LA--11601-MS

DE89 014261

LA-11601-MS

UC-000
Issued: July 1989

Proton Linear Accelerators: A Theoretical and Historical Introduction

*Pierre M. Lapostolle**

DISCLAIMER

**Consultant at Los Alamos. 3, rue Victor Daix, 92200 Neuilly Sur Seine, FRANCE.*

Los Alamos National Laboratory
Los Alamos, New Mexico 87545

TABLE OF CONTENTS

Preface

In 1986, a series of invited seminars on the theory of proton linacs was given at Los Alamos National Laboratory, AT Division, and CERN. This report is a presentation of the material given in these seminars.

The main documentation for the field of linacs includes (1) the 1971 book *Linear Accelerators* (North-Holland Publishing), which is now out of print and also out of date in a few areas, and (2) the proceedings of accelerator conferences. This last source of material is very detailed and accurate, but is generally in the form of short contributions that do not give a comprehensive view of the problems involved. The aim of the seminars and of this report is to present the basic general principles that substantiate the many developments, which have sometimes been spectacular, presented at conferences devoted to this type of accelerator.

As was the case twenty years ago when a similar CERN report had been the origin of the book (mentioned above) on linear accelerators, it is hoped that this report, which does not go into complex detail, will be followed by a new book. If such a new book appears, it will have been greatly due to the support received from Los Alamos National Laboratory and CERN in the preparation of the seminars and to their continuing interest. Such a book will deal only with proton and ion linacs. It is hoped that the preparation of a new book on electron linacs by another author will be supported in the future.

Acknowledgment

The technical clarity of this report has greatly benefited from the help of Dr. R. K. Cooper. The style and editorial clarity has likewise been enhanced by L. H. Schilling. The author wishes to express his gratitude for their help and patience and heartily acknowledge their contributions.

As said in the preface, this report is a step towards the preparation of a new book. This means that if derivations are missing in the report, the subjects treated and the way they are presented would be the same in the book.

In order to make this book correct, useful, and profitable for future readers, all comments, criticisms, and suggestions on the content as well as on the presentation would be greatly welcome; these would help in arriving at a reasonable compromise between a good book and what the author will be able to achieve.

Please do not hesitate, then, to send me your comments. Thank you in advance.

P. M. Lapostolle

Pierre Lapostolle

3, rue Victor Daix

9220 NEUILLY SUR SEINE

FRANCE

PROTON LINEAR ACCELERATORS: A Theoretical and Historical Introduction

by

Pierre M. Lapostolle

ABSTRACT

From the beginning, the development of linear accelerators has followed a number of different directions. This report surveys the basic ideas and general principles of such machines, pointing out the problems that have led to the various improvements, with the hope that it may also aid further progress. After a brief historical survey, the principal aspects of accelerator theory are covered in some detail: phase stability, focusing, radio-frequency accelerating structures, the detailed calculation of particle dynamics, and space-charge effects at high intensities. These developments apply essentially to proton and ion accelerators, and only the last chapter deals with a few aspects relative to electrons.

CHAPTER 1

HISTORY AND INTRODUCTION TO THE THEORY OF LINEAR ACCELERATORS

Since 1924, the history of linear accelerators (linacs) has included not only many obstacles, which were sometimes considered insurmountable, but also breakthroughs that, though often spectacular, sometimes presented unexpected or even paradoxical results. Ultimately, theory and practice became more accurate, and sophisticated tools exist today for designing linacs. New work, however, must still be done in order to understand and to master all the phenomena taking place.

1. LINAC PRINCIPLE

1.1 Origin of the Principle

In an electrostatic device, the potential difference V must exist between two points of the system to give particles of charge q an energy equal to $q \cdot V$. This energy is necessarily limited by electrical breakdown. Ising, in 1924 [Ising], proposed the following device to avoid this limitation: positive particles, coming out of a discharge tube, cross a succession of *"drift tubes"* made of electrodes with a hole for letting the beam go through (Fig. 1). Pulsed electric voltages, properly synchronized, are applied on each of the drift tubes. If the pulses are applied between the time the particles enter the hole and the time they exit (or vice versa), one may achieve additional acceleration. This principle was not tested at the time it was proposed.

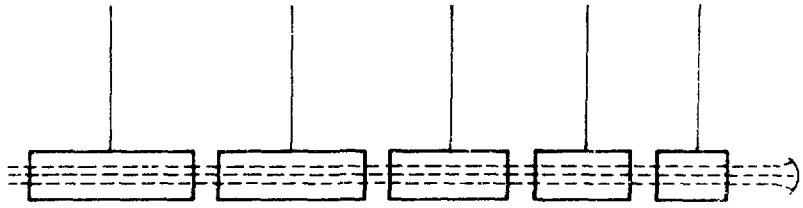

Fig. 1. Ising proposal.

1.2 First Experiment

In 1928, Wideröe [Wideröe], then in Aachen, Germany, proposed a new device. Instead of pulses, he suggested the use of a radio-frequency (rf) voltage, choosing drift tubes whose length increased with particle velocity, such that particles always find an accelerating voltage when going from one tube to the next. (It is this description of the linac principle that led E. O. Lawrence to the invention of the *cyclotron*.)

Wideröe built a machine with a single drift tube to test the validity of his principle: using a voltage of 25 kV between two grounded electrodes, singly charged Na and K ions (coming out of a heated filament) were accelerated to an energy of 50 keV (two successive accelerations).

1.3 A Larger Experiment

In 1931, Sloan and Lawrence at Berkeley [Sloan et al., 1931] proposed to test the method on a large device. Applying an rf voltage of 42 kV at a frequency of 10 MHz to a sequence of 30 drift tubes (Fig. 2), they obtained an energy of 1.25 MeV with mercury ions. A few years later, in 1934, they reached 2.8 MeV using a sequence of 36 drift tubes with 79 kV [Sloan et al., 1934].

However, such a device remained purely experimental, because the needs of physics, at least for protons, were better satisfied by cyclotrons as developed by E. O. Lawrence (a linac would have had to be too long, at that time, to reach similar energies).

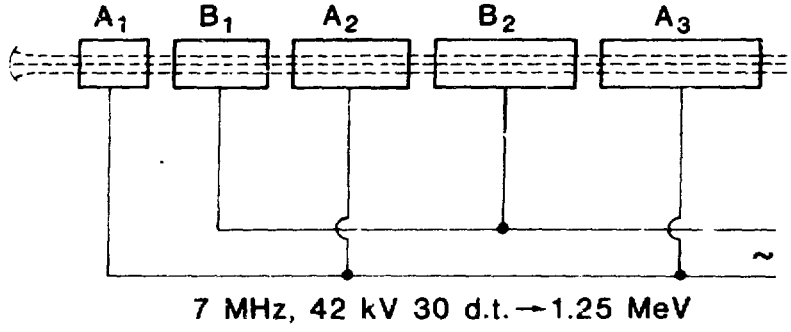

Fig. 2. Principle of the Sloan and Lawrence machine.

2. FIRST PROTON LINAC

In 1945, under the leadership of Luis Alvarez, a team of scientists that included many individuals who were to become well known in the field of accelerators (such as W. Panofsky) started the construction of the first true proton linac [Alvarez et al.]. The structure, the so-called Alvarez structure, can be considered as a section of circular waveguide excited in a TM_0 mode and loaded with a succession of drift tubes whose length and position are chosen to insure synchronism of accelerated particles while keeping the resonant frequency of the cavity constant (Fig. 3). The axial electric field of the TM_0 mode is then concentrated in accelerating gaps between drift tubes, the voltage between them being proportional to their length and not constant as in previous devices. It is thus possible to obtain a fast acceleration, even when the velocity increases. With a frequency of 200 MHz (because of the availability of radar amplifier tubes), the 12-m-long machine accelerated protons from 4 MeV to 32 MeV.

Besides the development of the rf structure, such a linac provided an opportunity to delve more deeply into the theory of linacs, in particular the beam dynamics, longitudinal as well as transverse.

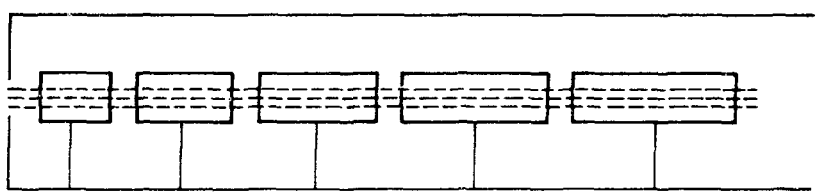

Fig. 3. Alvarez-type cavity.

2.1. Phase Stability

The principle of phase stability is illustrated in Fig. 4. The successive lengths of drift tubes are such that at gap N, exactly one rf period before gap $N + 1$, the energy gain must have a given value qV, lower than peak value, qV_0, that the sinusoidal voltage could deliver.

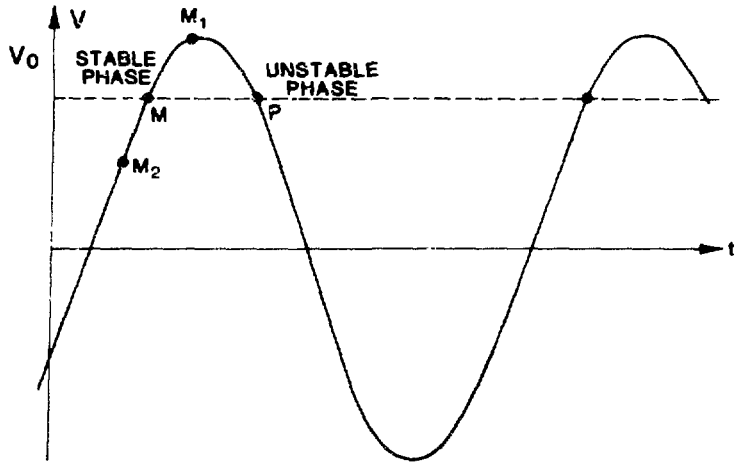

Fig. 4. Stable and unstable phases.

Letting

$$qV = qV_0 \cos \phi \ ,$$

one sees that there exists, per rf period, two phases for which the condition is satisfied. Let M and P be the corresponding points in Fig. 4. If particles must cross gap N exactly with one of these two phases, only a very few will be correctly accelerated.

Let us consider, however, what will result from a late arrival—at M_1, for instance. At M_1, the voltage is higher than V. The particle will then receive more energy, and it will go faster and catch up its delay. At M_2, on the opposite side, an early particle will be slowed down. There is phase stability, and particles are attracted toward the stable point M. Conversely, around P an instability exists.

There is stability around the phase for which the field is increasing with time. A detailed analysis of this stability will be given in Chap. 2.

2.2 RF Defocusing

When crossing an accelerating gap where there is phase stability, particles are defocused.

Let us consider the field distribution around the holes of the drift tubes in a gap (Fig. 5). For an accelerating field, there is a focusing effect at the entrance and a defocusing

effect at the exit. If the field was constant with time, there would be a compensating effect (at least to the first order). But for phase stability, the field must be rising. Defocusing then overcomes focusing.

Chapter 3 will show what tricks were invented to circumvent this difficulty, which results directly from electromagnetic field properties. Only the early milestones will be indicated here along with the solution of this difficult overall stability problem.

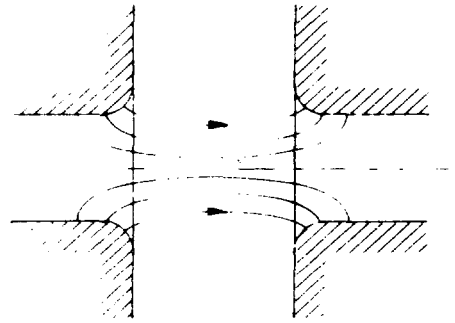

Fig. 5. Radio-frequency defocusing when the field is rising.

2.3 Foil and Grid Focusing

One way to avoid the global defocusing effect is to suppress the defocusing effect at the gap exit by closing the drift-tube hole with a foil thin enough to be crossed by fast particles (Fig. 6). This foil, to which electric field lines are locally normal, becomes charged, counteracting the incompatibility condition. There can be, then. longitudinal stability with transverse focusing.

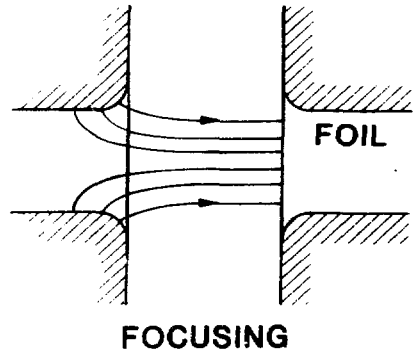

Fig. 6. Foil or grid focusing.

However, the test of this method turned out to be unsuccessful because electrical breakdowns that usually occur during electric conditioning destroyed the foils.

Grids were then proposed instead of thin foils, the microscopic mesh of which particles were supposed to penetrate. It is true that no focusing is obtained through aligned grid holes; particles must oscillate around aligned grid wires (and not run into them) as they pass through. Several grid configurations were considered, such as shown in Fig. 7. It is obvious that one can expect a loss of particles with such a system. Until the final tests, in particular during tests that were unsuccessful for other reasons, doubt as to the efficiency of grids persisted. In 1947, however, the first beam was accelerated in the Alvarez machine.

Before being transported to the University of Southern California in 1958, this machine was used in 1952 to test the alternating gradient (AG) electric focusing [Blewett] concept that had been recently invented by Blewett.

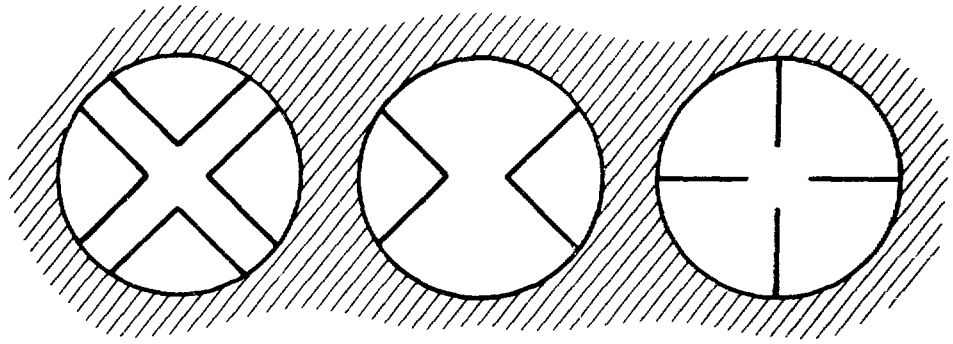

Fig. 7. Various shapes of grids.

3. CERN LINAC I

After the Alvarez machine, another linac with an energy of 68 MeV was built at the University of Minnesota in 1953. Apart from the use of three rf cavities and a lower injection energy (500 keV), this machine was very similar to the first one. Another machine, a 20-MeV linac, was built at Berkeley (the Bevatron injector).

During the second half of the 1950's, linacs were built to use AG focusing in its magnetic version, only applicable when the particle velocity becomes high. Two machines

were built simultaneously, one at Brookhaven (50-MeV AGS* Injector) and one at CERN (PS** Injector I). The CERN linac was made of three cavities, the first one of them being designed simultaneously with the NIMROD injector at Harwell (England).

3.1. First Tests (Grid Focusing)

At the beginning of 1959, the first cavity in its initial Harwell version (with grids) seemed ready to accelerate protons produced by an rf source through a 500-kV column. Measurements had been made of the cavity's Q (around 50,000) and of the metallic bead perturbation of the axial electric field (frequency displacements of a few hundred hertz). These measurements gave a value of the shunt impedance Z_s (see Chap. 4). Eventually, a measurement of rf power (calorimetric measurement of about one hundred watts, average, with a peak power close to a magawatt) seemed to show that the electric field, reached by conditioning, should be enough for acceleration.

After several unsuccessful tests, a very weak current was observed at the output from a faint quartz plate illumination. The energy, however, was much smaller than the 10 MeV expected, because the beam was stopped by a very thin copper plate. This surprising and completely unexpected result was to be explained from an acceleration at half velocity (previously unexpected) in which the transit time between gaps is two rf periods instead of one. The electric field was too small for normal acceleration but large enough for this reduced energy.

It remained unexplained, however, how such a phenomenon could take place with the nominal injection voltage. Acceleration, which was a little more intense at 125 kV (and zero below), still existed up to 500 kV. One had then to invoke field irregularities to explain a beam capture at some points along the structure. A more detailed theory of phase stability, including the "golf club" (Fig. 8, see Chap. 2 for details), which takes rapid acceleration into account, was not yet known!

Normal operation was obtained two weeks later by better conditioning of the cavity.

---

* AGS -- Alternating gradient synchrotron.

** PS — Proton synchrotron.

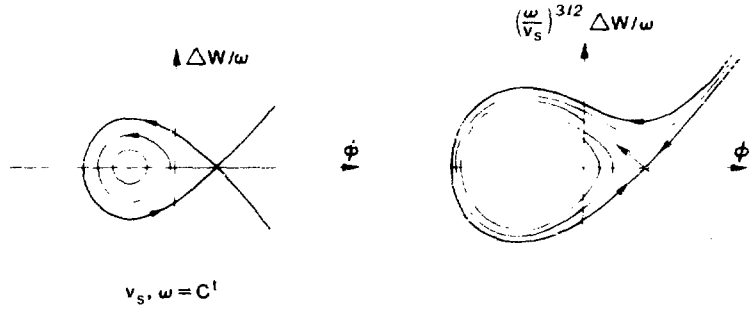

Fig. 8. Bucket and golf club.

3.2. Tests with AG Focusing

A few months later, in the Spring of 1959, gridded drift tubes in Cavity I were replaced by drift tubes containing pulsed quadrupoles (technology did not permit high enough dc fields). Design, made according to the new principle of AG focusing, which was itself derived from Floquet's theory and the Hill and Mathieu equations, had led to the adoption of very strict tolerances for quadrupole field adjustments in order to remain inside a relatively narrow stability region (Fig. 9, see Chap. 3 for details).

From the first tests, a good intensity was obtained from Cavity I. However, beam observation, accomplished by blackening a quartz plate, revealed a flat, slightly cross-shaped beam. The focusing system was suspected and, despite the strict tolerances, it was decided to invert, one after the other, the 44 quadrupoles of the cavity and observe the effect on the beam shape. Apart from the first quadrupoles, the inversion (or switch off) of which entailed a noticeable loss of beam, the effect on the others was not at all fatal and was hardly visible in the intensity. However, from the beam-shape observation (which still remained partly cross-shaped because of aberrations), two quadrupoles were found to have their polarity reversed (the 34th and the 43rd).

The concept of instability, which led to the design of the machine (under the influence of parallel studies made for the CERN PS), still had to be completed by the understanding of nonperiodic focusing errors in order to deal with practical operation.

Cavities II and III of the CERN linac (with dc magnetic focusing) were installed without difficulty, and beam was injected into the PS in September 1959.

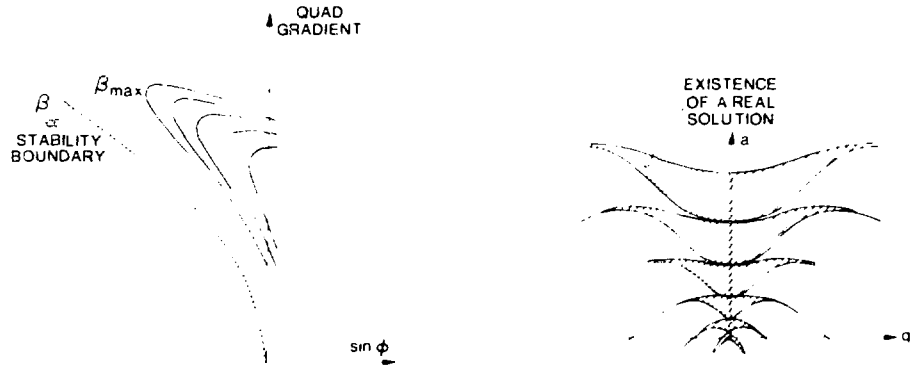

Fig. 9. Mathieu's equation stability area and linac focusing stability limits.

4. MORE RECENT EXPERIENCE WITH LINACS

4.1. Field Distribution

From the design of the first linacs [Alvarez et al.], the adverse effect of a field variation (usually regular and monotonic) along a long cavity had been suspected. This variation was corrected with the help of movable walls or plungers put along the structure, mainly near the ends. In addition, similar elements were used to correct the resonant frequency, an essential operation in cavities with Q of the order of 50,000.

The SATURNE 20-MeV linac injector, built in Saclay in the 1960s, made use of a set of ball tuners that were moved in the cavity volume around neutral points where electric and magnetic field perturbation effects, which are of opposite sign, become equal (see Chap. 4). Later the adjustment of the balls was done empirically by studying the injection efficiency of SATURNE, a relatively loose criterion that is due to the not very stringent injection requirements.

Near the end of the 1970's, it was decided to accelerate deuterons and α particles, and then heavier ions. This could only be done in a half-velocity mode (see Sec. 3.1). The efficiency, however, was found to be relatively low, noticeably lower than expected (inconsistent with the more detailed knowledge of beam dynamics as it was then developed — see Chap. 5). This situation became unacceptable when polarized particles (with very low source intensity) were accelerated.

Empirical adjustments being unsuccessful, the field distribution was suspected and various laws were proposed to use in beam dynamics computation [Chamouard et al.]. It was then possible to conclude that a low-energy ball tuner was producing a dip in the field distribution and not just a tilt, as had been previously assumed; this dip was responsible for the unsatisfactory operation. After moving the tuner had corrected the field distribution, a parallel study of focusing led to a new adjustment, which gave a normal acceleration efficiency. It will be seen in Chap. 4 that a field tilt can be interpreted from the addition of two modes, TM_{010} and TM_{011}, in the cavity. A more complicated distribution can result from the addition of more modes of higher order.

Another interpretation, introduced later [Dôme et al.], refers to the properties of the 0 mode (Fig. 10) for which the phase velocity is infinite, and one cannot speak about forward and backward waves. The solution of the wave equation

$$\frac{\partial^2 E_z}{\partial z^2} + k^2 E_z = 0 \quad ,$$

which, in general, has two solutions when $k \neq 0$, becomes, when $k = 0$,

$$E_z = \text{Const.} \qquad \text{and} \qquad E_z = z \times \text{Const.} \quad .$$

The first of these solutions is the normal 0 mode. The second one, for which $z = 0$ would be a magnetic boundary (Fig. 11), cannot exist in a perfect cavity; it is a degenerate mode. A computation of Poynting's vector in this mode shows that there is a circulation of reactive energy to maintain field and a stored energy inequality along the z axis of the structure.

If such a mode does not exist in a perfect cavity, it can, however, be excited by perturbed end boundaries; local perturbations, changing the resonant frequency locally, can also behave like a source or a sink of reactive energy, which then has to flow along the structure to maintain equilibrium, entailing a variation of field level. Ball tuners, if they are localized and their perturbation is large, may produce such effects.

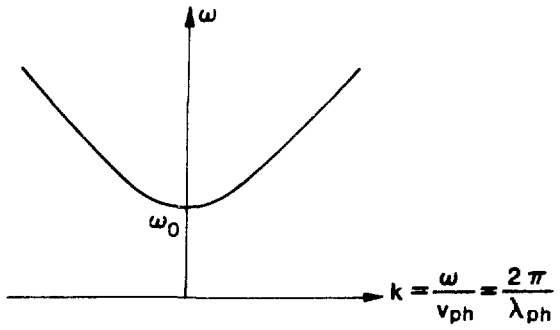

Fig. 10. Dispersion curve and cut-off mode (zero mode).

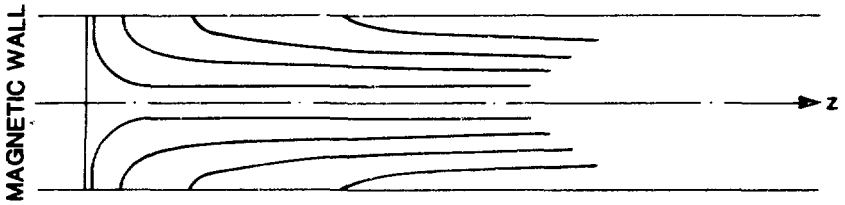

Fig. 11. Degenerate mode.

4.2. Field Stabilization

Concerns about the difficulty of field adjustments or the avoidance of situations such as that described above have led to a search for structures that are insensitive to field perturbations. Chapter 4 will show that this sensitivity can be characterized by a mode separation in frequency around the operating 0 mode. In the degenerate-mode approach presented above, the Poynting vector flux for a given slope of the field is larger when the frequencies are distant and, in particular, if the group velocity is not zero as it is normally at the 0 mode. The possibility of having a nonzero group velocity at the zero mode, as shown on the dispersion curve of Fig. 12 (see Chap. 4), can be obtained with the use of coupled circuits. Another advantage is that this nonzero group velocity makes the propagation of transients faster, particularly for filling the cavities and for beam-loading compensation.

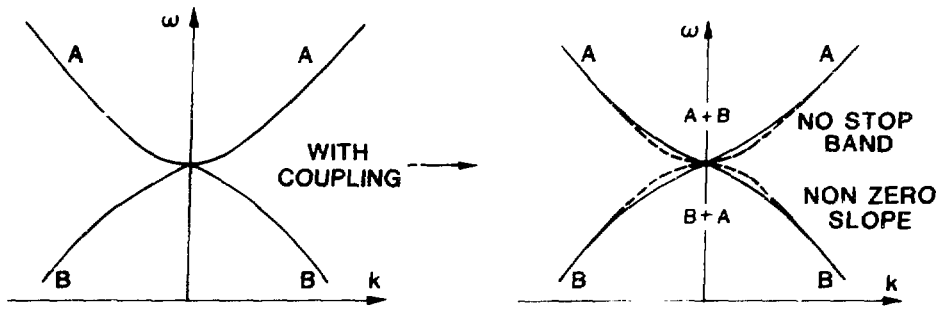

Fig. 12. Dispersion curve at confluence of two coupled modes.

5. HIGH-INTENSITY ACCELERATION

When the intensity is increased in a linac, one perturbing effect is the mutual repulsion of particles due to their electric charge. This repulsion affects phase stability as well as focusing. The computation of such effects requires a knowledge of the charge distribution in the beam. The first theory, presented in 1959 by Kapchinskij and Vladimirskij [Kapchinskij et al.], treats the case of a continuous beam and assumes a uniform distribution. This case is the only one consistent with linear equations. Kapchinskij and Vladimirskij computed the corresponding four-dimensional phase-space distribution (configuration and transverse velocity spaces) assuming the same longitudinal velocity for all particles. This distribution is a surface distribution on a hollow hyperellipsoid. Such a distribution is not physical. Very often medium intensity beams do not exhibit uniform distributions, but rather distributions that decrease toward the edges.

More recently, in the early 1980's, experiments at Berkeley on very intense beam transport showed a practically uniform distribution, falling sharply to zero on the edges [Kim et al.]. Such a distribution, corresponding, for instance, to a uniform or Gaussian distribution in phase space, had been derived before 1969 [Kapchinskij] and also [Lapostolle] but had been forgotten. For very high intensities, the beam, circulating in a focusing system, behaves somewhat like a plasma. Its density becomes such as to cancel out external fields. Particles then move freely across the beam in the transverse direction, being reflected at the edges.

Studies relative to high-intensity beams, as described in Chap. 6, are far from being complete, even though more and more powerful and accurate simulation codes allow a

relatively good representation of experimental observations. Theoretical work remains to be done for a more complete interpretation of the physical phenomena, even though important milestones have already been achieved.

CHAPTER 2

PHASE STABILITY IN LINACS

The principle of phase stability that governs the longitudinal motion of particles was invented by E. O. MacMillan and V. I. Veksler in 1945 [MacMillan] and [Veksler]. It was applied to linear accelerators by L. Alvarez in 1946 [Alvarez]. This principle, described in Chap. 1 and recalled in Fig. 1, is closely linked to the concept a of synchronous accelerating wave. To explain this principle we will first examine the synchrotron case, even though there will be limitations for the definition of this synchronous wave for the linac case.

In developing phase stability theory, the effects of some necessary approximations resulting from the previous limitations will be described, as well as methods to counteract the effects. Pitfalls that were encountered in early research will also be discussed. A more detailed and more accurate computation, valid for all cases, will be described in Chap. 5.

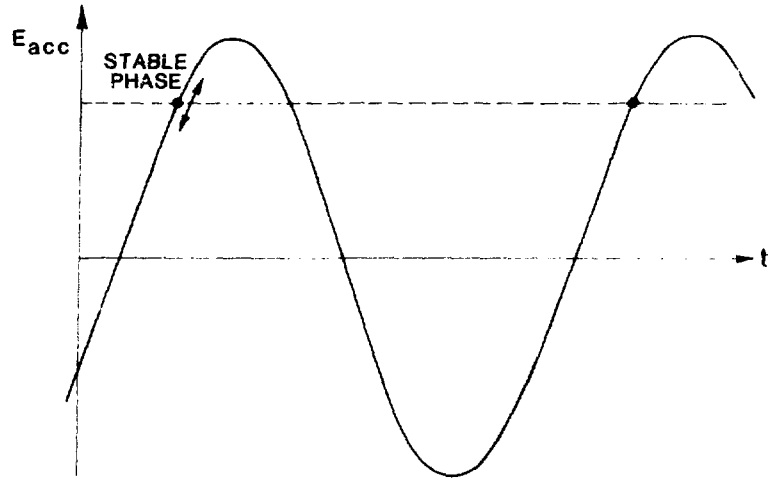

Fig. 1. Traditional presentation of phase stability.

1. SYNCHRONOUS WAVE

1.1 Synchronous Wave in a Synchrotron

One may compare the acceleration in a synchrotron to the operation of a synchronous motor. In a single-phase synchronous motor, the magnetic field of the stator can be considered as the sum of two rotating fields, rotating in opposite directions. The rotor is driven by one of them.

Let us consider a synchrotron with a single accelerating cavity (or two cavities diametrically opposed, see Fig. 2). Taking the circumference as a period, the accelerating field can be expressed in the form of a Fourier series as a function of the azimuth, a sum of terms in the harmonic number h. In the special case of infinitesimally short cavities (δ function), each harmonic has the same amplitude. Two rotating waves of opposite direction correspond to each harmonic representing a stationary field.

Each rotating wave of different h has a corresponding revolution period, a multiple h of the rf period, and a revolution velocity. A synchrotron can accelerate on various harmonics h, i.e., particles of different velocities can be accelerated.

When several cavities are installed around the circumference, Fourier analysis still gives the possible modes of acceleration. If all the cavities are not in phase or in opposite phase, there is not necessarily a symmetry between the two senses of rotation.

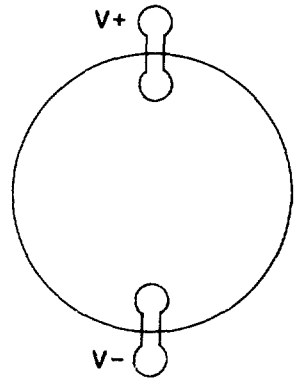

Fig. 2. Synchrotron orbit with two accelerating cavities.

1.2 Transit Time Factor

Accelerating gaps are never infinitely short. Fourier analysis then shows that beyond some harmonic number, the amplitude drops instead of remaining constant, as for a true δ function. To this effect, one may add that the accelerating field enters the beam holes beyond the faces of the electrodes (Fig. 3); the axial field is not the same on the axis as on the borehole edge.

The usual expression that will be justified in Chap. 5 is [Alvarez et al.]:

$$T(k,r) = \frac{I_0(k_r r)}{I_0(k_r a)} \frac{\sin\, kg/2}{kg/2} \quad . \tag{1}$$

The transit time coefficient T, less than 1, is the reduction factor of the accelerating synchronous wave amplitude with respect to what it would be for an infinitesimally short gap with no field penetration effect.

In this relation, g is the gap length,

$$k = \omega/v \tag{2}$$

with ω being the rf angular frequency and v the velocity of the particles, and

$$k_r^2 = k^2 - \omega^2/c^2 \quad . \tag{3}$$

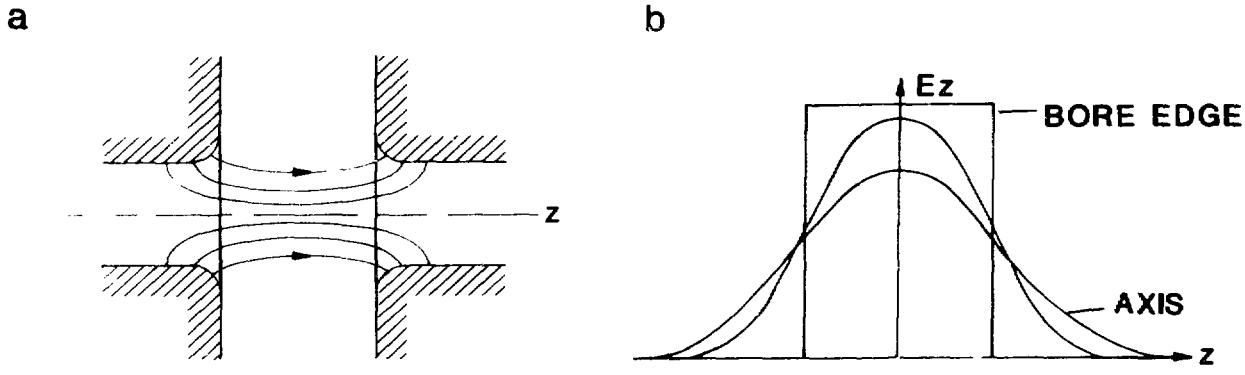

Fig. 3. Electric field distribution across a gap.

The quantity a is the radius of the beam hole and r is the distance to the axis at which T is computed. The kg term corresponds to the Fourier analysis mentioned above.* The terms involving I_0 Bessel functions correspond to the field penetration effect (one sees that $T = 1$ for $g = 0$, and $z = r = 0$). The transit time factor reduces acceleration on high harmonics: for a synchrotron of average radius R, the quantities g/R and $a/R \ll 1/h$. In practice, for synchrotrons this reduction is small, but as will be seen, it is not small for linacs.

1.3 Synchronous Wave in a Linac

The comparison between a synchrotron and a synchronous motor leads us to consider a linear induction motor for a linac. Here, however, because the velocity changes, there is no strict periodicity in space (in a synchrotron, only the frequency changes). On the contrary, one endeavors, by construction, to maintain the time periodicity by a change in space periodicity. This is, however, seldom achieved in practice for several reasons:

1. the accelerating field may vary along the structure;
2. the absence of exact scaling in the gap geometry, according to the velocity increase, may lead to a change in transit time factor;
3. in the low energy part of the machine, the relative energy increase may be very fast; and
4. any error in construction or adjustment entails almost inevitably the absence of a synchronous particle.

Nevertheless, the general theory of stability and phase oscillations gives a simple and generally valid interpretation of the phenomena, and it remains of current use even if it may lead to errors in some cases. Detailed methods available today, as described in Chap. 5, are necessary for checking some results.

---

* As will be mentioned in Chap. 5, Sec. 1.1, it is possible to take into account the effect of the chamfer radius ρ_c in the borehole (Fig. 3) by replacing g by a corrected value g_c.

1.4 Higher Order Mode Operation

Alvarez structure [Alvarez, et al.] (Fig. 4) operation is usually at the $h = 1$ (or 2π mode). It can, however, be at the $h = 2$ (4π mode) for half-velocity particles (see Chap. 1, paragraph 3.1). Because the field at the 2π mode extends in gaps over a relatively long length (1/4 rf period), the transit time coefficient is greatly reduced (at least by 30% to 40%) for operation at the 4π mode, particularly at low energy [$I_0(k_r a)$ term].

The Sloan-Lawrence [Sloan, et al.] and interdigital or H-type structures (Fig. 5) normally operate at the π mode. The first higher order mode would be 3π, but T is then reduced by a factor of about 3 unless the gap geometry has been designed for that case.

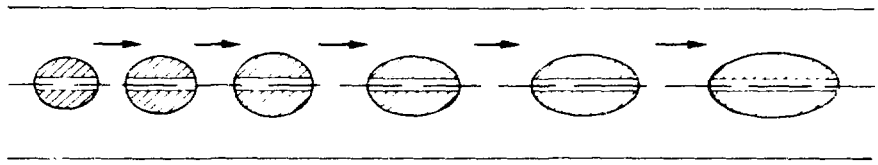

Fig. 4. Field orientation in the gaps of an Alvarez structure.

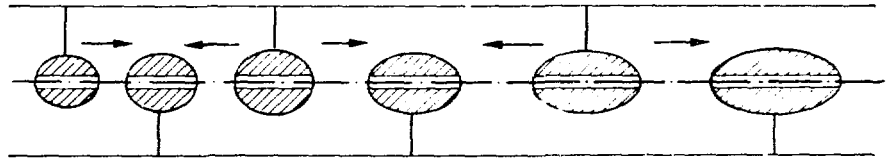

Fig. 5. Field orientation in the gaps of a Sloan-Lawrence interdigital structure.

1.5 Acceleration with Several Harmonic Frequencies (Flat Topping)

In some machines, two sets of accelerating cavities excited at harmonic frequencies and operating simultaneously are used (this has so far only been done in circular machines). The Fourier analysis previously described can be made for all the frequencies used.

Wave addition, for a given mode of operation (h for fundamental frequency and kh for harmonics), gives a nonsinusoidal distribution, the shape of which can be modeled around the stable phase point.

It is then possible by adjusting amplitude and phase to obtain a flat (for cyclotrons) or linear profile (Fig. 6) over almost the full extent of beam bunches. This linearizing effect is obtained at the cost of some loss of acceleration. The choice of the order and number of harmonics used for "flat topping" depends on the required extent in phase.

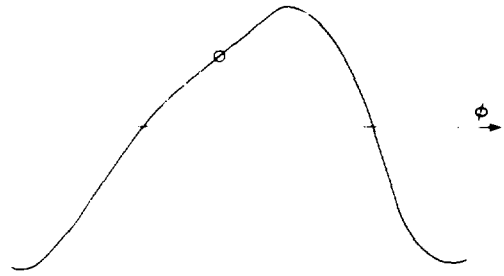

Fig. 6. Linear field variation obtained with two harmonics ($h = 1$ and 2).

2. PHASE STABILITY DYNAMICS IN FIRST APPROXIMATION

Phase stability results from the capture of accelerated particles in the synchronous wave. In an induction motor, the locking of the rotor to the rotating or linear wave results from a force that makes it move, producing a certain work.

In a linac (or a synchrotron), the energy given to the particles causes the velocity to increase (at least in the nonrelativistic case: protons, heavy ions). Under such conditions, the space period of the wave also has to increase, changing the depth of the potential well where particles are captured. As will be seen, this potential is as shown in Fig. 7, where the change in period has been exaggerated.

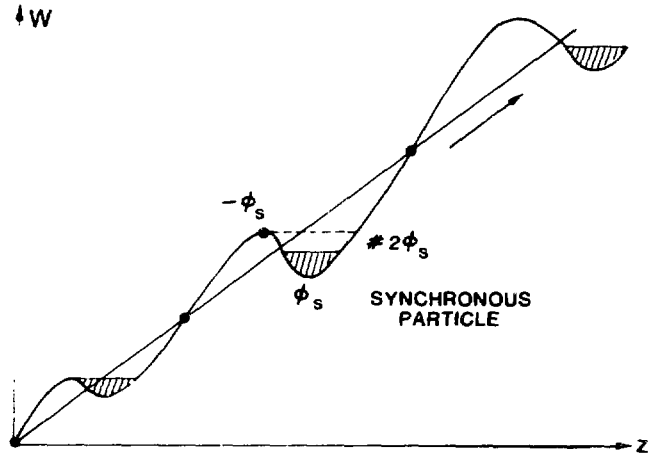

Fig. 7. Motion of accelerating buckets.

2.1 Hypothesis for a First Approximation

It can be said that the usual classical theory of phase stability is a first approximation in which velocity change is neglected. Such a model, similar to the induction motor, would correspond to the case where particles should fight against an external braking force while receiving acceleration, thus keeping a constant kinetic energy.

2.1.1 Nonrelativistic Case

The motion of one particle (abscissa z) of mass m with respect to the synchronous particle (z_s) of fixed phase ϕ_s, with respect to the wave of velocity v_s, can be written with time t as a variable. Putting

$$u = z - z_s \tag{4}$$

and letting ET be the peak value of the accelerating field in the wave, one has

$$mu'' = eET\left[\cos\left(\frac{\omega u}{v_s} - \phi_s\right) - \cos\,\phi_s\right] \;; \tag{5}$$

by integration after multiplying each member by u', one has, if $u' = u'_0$ when $u = 0$,

$$m\left(u'^2 - u_0'^2\right) = 2eET\left[\frac{v_s}{\omega}\,\sin\left(\frac{\omega u}{v_s} - \phi_s\right) - u\,\cos\,\phi_s + \frac{v_s}{\omega}\,\sin\,\phi_s\right] \;. \tag{6}$$

The kinetic energy of the particles in a frame moving at the wave velocity v_s is shown on the left-hand side, while the right-hand side shows the potential in which particles are captured, as shown previously in Fig. 7. In this figure, the variable u can be replaced by the phase

$$\phi = \phi_s - \frac{\omega u}{v_s} \quad . \tag{7}$$

The potential dip (stability zone) is limited by $\phi = -\phi_s$ and $\phi \approx 2\phi_s$, where $\phi = 0$ is the crest of the accelerating wave (if the potential law around $\phi = -\phi_s$, 0, and ϕ_s is replaced by a cubic curve, the upper limit is exactly $2\phi_s$).

This variable ϕ is often preferred to u. Its conjugate momentum is easily obtained from the derivative of kinetic energy with respect to ϕ':

$$\left| \frac{d\left(\frac{1}{2}mu'^2\right)}{d\phi'} \right| = \frac{d\left(\frac{1}{2}mu'^2\right)}{\frac{\omega}{v_s}du'} = \frac{mv_s u'}{\omega} \simeq \frac{\delta W}{\omega} \quad ,$$

where δW is the energy difference between the particle under consideration and the synchronous particle.

Remark. The motion described by Eqs. (5) and (6) is sometimes compared to that of a forced pendulum (Fig. 8). This analogy is frequently used in the theory of the synchrocyclotron.

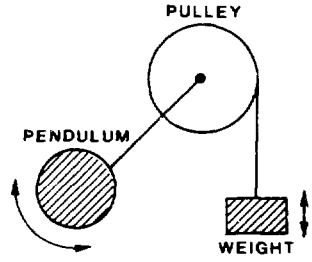

Fig. 8. Forced pendulum analog.

2.1.2 Relativistic Case

It is easy to introduce relativistic corrections in the previous equations. It is common practice then to replace the variable t by the abscissa s of the crest of the accelerating wave

[Smith, L.]. Introducing classical relativity symbols β and γ one gets

$$\delta\gamma = \frac{\delta W}{m_0 c^2} \tag{8}$$

and

$$\begin{cases} \dfrac{m_0 c^2}{\omega}\dfrac{d(\delta\gamma)}{ds} = \dfrac{eET}{\omega}(\cos\phi - \cos\phi_s) \\ \\ \dfrac{d\phi}{ds} \simeq -\dfrac{\omega}{c}\dfrac{\delta\beta}{\beta_s^2} = -\dfrac{\omega}{c}\dfrac{\delta\gamma}{\beta_s^3\gamma_s^3} \end{cases} , \tag{9}$$

whence

$$m_0 c^3 \frac{d}{ds}\left(\frac{\beta_s^3\gamma_s^3}{\omega}\frac{d\phi}{ds}\right) = -eET\,(\cos\phi - \cos\phi_s)\ . \tag{10}$$

Supposing $\beta_s^3\gamma_s^3/\omega$ = const (not a function of s), this equation is easy to integrate, and a solution similar to the nonrelativistic case is found.

It is also possible to deduce the relation between conjugate variables ϕ and $\delta W/\omega$ or ϕ and $\delta\gamma$:

$$\delta\gamma^2 + \frac{2eET\beta_s^3\gamma_s^3}{\omega m_0 c}(\sin\phi - \phi\cos\phi_s) = \text{Const.}\ . \tag{11}$$

One recognizes the usual form of the stability diagram (Fig. 9) in phase space (conjugate variables) [Bruck, Chap. XVI]. Between the limiting points in ϕ: $\approx 2\phi_s, -\phi_s$, the separatrix shows the limits in $\delta W/\omega$ or $\delta\gamma$. Inside this separatrix, particles, during acceleration, move along quasi-elliptic curves around stable phase ϕ_s, such curves departing more and more from ellipses as they come closer to the separatrix.

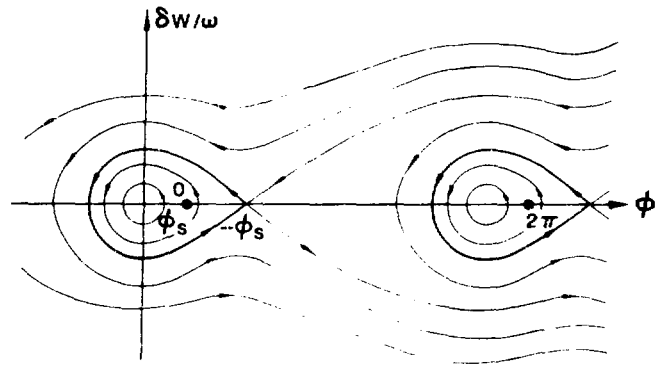

Fig. 9. Trajectories in phase space.

When the stable phase ϕ_s approaches $-\pi/2$ and the acceleration goes to zero, the stability limits join; the separatrix takes the shape shown in Fig. 10, symmetrical with respect to $\phi_s = -\pi/2$.

The stability area, limited by the separatrix, is currently called a bucket, evoking the possibility of raising in energy the particles enclosed there (the term "fish," referring to the shape of the separatrix, is seldom used).

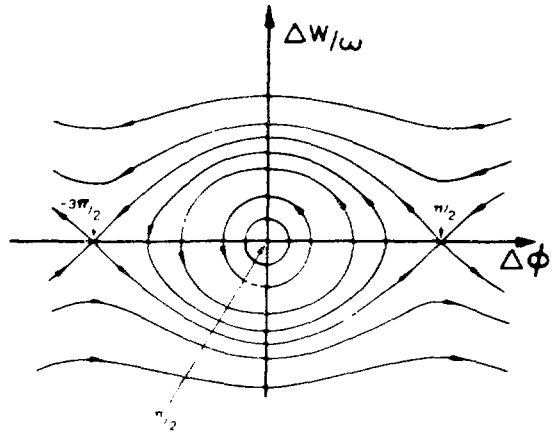

Fig. 10. Nonaccelerating case.

2.2 Hamiltonian of the Motion

It is worth noticing that if

$$H = -m_0 c \frac{(\delta\gamma)^2}{2\beta_s^3\gamma_s^3} - \frac{eET}{\omega}(\sin\phi - \phi\cos\phi_s) \quad , \tag{12}$$

one has, for Eq. (9):

$$\begin{cases} \dfrac{d\phi}{ds} = \dfrac{\partial H}{\partial(\delta\gamma)} \dfrac{\omega}{m_0 c^2} \\ \\ \dfrac{m_0 c^2}{\omega} \dfrac{(\delta\gamma)}{ds} = -\dfrac{\partial H}{\partial\phi} \end{cases} , \tag{13}$$

which means that the motion of particles described by conjugate variables ϕ and $\delta W/\omega = m_o c^2\, \delta\gamma/\omega$ is derived from the Hamiltonian H.

3. SECOND APPROXIMATION

The hypothesis of constant velocity and energy can only provide a local representation. If one wants to know the motion of particles in the course of the acceleration, one needs to introduce a change in energy, and perhaps also changes in other parameters such as the accelerating field ET and stable phase ϕ_s. To first order, one may, however, assume such quantities will change slowly (adiabatically) without ever compromising the existence of a "synchronous particle."

Because the motion is derived from a Hamiltonian, it satisfies *Liouville's theorem* [Becker], [Corben et al.] and [Lichtenberg].

3.1. Liouville's Theorem

According to Liouville's theorem, the area occupied in phase space (space where coordinates are conjugate variables) by a set of particles is an invariant of the motion. This set of particles than behaves, in phase space, as an incompressible fluid.

Let $q = \delta\phi$ and $p = \delta W/\omega$ be these conjugate variables, and let us consider their evolution between two successive points s_1 and $s_2 = s_1 + ds$.

Let

$$A_1 = \int\int dq_1 dp_1 \tag{14}$$

and

$$A_2 = \int\int dq_2 dp_2$$

be the phase-space extensions (area in phase space) of the same set of particles at points s_1 and s_2.

According to the theorem of the Jacobian;

$$A_2 = \int\int dq_2 dp_2 = \int\int J dq_1 dp_1 \tag{15}$$

with

$$J = \begin{vmatrix} \dfrac{\partial q_2}{\partial q_1} & \dfrac{\partial p_2}{\partial q_1} \\ \\ \dfrac{\partial q_2}{\partial p_1} & \dfrac{\partial p_2}{\partial p_1} \end{vmatrix} . \tag{16}$$

But

$$q_2 = q_1 + \frac{dq}{ds}ds = q_1 + \frac{\partial H}{\partial p}ds \tag{17}$$

$$p_2 = q_1 + \frac{dp}{ds}ds = p_1 - \frac{\partial H}{\partial q}ds$$

then

$$J = \begin{vmatrix} 1 + \dfrac{\partial^2 H}{\partial p \partial q}ds & \dfrac{-\partial^2 H}{\partial q^2}ds \\ \\ \dfrac{\partial^2 H}{\partial p^2}ds & 1 - \dfrac{\partial^2 H}{\partial p \partial q}ds \end{vmatrix} \tag{18}$$

such that

$$\frac{dJ}{ds} = 0 .$$

Phase extension is invariant because *even if H is a function of s*, since $\partial H/\partial s$ does not appear in the expression of the Jacobian, it does not affect it. On the contrary, Liouville's theorem does not apply if the system is not conservative. It is the case, for instance, of friction for which Hamiltonian mechanics does not apply.

3.2. Application

If now one considers a set of particles occupying an area A limited by one of the curves given by Eq. (11) corresponding to their input into the linac, this set will occupy at output a surface of equal area (but with the values of β, γ, ET, and ϕ_s corresponding to output). For example, if one considers small oscillations (elliptic curves in the central

part of the bucket), one has during acceleration

$$\begin{cases} \delta\phi_{max} = \sqrt{A}\ \sqrt[4]{\dfrac{2\pi\omega^2}{m_0c^2\beta_s^3\gamma_s^3\ eET\ \mid \sin\phi_s \mid \lambda_0}} \\ \\ \dfrac{\delta W_{max}}{\omega} = \sqrt{A}\ \sqrt[4]{\dfrac{m_0c^2\beta_s^3\gamma_s^3 eET \mid \sin\phi_s \mid \lambda_0}{2\pi\omega^2}} \end{cases} \tag{19}$$

where

$$\lambda_0 = 2\pi c/\omega \quad . \tag{20}$$

One sees that if ET and ϕ_s remain constant, there is, during acceleration, a bunch compression in phase and an energy spread increase.

In the case that a set of particles would not be "matched" [Bruck, Chap. VIII] in phase space, i.e., limited by a curve (11), it would "rotate" at a speed corresponding to "synchrotron oscillations" with a space period given by

$$\Lambda = \lambda_0\sqrt{\frac{2\pi m_0c^2\beta_s^3\gamma_s^3}{eET \mid \sin\phi_s \mid \lambda_0}} \quad . \tag{21}$$

Such properties are currently employed, and they offer a usually correct representation of accelerating beams. However, at very low energies, where changes are not necessarily adiabatic, it may be safer to make use of more accurate computations. Similarly, in case of field errors or of any other fast change of parameters, checks are necessary even if previous considerations are successfully used for "beam gymnastics" operations similar to the ones used to achieve matching in the transverse direction.

3.3. Adiabatic Changes — Golf Club

One may illustrate some of the effects that parameter changes, of adiabatic type, may introduce to classical beam dynamics representation and phase stability. It was shown that the energy increase changed the axis ratio of small amplitude oscillations. If one now considers the separatrix itself and the area it limits, it is obvious that this area increases with energy. A consequence of this apparent paradox has already been illustrated in

Chap. 1: it must be possible, as the energy increases, that *particles penetrate into the separatrix,* since Liouville's theorem is not violated.

R. Taylor [Taylor] has studied this mechanism. Computing the motion of particles with $\beta_s\gamma_s$ nonconstant, one obtains nonclosed curves. Figure 11 shows the type of trajectories obtained in a plane ϕ, $\omega^{1/2}\,\delta W/(\beta_s\gamma_s)^{3/2}$: the choice of these coordinates that are non-canonical avoids crossing and shows more clearly how the stability area can be filled. One understands that way how particles can be accelerated in a linac even if their injection energy is too high (Chap. 1, paragraph 3.1).

Instead of changing only the energy, one may also change E and synchronous phase ϕ_s. Provided such changes are slow enough, similar results apply. One may also keep the area of stability *constant.* Such methods are currently used to improve the operation at high intensity. They also allow a better matching of longitudinal emittances at injection or output of a linac section. They are currently used in radio-frequency quadrupoles (see Chap. 3, paragraph 5.3). Because of a change of E and ϕ_s, the area inside the separatrix may also shrink along the machine. Instead of Fig. 11, there will be a situation where there is a "leak" of particles. This leak has been used to produce a reduced energy from a linac. If experience confirms this phenomenon, the simple theory described here does not allow an accurate prediction of the results.

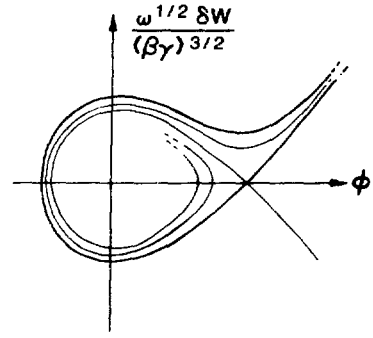

Fig. 11. Golf club.

4. IRREGULARITIES IN THE STRUCTURE

4.1. Nonadiabatic Changes

Instead of a progressive change, it is possible, for instance, to move suddenly the input phase of particles in a gap by changing either a drift-tube length if this is made inside a cavity, or a cavity phase if the change is made in between cavities. A particular application may consist of jumping quickly to the unstable point (Fig. 12). There the bunch will extend along the separatrix. Coming back to stable phase will then induce a rotation of the area leading, after a convenient length, either to very short bunches or to very small energy spread. Such "beam gymnastics" are not much used in linacs but are current practice in synchrotrons.

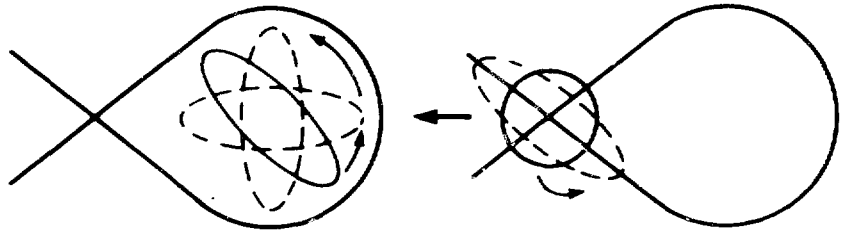

Fig. 12. Example of beam gymnastics — compression in phase or energy spread.

4.2. Constructional Errors — Field Errors

Various types of errors can occur: an error in the longitudinal position of drift tubes changes slightly not only the phase of particle crossing but also voltage amplitude; in a long cavity, one may observe a field modulation caused by slight mechanical imperfections (tilt ...). With errors of the first type, usually a synchronous particle no longer exists. As will be justified in Chap. 5, however, one may say that a modified gap behaves as a

perturbed "longitudinal lens." This error may, as it requires a higher acceptance, entail a loss of particles. In most cases, however, the effect is hardly visible. Even the temporary absence of stability is not necessarily fatal, as can be seen in the beam gymnastics operation described above. Needless to say, a more detailed computation is necessary to elaborate on specific considerations.

The case of a field modulation may result from the presence of parasitic modes. Even though it may be small, it is not certain that such an unwanted modulation does not prevent the existence of a synchronous particle, with small and slow enough phase oscillations not to break any adiabaticity criterion.

In some cases, one may also come back to the Fourier analysis to obtain synchronous waves. A modulation may then appear as the addition to the fundamental wave of satellites of nearby velocity; their amplitude is, however, usually too small to trap particles. It may, however, be large enough to affect the stability on the fundamental. In this case, too, sufficient knowledge requires detailed computation. If the amplitude of the satellites is large enough to capture particles and if stability areas of the various waves overlap, one may observe a "chaotic" phenomenon: with only very slight changes in initial conditions particles may be trapped by one wave or another.

In Chap. 5 will be described how relatively simple codes can be written to treat all possible configurations. If such a method is accurate, however, it still may not lead to a clear understanding of the conditions of stability. These conditions, as described in the present chapter, remain useful as a general reference guide.

CHAPTER 3

FOCUSING IN LINACS

Earnshaw's theorem shows that it is impossible to have, for the motion of particles in the accelerating wave of a linac, both phase stability for the longitudinal motion and focusing for the transverse motion [MacMillan]. The first proposal to overcome this difficulty used thin foils, which were unsuccessful; subsequently, grids were used.

Since the advent of alternating gradient focusing [Blewett], quadropoles have been generally used. Other methods discovered to provide focusing for the transverse motion include alternating phase focusing (APF) and radio-frequency quadrupole (RFQ) focusing; the latter is now widely used. The principles and limitations of these various types of focusing will be surveyed in this chapter.

1. IMPOSSIBILITY OF SIMULTANEOUS LONGITUDINAL AND TRANSVERSE STABILITIES

Phase stability requires that particles cross accelerating gaps when the rf field is *rising*. Figure 1 shows a typical electric field line distribution in such a gap: if accelerating, the field is focusing at input and defocusing at output. If the field level is increasing while particles cross the gap, the defocusing effect is larger. (One must notice that in a purely electrostatic system, the overall effect is focusing, but the effect arising from the change in field level with time strongly overcomes this electrostatic focusing strength.)

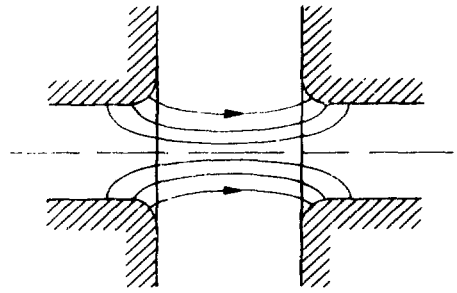

Fig. 1. Focusing and defocusing effects at the input and output of a gap.

This incompatibility property is very general [MacMillan] and cannot be avoided by a proper shaping of the circular hole entrances of drift tubes. It was shown in Chap. 2 that in order to study phase stability, it was appropriate to select, in the series of waves representing the field, that wave which propagates at the average particle velocity and which captures particles. Instead of considering this wave in the laboratory frame, one may then choose a frame moving at the synchronous velocity; the wave then becomes electrostatic.

If the effect of the beam charges is neglected, the field in this frame must satisfy the Laplace equation and the potential has no extremum except on boundaries where charges lie. If one then has phase stability, the potential must present a saddle, and there is transverse instability, and vice versa. Because

$$\frac{\partial E_x}{\partial x} + \frac{\partial E_y}{\partial y} + \frac{\partial E_z}{\partial z} = 0 \ , \tag{1}$$

then if

$$\frac{\partial E_z}{\partial z} < 0 \qquad \text{(phase stability)} \ ,$$

one has

$$\frac{\partial E_x}{\partial x} = \frac{\partial E_y}{\partial y} > 0 \qquad \text{(focusing)} \ .$$

The effect of the beam charges can only worsen the situation; this will be studied in Chap. 6.

2. FOIL AND GRID FOCUSING

Foils are put at the entrance of each drift-tube hole to close them (Fig. 2). Defocusing is then suppressed, leaving the focusing effect at gap entrances.

This method does not contradict the previous incompatibility proof because when field lines stop on the foil, they develop charges there. On that side of the interval, their sign produces an attractive potential such that there may be stability in all directions. (Put at the gap entrance, the foils would have a defocusing effect.)

In practice, the thin foils (thin enough not to degrade the energy nor to cause too much loss) were very quickly destroyed by electric breakdown (which cannot be avoided during conditioning) and their use had to be abandoned. Therefore, foils were replaced by grids, which were a large-scale replica of the foil lattice. To insure good cooling, these grids were often strips in a cross-shaped arrangement that were parallel to the beam (see Fig. 7 of Chap. 1). In the case of aligned crosses, the space offered to the beam would be divided into four parts; each part is unstable by itself and stability requires that particles from transverse oscillations jump from one hole to another.

Obviously such a device cannot avoid particle loss. Furthermore, one may guess that such thick grids are not aberration free so beam quality cannot be very good.

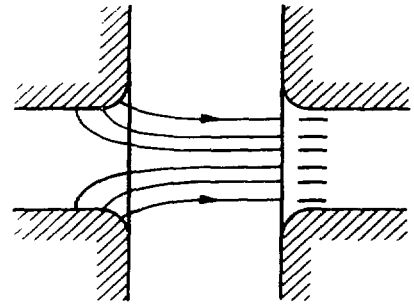

Fig. 2. Foil or grid focusing—the defocusing effect is suppressed.

3. EXTERNAL ALTERNATING GRADIENT FOCUSING [Blewett]

The first tests of AG focusing with electrostatic quadrupoles were made in Berkeley in 1952. The method became operational, in its magnetic version, in 1959 at CERN and in 1960 at Brookhaven.

3.1 Principle of AG Focusing in Linacs [Teng] - [Smith et al.]

Phase stability results from the choice of synchronous phase ϕ_s. From Eq. (21) of Chap. 2, one easily obtains the phase advance of longitudinal oscillations per rf period (2π mode Alvarez structure),

$$\sigma_\ell = 2\pi \frac{\lambda_0 \beta_s}{\Lambda} = \sqrt{\frac{2\pi e E T |\sin \phi_s| \lambda_0}{m_0 c^2 \beta_s \gamma_s^3}} \quad , \tag{2}$$

which can also be written

$$\sigma_\ell = \pi \sqrt{\frac{\Delta W_s}{W_s} \left| \frac{\tan \phi_s}{\pi} \right|} \quad , \tag{3}$$

where ΔW_s is the synchronous energy gain per rf period (Alvarez drift tube), and W_s is the synchronous energy. Usually $\phi_s \sim 30°$, then

$$\sigma_\ell \sim 0.4\pi \sqrt{\frac{\Delta W_s}{W_s}} \quad . \tag{4}$$

(One may notice that if ϕ_s were raised to 75°, σ_ℓ would be multiplied by 2.5; the energy gain, however, would be divided by almost 3).

Because at injection $\Delta W_s / W_s < 0.15$ and goes down afterwards, during the first phase oscillation the average value of σ_ℓ is

$$\sigma_\ell \gtrsim 0.1\pi \quad . \tag{5}$$

Stability conditions for an AG system have been derived by several authors [Courant et al.] and also [Laslett], but we shall use Bruck's results [Bruck, p. 72] and in particular the "necktie diagram" presented there (Fig. 3). In his derivation, Bruck introduces for each section, focusing or defocusing, an action term P or Q proportional to the integral of the force gradient (positive or negative) acting on the particles. In the longitudinal direction (phase stability), one has

$$P_z = (\sigma_\ell / \pi)^2 = -\frac{\Delta W_s \tan \phi_s}{\pi W_s} \quad . \tag{6}$$

The resulting transverse defocusing in x and y is, from the divergence property, assuming a circular symmetry,

$$P_x = P_y = -P_z/2 \quad . \tag{7}$$

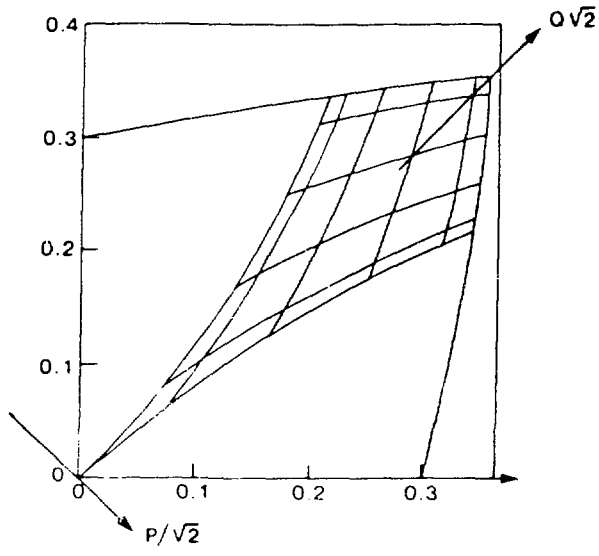

Fig. 3. Necktie diagram. For linac application, it will have to be rotated 45°.

In drift tubes, magnetic quadrupoles will add $\pm Q$ (we shall here first assume, to follow Bruck, that the filling factor of these quadrupoles is 100%, as if they were extended to the gaps, but we shall come back to this point later).

With a gradient $B' = \partial B_x/\partial y$ or $\partial B_y/\partial x$ and for a sign reversing at each drift tube ($+-+-$ focusing mode), in an Alvarez structure operated in the 2π mode (period $\lambda_0\beta_s$ per drift tube) one has

$$Q = \frac{eB'(\lambda_0\beta_s)^2}{\pi^2 m_0 c\beta_s} \quad . \tag{8}$$

(One must notice that for a $++--$ focusing mode, with sign reversing every other drift tube only, Q_2 would be multiplied by 4 and not 2, $Q_2 = 4Q_1$ and by n^2 for a reversal every n^{th} drift tube only. The same remark applies to P with $\sigma_{\ell,n} = n\sigma_\ell$).

Through a complete focusing period one has, then, in the transverse direction, the successive actions

$$Q - P/2 \quad \text{and} \quad -Q - P/2 \quad .$$

In the necktie diagram, the operating point is therefore never on the diagonal. One may obtain a diagram in $P/\sqrt{2}$ and $Q\sqrt{2}$ by a 45° rotation of the classical necktie. Figure 4, obtained by such a rotation, gives $\sigma_x = \sigma_y$ as a function of P and Q.

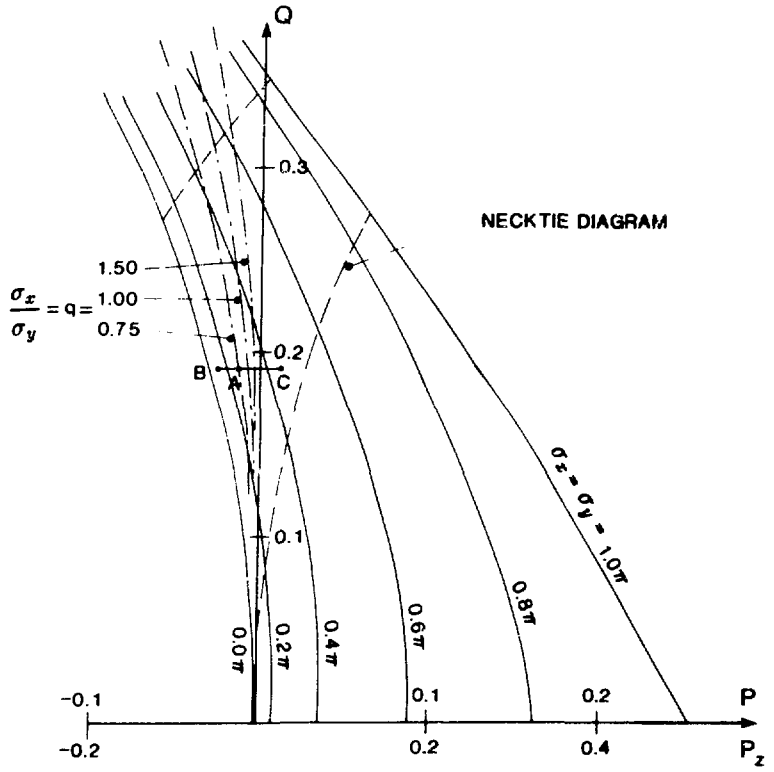

Fig. 4. Stability diagram.

For a $+ - + -$ focusing in which $\sigma_z = 2\sigma_\ell$,

$$\sigma_z = 2\pi\sqrt{P} \quad , \tag{9}$$

and Fig. 4 gives the values of

$$q = \sigma_x/\sigma_z \quad . \tag{10}$$

It is possible to compute the β function (form factor of the focusing envelope). As can be expected, $\beta_{\max}/\beta_{\min}$ increases for operating points closest to the stability limits. A similar computation can be performed for the actual filling factor of the quadrupoles (usually of the order of 1/2). Results remain very similar if one uses for Q the same gradient integral per quadrupole (equal power lens); there is, however, some increase of $\beta_{\max}/\beta_{\min}$. For a $+ + - -$ focusing mode, the previous diagram applies ($P_2 = 4P_1$). The

required value of Q_2 is then not much higher than Q_1, and the required gradients are smaller. Nevertheless, β_{max}/β_{min} increases.

3.2 Discussion

Point A of Fig. 4 is a typical operating point. The gradient required at low energy is high. Therefore, early machines used $++--$ focusing mode, at least at the beginning of acceleration. In fact, A corresponds to synchronous particles. For non-synchronous particles, which oscillate in phase, the local value of the defocusing action P is such that

$$P/2 = -\frac{\Delta W_s \sin \phi}{2\pi W_s \cos \phi_s} \quad , \tag{11}$$

where ϕ is the actual phase value; around A one may then have oscillations between B and C (separatrix). This phenomenon produces a coupling between longitudinal and transverse motions; a detailed computation [Hereward et al.] has, however, shown that this effect was not important except in the case of the resonance

$$q = \sigma_x/\sigma_z = 0.5 \quad ,$$

which must be avoided.

In practice, $q \approx 1$ (ranging from 0.75 to 1.5 or even more) and $\sigma_x \lesssim \pi/3$ (one always takes $\sigma_x < \pi/2$, see Chap. 6).

3.3 Remark

Transverse oscillations are governed by a Hill's equation of Mathieu's type,

$$y'' + (a - 2q \cos 2z)y = 0 \quad ,$$

where a would represent the $-P/2$ term and $2q$ represents Q, with a sinusoidal variation instead of a square shape.

Stability conditions for Mathieu's equation can be found in mathematics books [Abramowitz et al., p. 724]. Figure 5 shows the graph from Angot [Angot, p. 471]

and the central portion is enlarged in Fig. 6. One can recognize, by permuting the axes, the diagram of Fig. 4.

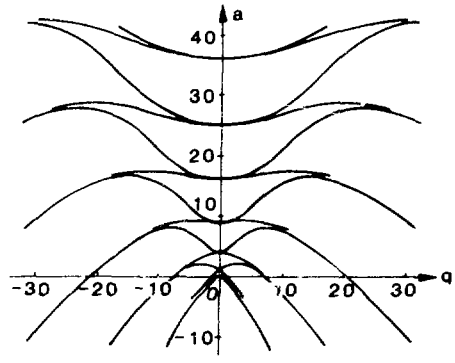

Fig. 5. Mathieu's stability diagram.

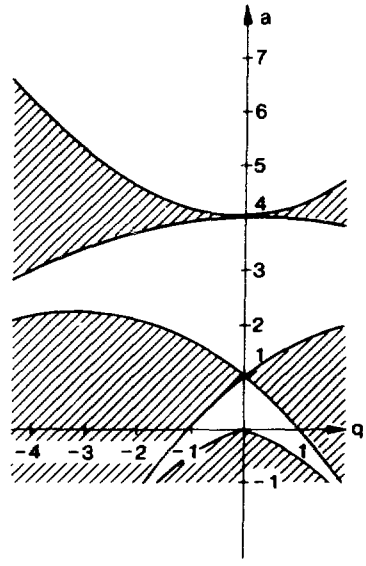

Fig. 6. Enlarged Mathieu's diagram rotated by 90°. It is very similar to Fig. 4.

3.4 Conclusions

Magnetic AG focusing, though complicated from a technological point of view, is extremely efficient for Alvarez-type linacs, the only linac used at medium energies.

For interdigital or H-type structures at low energy, one often replaces magnetic quadrupoles with electrostatic ones. Later the possibilities offered by RFQs will be shown.

For high energy, focusing is easier to achieve; it is normally made by separated quadrupoles, between accelerating cavities.

4. ALTERNATING PHASE FOCUSING

The APF principle, presented for the first time in 1953 by J. H. Adlam [Adlam] in an AERE* report and by Good [Good], was described again in the USSR by Fainberg [Fainberg] in 1956, but not tested til the 1970s in the USSR and at Los Alamos in the PIGMI project [Knapp et al.]. Several studies were devoted to this principle; the study results were presented at the Chalk River Linac Conference in 1976 by Swenson and also by Deitinghoff [Swenson] and [Deitinghoff et al.]. A detailed analysis has been made by [I. M. Kapchinskij].

The idea is to apply to longitudinal and transverse motions the AG focusing that is so successful for transverse directions. By changing the drift-tube lengths, it is possible to give to the average phase crossing ϕ_s of the particles alternatively a positive and a negative value.

In such a situation, the longitudinal action term P of Sec. 3.1 is no longer constant, but it may oscillate between $-P_1$ and $+ P_2$. Simultaneously, the transverse action will oscillate between $+ P_1/2$ and $- P_2/2$. Using the graph of Fig. 3 from Bruck, one may then obtain a diagram referring to this case (Fig. 7). The necktie is now unsymmetrical; and in order to have $q = \sigma_x/\sigma_z \approx 1$, one should choose $P_1 \neq P_2$.

According to the diagram, the P values should range from 0.15 to 0.25 (instead of ≈ 0.01 for $\phi_s = 30°$ with a reversal every drift tube).

* Atomic Energy Research Establishment, Harwell, Great Britain.

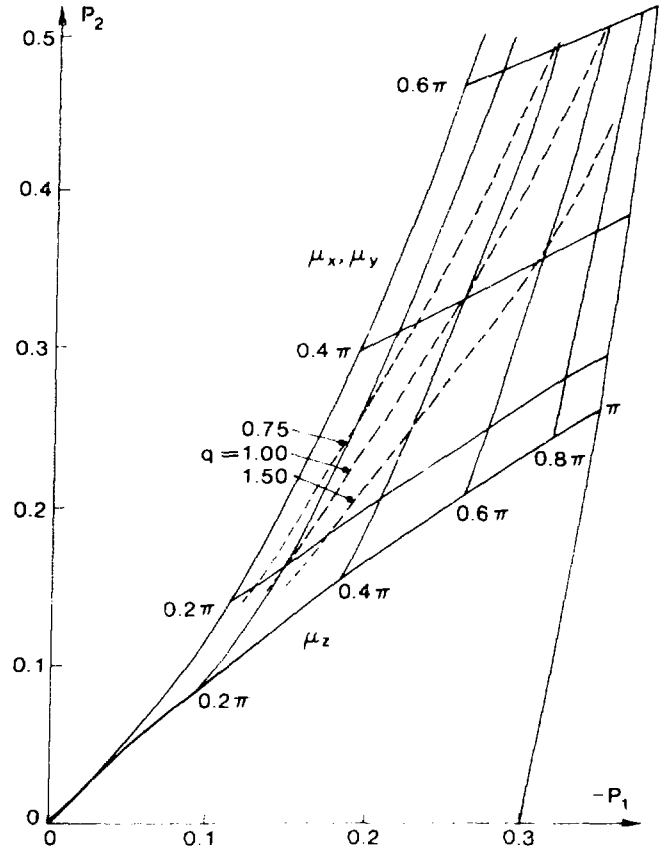

Fig. 7. Stability diagram for APF focusing.

One is then led to increase the field and to reverse phase only every 3 or 4 drift tubes, or at the very least 2, if ϕ_s is also increased as well as E_z.

Whatever one does, the focusing period is always very much longer than with quadrupole lenses, perhaps by as much as a factor of 4; the focusing is much weaker (by a factor of 10 to 20) in the transverse as well as in the longitudinal direction. With external focusing lenses, one had $Q \gg P$; here P_1 and P_2 are both limited.

The phase acceptance may nevertheless be reasonable (up to a total of 40° to 60°).

Alternating phase focusing is an extremely simple method, but unfortunately it is not very efficient. It could not be used for high intensity (a few tens of mA and probably less in a small emittance).

5. RADIO-FREQUENCY QUADRUPOLE FOCUSING

5.1 Initial Proposal — Finger Tips

This proposal was made by V. Vladimirskij in 1956 [Vladimirskij]. The idea was to put on each drift-tube face two diametrically opposed finger tips with alternate rectangular directions in order to produce a transverse quadrupolar field (Fig. 8) in the gaps.

This quadrupolar field is rf, but always has the same sign when particles cross the gap around synchronous phase. Alternating the polarity in successive gaps produces AG focusing. This device was experimentally studied in detail by D. Boussard in Orsay in 1965 and by Maltsev and Teplyakov, in particular, with a view toward a possible application for low-energy heavy ions [Boussard], [Maltsev et al.]

The focusing is efficient, but electric fields on the tips can have high levels; in order to avoid sparking, acceleration must be slow.

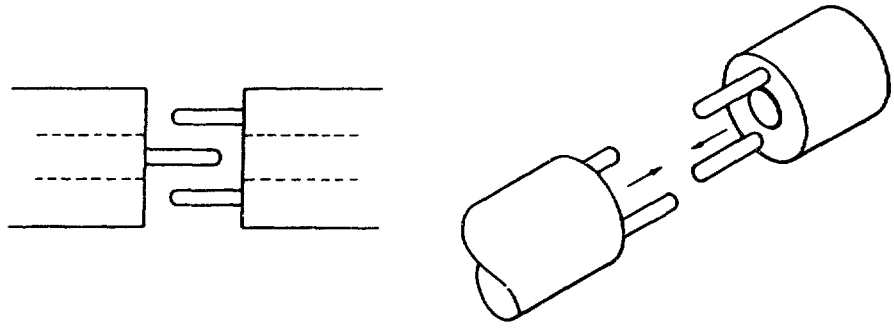

Fig. 8. Finger focusing.

5.2 Second Proposal — Match Boxes

The match box shape was proposed in 1963 by I. M. Kapchinskij and P. Lapostolle [Anisimov et al.] and [Lapostolle et al.]; the idea is to replace the circular shape of drift tubes, or at least the beam hole, by a rectangular shape of alternate orientation (Fig. 9: each tube might be like a "match box").

As shown in the figure, the transverse divergence of the field takes place only in one transverse direction x or y at each end of the gap and is inverted from input to output. There is no longer overcompensation by output as there was with circular holes (Fig. 1), but there is a quadrupolar effect.

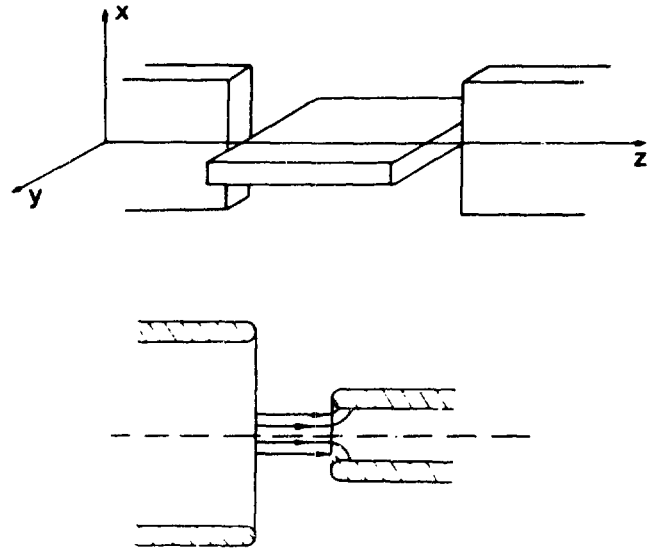

Fig. 9. Match box focusing.

At the input, for instance, the focusing effect can be approximated from the relations

$$-e\int \frac{E_x}{x}dz \simeq -e\int \frac{\partial E_x}{\partial x}dz = e\int \frac{\partial E_z}{\partial z}dz = eE_g \quad , \tag{12}$$

where E_g is the accelerating field in the gap at the time of input, supposedly fast. At output, there is a larger defocusing effect, but in the y direction.

As can be seen, there is an advantage to having a high accelerating field, i.e., for a given voltage, short gaps. One is again limited by breakdown risks. Computation shows that this simple device is satisfactory, but only at very low energy. Of course, the device can be applied (as the finger tips) not only to Alvarez-type structures (2π mode), but also to Wideröe, interdigital, or H-type structures (π mode).

5.3 Present RFQ

In the previous structure, when operated in the π mode, one can omit from the boxes the farther sides and make the closer sides round, in the form of bars; each pair of opposite bars can then successively be connected to the terminals of an rf voltage source (Fig. 10).

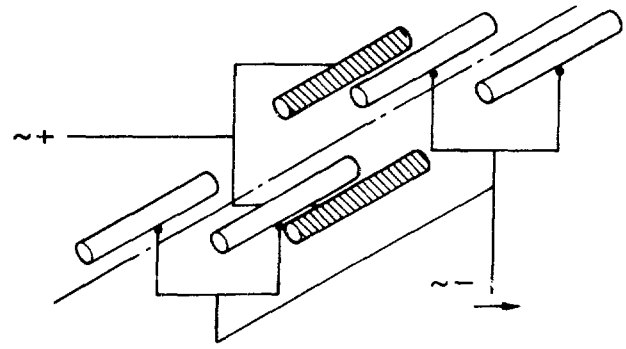

Fig. 10. Bar focusing.

Such a device was developed by H. Klein in Frankfurt, then modified and improved by R. Müller in Darmstadt (Germany) [Müller] and [Klein et al.].

Bars of equal potential can still be joined by a conductor further away from the axis, with an equipotential boundary of quasi-sinusoidal shape, of opposite phase in the two planes of bars. All these bars can be put in an rf cavity divided into four sections (Fig. 11). This is the most common configuration for RFQ structures. The original idea of Kapchinskij and Teplyakov in 1970 [Kapchinskij et al.] emerged in 1979 into real devices tested in Los Alamos and Moscow [Kapchinskij et al.], [Swenson], [Potter et al.], and [Stokes et al.].

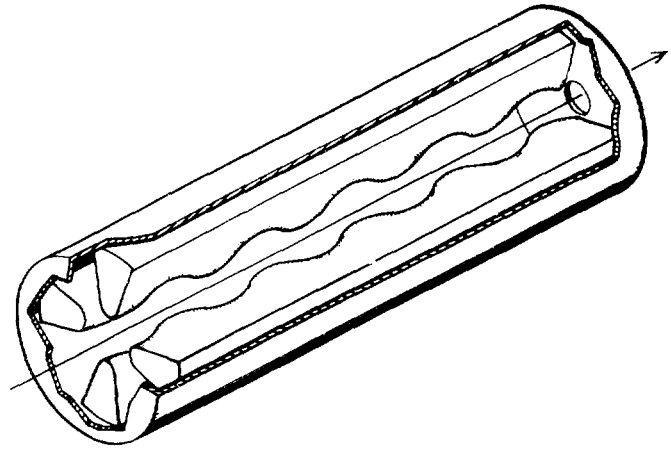

Fig. 11. Classical RFQ device.

In the classic RFQ structure there is a superposition of two fields or waves: a standing accelerating wave of amplitude AV (the sum of two traveling waves with opposite velocity) and an rf quadrupolar field independent of z of amplitude XV. The total field has the form

$$\left.\begin{aligned} E_r &= \frac{-XV}{a^2} r \cos 2\psi - \frac{kAV}{2} I_1(kr) \cos kz \\ E_\psi &= \frac{XV}{a^2} r \sin 2\psi \\ E_z &= \frac{kAV}{2} I_0(kr) \sin kz \end{aligned}\right\} \times \sin(\omega t + \phi) \quad . \tag{13}$$

Bar or pole profiles are shaped to fit the boundary conditions of this field.

Such a device has proved to be extremely efficient, even at high intensity for very low energies. It is used to produce transverse matching of the beam, progressive bunching (adiabatic), and acceleration. Beam efficiency can be close to 100% for intensities in the range of 100 mA. This device increasingly is replacing previous electrostatic injectors and bunching cavities.

6. REMARK ON THE POSSIBILITY OF SIMULTANEOUS STABILITY IN LONGITUDINAL AND TRANSVERSE DIRECTIONS

6.1 Alternate Focusing Effect

Looking at a field as given by Eq. (13) in a frame moving at the velocity v of the synchronous wave, the forward component of the accelerating field becomes electrostatic, while the quadrupolar field is oscillating (in addition to the static part of the accelerating wave).

If the frequency variation of the focusing is very fast, there is obviously hardly any effect; if it is too slow, the situation may become unstable. There is, however, a range of frequencies in which the global effect is focusing. This is the basic principle of AG focusing, which can be presented as resulting from the focusing effect of a two-lens system:

$$\frac{1}{F} = \frac{1}{f_1} + \frac{1}{f_2} - \frac{d}{f_1 f_2} \quad . \tag{14}$$

For $f_2 = -f_1$ (equal and opposite focal lengths of the two lenses), thanks to the third term the global focusing effect can be significant if the distance d between the lenses is convenient.

It is also possible, considering the shape of a trajectory crossing a succession of focusing and defocusing lenses (Fig. 12), to notice that the axial distance of the crossing points in the focusing lenses is, on the average, always larger than in defocusing ones. It is indeed the same property that appears in the betatron function β, which is maximal in focusing sectors and minimal in defocusing ones.

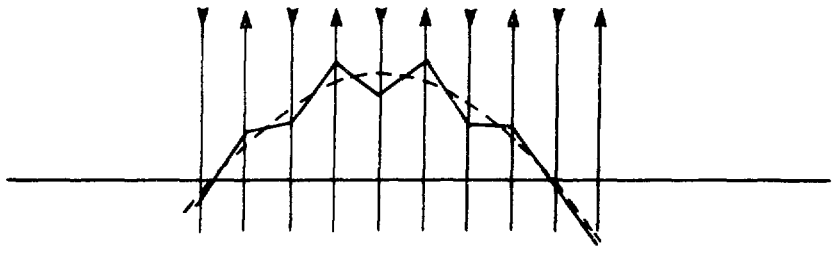

Fig. 12. AG focusing effect.

6.2 Comparison Between APF and RFQ Principles

AG focusing, if made in two or three directions (the Laplace equation forbids it to be done in only one), may provide stability in all three directions. In the APF system, there is AG focusing in z and in r (circular symmetry in x and y). In the RFQ device, there is AG focusing in x and y and smooth focusing in z.

6.3 Fast Wave Focusing

Instead of using, as in the RFQ, an accelerating wave and a quadrupole rf field that is stationary in the laboratory frame or, as in the APF, a stationary phase modulation of the accelerating wave, one might superimpose two longitudinal waves of different velocities. One of them, in phase with the beam, is then accelerating; the other, which may have a different amplitude and which oscillates in phase with respect to the beam because its phase velocity is different, provides stability both transversely and longitudinally.

Such a device, invented in the USSR [Baev et al.] and named FWF (fast wave focusing) has not shown yet its real potential.

CHAPTER 4

RF STRUCTURES FOR LINACS

A good accelerating structure should exhibit a large accelerating field with limited rf power and good stability. This assumes that for a given accelerating field, the electromagnetic (EM) field distribution is such that the peak electric field has been minimized to avoid breakdown risks, and currents in the wall have been minimized to reduce losses. This also assumes a structure that is not very sensitive to perturbations, both intrinsic (beam loading, transient phenomena during cavity filling) and extrinsic (mechanical imperfections, distortions resulting from temperature, etc.). Finally, and somewhat contradictorily to this last requirement, one may wish for a structure that is flexible enough to be used in different operating conditions (with other particles, other modes, etc.).

These electrical requirements have, of course, an impact on mechanical fabrication problems: value of tolerances, possibility of adjustments, cooling and temperature control, etc., and solving these problems/meeting these conditions at minimum cost.

1. QUALITIES OF A STRUCTURE FOR ACCELERATION

1.1 Shunt Impedance Z_s

Let us consider an EM resonant cavity with standing waves. The accelerating peak electric field E_z on the axis is, for instance, as shown in Fig. 1 [Alvarez et al.].

Fig. 1. Typical axial field distribution.

One may compute an average field over the cavity length L or an integral number of periods,

$$\overline{E_z} = \frac{1}{L}\int_0^L E_z\, dz \quad ,$$

or the Fourier component of the synchronous accelerating wave,

$$\overline{E_z}\, T \quad . \qquad (T \text{ is the transit time factor, see Chaps. 2 and 5.})$$

The shunt impedance, nominal or effective, is defined as

$$Z_s = \frac{\overline{E_z}^2}{P} \quad \text{or} \quad Z_{s,e} = \frac{(\overline{E_z}T)^2}{P} \quad , \tag{1}$$

where P represents the rf power losses in the walls per unit length of the structure. (Such quantities may, of course, change along a long cavity, and one can define a local and an overall value.) The terms Z_s and $Z_{s,e}$ are usually expressed in megohms per meter.

One may notice that, for a structure of length L, the total shunt impedance

$$(Z_{s,e}) = L \cdot Z_{s,e} \tag{2}$$

is such that the total power $(P) = L \cdot P$ can offer a total accelerating voltage (V) to the particles:

$$(V) = \sqrt{(P) \cdot (Z_{s,e})} = L \cdot \sqrt{P \cdot Z_{s,e}} = L \cdot V \quad , \tag{3}$$

i.e., L times the voltage per meter.

1.2. Quality Factor Q

By definition, the quality factor Q is 2π times the ratio of the EM stored energy W_s in the cavity to the joule losses in the walls during an rf period.

1.3. Field Measurements — Bead Perturbation Method

From previous definitions one has

$$\omega Z_s/Q \propto \overline{E}^2/W_s \quad .$$

Now one may measure locally the ratio of the square of the electric field (or magnetic field) to the stored energy. This fact results from Slater's perturbation method [Slater]. At resonance, in an EM cavity, there is a continuous interchange between electric and magnetic energies such that their peak values must be equal. Any modification in one of them entails a change in frequency to restore equilibrium (with some analogy to what happens in an LC circuit where the capacitance or the inductance would be changed). A metallic ball or bead on the axis of a cavity (where the magnetic field is normally negligible) modifies the electric energy (by forcing the field out) and changes the frequency. If such a bead is moved along the axis, one gets a measurement of the field distribution and, by a proper standardization, Z_s/Q. Such a method is currently used for the initial adjustment of cavities.

Away from the axis, the introduction of metallic (or dielectric) balls can be used as a way to change the resonant frequency. If the ball is put in a region where the electric field or magnetic field dominates, the change in frequency will be of a different sign; in a transition region, there is no net effect.

1.4 Traveling Wave Cavity — Attenuation

At a power [P] circulating along a cavity, there is a corresponding accelerating field $\overline{E_z}$ on the axis. Because of wall losses, the circulating power decreases and the amplitude of the field also decreases exponentially along the cavity:

$$\overline{E_z}(z) = \overline{E_z}(0)e^{-Az} \quad . \tag{4}$$

Circulating power absorbed in the walls decreases as $\overline{E_z^2}$. Then

$$[P] = \overline{E_z^2}/2AZ_s \quad . \tag{5}$$

2. DISPERSION CURVE — CAVITY AND STRUCTURE MODES

2.1 Dispersion Curve

In a lossless waveguide, the field on the axis z of a given mode is given as a function of z and t by

$$E(z,t) = E(0,0)e^{j(\omega t - k_z z)} \tag{6}$$

with

$$k_z = \omega / v_\phi \quad , \tag{7}$$

where v_ϕ is the phase velocity. In a periodic structure used as an accelerating structure, by corresponding points separated by a multiple of the period, considering periodic points, it is still possible to define a v_ϕ and hence a k_z.

In the frequency band in which a given mode exists, there is a relation between k_z and angular frequency ω. On the dispersion curve (Fig. 2) expressing this relation, the slope of OM is the phase velocity v_ϕ. The slope of the tangent at M is the group velocity v_g, that is, the velocity of a wave packet of frequencies close to ω corresponding to M.

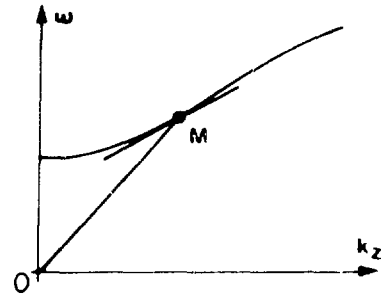

Fig. 2. Dispersion curve. Phase and group velocities.

Let us consider the sum of two waves around M. One has

$$\begin{aligned} &\cos[\overline{(\omega - \Delta\omega)}\, t - \overline{(k_z - \Delta k_z)}\, z] \;+\; \cos\,[\overline{(\omega + \Delta\omega)}\, t - \overline{(k_z + \Delta k_z)} z] \\ &\qquad = 2\,\cos\,(\omega t - k_z z)\,\cos\,(\Delta\omega t - \Delta k_z z) \quad . \end{aligned} \tag{8}$$

In this expression, the first term expresses the propagation at phase velocity v_ϕ (Eq. 7); the second term represents the amplitude, which moves at group velocity

$$v_g = \Delta\omega/\Delta k_z \quad . \tag{9}$$

In some way, this velocity can be considered as the velocity of energy propagation and as the velocity of transients.

2.2 Cavity Mode — Structure Mode

In a resonant cavity, the length L of the structure must be such that

$$k_z L = N\pi \quad , \tag{10}$$

with $N = 0$ or an integer; N denotes the *cavity mode.*

In most cases, boundary conditions are made such that $N = 0$ is possible; then the field amplitude is constant. For $N \neq 0$, there are standing waves with a sinusoidal variation of the field. This configuration can be considered as a non-optimum use of the structure, in which some portions are not (or are barely) accelerating.

In an Alvarez structure, which is normally used in the zero mode, if the frequency is increased slightly, modes N =1, 2, ... are excited.

In a traveling wave operation, the relation in Eq. (10) does not have to be satisfied, and there is no advantage to having $N = 0$; in fact, as will be seen later, it is better to have $N \neq 0$.

In a periodic structure of period p, $k_z p$ is the structure mode. For the beam, this mode can take values

$$k_z p + 2h\pi \qquad (h = 0 \text{ or integer}) \quad ,$$

or, when the field is reversed in successive gaps,

$$k_z p + 2h\pi + \pi \quad .$$

As was already mentioned in Chap. 2, because of the value of the transit time factor T, only one or two such beam modes can be used:

2π or 4π (Alvarez)

π(or 3π?) (interdigital or H structure).

3. TRANSIENTS, BEAM LOADING, SENSITIVITY TO PERTURBATIONS OR IMPERFECTIONS

3.1 Transients and Beam Loading

In the pass band of a mode, the dispersion curve is usually as shown in Fig. 3. There, simply because of the periodicity, the slope is 0 for the zero and π structure modes. For the zero mode, which also corresponds to $N = 0$, one then has $v_g = 0$.

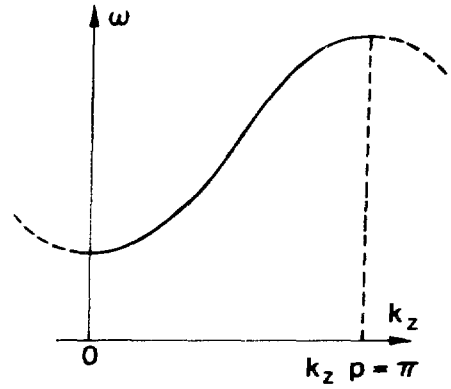

Fig. 3. Zero and π modes.

In such conditions, cavity filling is slow. A computation based on the telegrapher's equation (see Sec. 8 of this chapter for more details) shows that the field penetration in a *long* structure is proportional to $c/\sqrt{Q}$. It is only through the phase shift caused by losses (as will be seen later) and maybe with the help of higher order modes (particularly in the case of very low losses) that energy can propagate.

In a similar way, when the beam suddenly absorbs stored energy from the cavity, refilling will take some time, during which the field distribution is modified in amplitude and phase.

3.2 Sensitivity to Mechanical Imperfections and Perturbations

Another drawback of structures operated in the zero mode is their great sensitivity to geometrical errors, which can induce large field perturbations. In order to describe such

an effect, let us consider the simple case of a circular waveguide cavity where there is a field modulation resulting from the existence of two modes:

$$\mathrm{TM}_{010} + a\ \mathrm{TM}_{011} \qquad (\text{with } a < 1)\ ;$$

the two modes having simultaneously *the same frequency* with, according to usual notation, $N = 0$ for the first mode, assumed to be amplitude 1, and $N = 1$ for the second mode of amplitude a.

At the two ends, the field on the axis will be (Fig. 4):

$$1 \pm a\ .$$

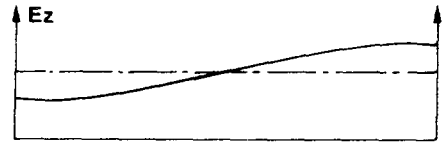

Fig. 4. Field modulation or tilt of a cavity.

The radial field distribution is governed, for these circularly symmetric modes, by the Bessel function J_0 in such a way that, in order that the E_z field be 0 on the lateral wall of the cavity, one must have at each end

$$J_0(k_{r0}\ r)\ \pm\ a\ J_0(k_{r1}\ r) = 0\ , \tag{11}$$

where k_{r0} and k_{r1} refer to modes 0 and 1 with

$$k_{r0}^2 - k_{r1}^2 = (\pi/L)^2\ . \tag{12}$$

This condition assumes a slightly "conical" cavity. The diameter must be larger (the local resonant frequency lower) at the end where the field is higher.

The problem treated here would correspond in actuality to a sinusoidal diameter modulation (and variation of local resonant frequencies). For a linear variation, the result, however, is similar.

Then, for a frequency perturbation $\delta\omega$, there is a field modulation δE with

$$\frac{\delta E}{E} = -\frac{1}{S}\frac{\delta(\omega^2)}{\omega^2} \quad . \tag{13}$$

The quantity S is a sensitivity factor such that

$$S \propto (\omega_1 - \omega_0)/\omega_0 \quad , \tag{14}$$

where ω_0 and ω_1 refer to 0 and 1 modes of the unperturbed cavity.

Then, for a zero mode cavity,

$$S \approx 2(c/\omega L)^2/\varepsilon\mu \tag{15}$$

(ε and μ are relative values); outside the zero mode, if $v_g \neq 0$,

$$S \approx 2(v_g/\omega L) \quad . \tag{16}$$

For most cavities, for which $\omega L \gg c$ and $0.1c < v_g < c$, one sees that cavities with the nonzero 0 mode are much less sensitive to mechanical imperfections.

As observed in Fig. 3, v_g is normally maximal near the $\pi/2$ mode. Unfortunately for such a mode, every other gap is a node where the field is zero. Acceleration is only half what it could be in the zero mode. (In fact, in a 0, π, ... mode, acceleration is provided by both forward and backward waves; this explains the factor 2 with the operation in $\pi/2$ mode).

4. VARIOUS TYPES OF STRUCTURES

4.1 Alvarez Structure [Alvarez et al.]

The Alvarez structure is schematically shown in Fig. 5, with its drift tubes of tapered length in a TM_{010} circular cavity. Most such structures operate at 200 MHz. The shunt impedance is high–$Z_{s,e} \sim 40$ MΩ/m for $0.03 < \beta < 0.5$. Zero mode operation makes this structure not very satisfactory for transients and from "sensitivity" points of view.

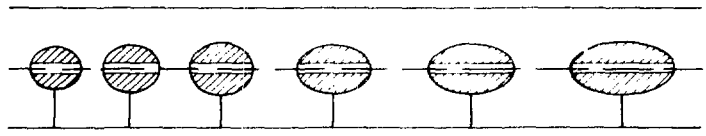

Fig. 5. Alvarez structure.

4.2 Interdigital or H-Type Structures [Sloan et al.][Zeidlitz]

Several different designs follow the same principle (see, for instance, the Sloan and Lawrence device [Nassibian et al.] mentioned in Chap. 1 (Sec. 1.3)). Figure 6a [Kaspar], [Moretti et al.] and [Watson et al.] and Fig. 6b [Nolte et al.] and [Fukushima et al.] only give a sketch of the main structures.

The cavity, operated in a TE mode, is accelerating because of the drift tubes, which exhibit a π mode for the beam (sometimes π–3π or even π–5π, see Fig. 6c). With an open-end-type boundary, the cavity can be operated in the zero mode. The shunt impedance is very high for this structure at frequencies ranging from 20 to 100 MHz and for $\beta < 0.05$.

a

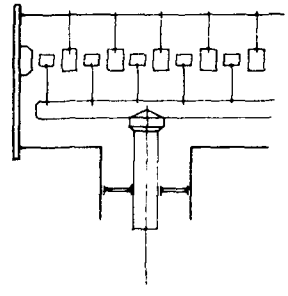

Fig. 6a. Sloan-Lawrence interdigital structures for medium energies.

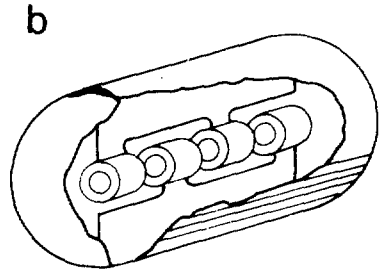

Fig. 6b. H-Type Structure.

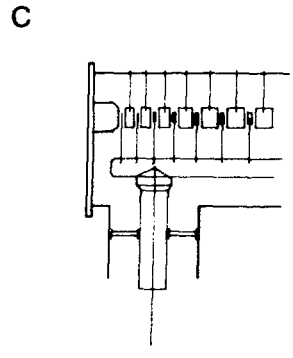

Fig. 6c. Low-energy interdigital structure.

4.3 Iris-Loaded Waveguide

The iris-loaded waveguide is a TM-excited circular waveguide where the phase velocity is reduced by iris loading (Fig. 7). This structure is normally used for electron acceleration with $\beta \approx 1$ in a $\pi/2$ or $2\pi/3$ structure mode, in a traveling wave, at a frequency of the order of 3 GHz (see Chap. 7).

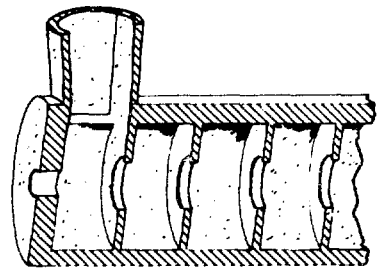

Fig. 7. Iris-loaded structure.

4.4 Side-Coupled Cavity Structure [Knapp et al.]

In the side-coupled cavity structure type of iris-loaded waveguide, small drift tubes in the irises prevent direct coupling from cell to cell. Coupling is then provided laterally through resonant cavities alternating diametrically (Fig. 8). From a field propagation point of view, these coupling cavities play a role similar to the accelerating ones. If they are considered as periods, the structure is operated in the $\pi/2$ mode. For accelerating cells, however, the phase shift is π (π-beam mode, except if through phase reversal in the geometry of the coupling, it is made 2π).

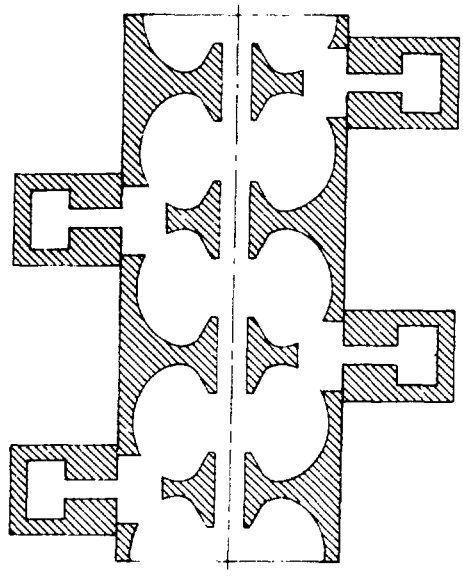

Fig. 8. Side-coupled cavity structure.

In standing-wave operation, only the accelerating cells are excited, and the field is weak in the coupling cells. The shunt impedance is high for $0.5 < \beta < 1$. The group velocity is high.

5. FIELD STABILIZATION OR "COMPENSATION"

The aim of this device is to modify zero- or π-mode properties in such a way that the group velocity should not be zero (as in the structure described in Sec. 4.4).

5.1 Alvarez Structure with Post Couplers (Los Alamos) [Swenson et al.]

In an Alvarez structure at zero mode, stored electromagnetic energy oscillates transversely in such a way that coupling is weak between successive gaps. If resonant posts are placed facing the drift tubes, they will couple with the Alvarez mode, inducing some kind of lateral coupling between successive gaps (Fig. 9).

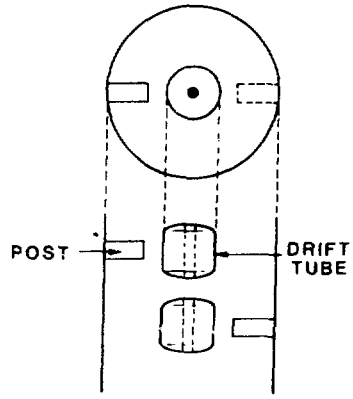

Fig. 9. Post-coupler compensation.

As in the side-coupled cavity structure, the group velocity is no longer 0 ($v_g \sim 0.1c$), especially if the posts alternate diametrically in position. Contrary to a normal side-coupled cavity structure, however, the Alvarez mode is still 0 (this could also be achieved with a side-coupled device). One may also consider that two modes are interacting on the same 0-mode frequency as will now be seen.

5.2 Coupled Mode Theory; Mode $\neq 0$ [Watkins] and [Vassallo]

Let us first consider a structure for which, at a given frequency, two modes may coexist for which the dispersion curves cross (Fig. 10). Let us assume, in addition, that the field distribution in these modes allows some coupling. For a frequency ω_0, the two modes will then have the same k_0 ($k_0 p \neq 0, \pi, 2\pi$) and will then propagate at the same velocity and interact, one of them exciting the other or vice versa (we shall here, in contrast with common practice that makes use of circuit theory, take a mode approach).

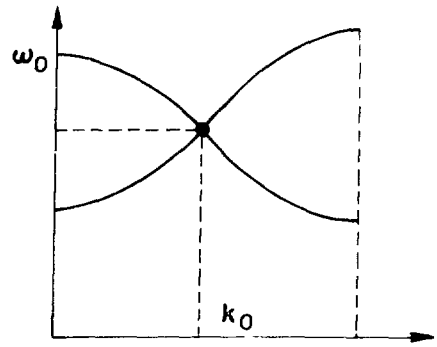

Fig. 10. Crossing of two uncoupled modes.

Let us consider each of the two modes independently first. Without coupling, and neglecting the losses, the amplitude of one of the modes is such that

$$X_{10} = C_1 e^{-ik_{10}z} \quad \text{with} \quad X'_{10} = -ik_{10}X_{10} \ , \tag{17}$$

and for the other mode

$$X_{20} = C_2 e^{-ik_{20}z} \quad \text{with} \quad X'_{20} = -ik_{20}X_{20} \ . \tag{18}$$

If the modes are coupled, Eqs. (17) and (18) are perturbed by the presence of the other mode. In the coupling zone, some amount α of the X_{20} mode 2 amplitude will add to the component X_{10} of the second half of Eq. (17). In a similar way, some fraction β of amplitude X_{10} will be subtracted from X_{20} of the second half of Eq. (18). (Of course, α and β are equal if modes are properly normalized.) These coupling coefficients α and β are frequency dependent, but in the small bandwidth considered, they may be assumed constant.

One may then write, instead of Eqs. (17) and (18):

$$\begin{cases} X_1' = -ik_{10}X_1 + i\alpha X_2 \\ X_2' = -ik_{20}X_2 - i\beta X_1 \end{cases} . \tag{19}$$

This set of equations can be solved by considering, for instance, that mode 1 of amplitude C_1 will excite, when propagating, the mode 2, whose amplitude will grow while C_1 diminishes. One may also try to seek couples of C_1 and C_2 modes for which the amplitudes remain constant (hybrid modes).

In case such hybrid modes exist, they will propagate at a different velocity with a new k. For each component of these hybrid modes one will have

$$X_1' = -ikX_1 \quad , \qquad X_2' = -ikX_2 \quad . \tag{20}$$

Hence, from Eq. (19)

$$\begin{cases} i(k - k_{10})X_1 + i\alpha X_2 = 0 \quad , \text{ and} \\ i(k - k_{20})X_2 - i\beta X_1 = 0 \quad . \end{cases} \tag{21}$$

In order for the hybrid modes to exist, the system (Eq. 21) must be compatible, i.e.,

$$\begin{vmatrix} i(k - k_{10}) & i\alpha \\ -i\beta & i(k - k_{20}) \end{vmatrix} = 0 \quad , \tag{22}$$

which gives

$$k = \frac{k_{10} + k_{20}}{2} \pm \sqrt{\left(\frac{k_{10} - k_{20}}{2}\right)^2 - \alpha\beta} \quad , \tag{23}$$

where k_{10} and k_{20} refer to uncoupled modes, and α and β are the coupling coefficients (related, as already mentioned, by reciprocity relations).

It can immediately be seen that when $k_{10} = k_{20}$, no wave exists, and there is a stopband where the hybrid waves are evanescent (Fig. 11).

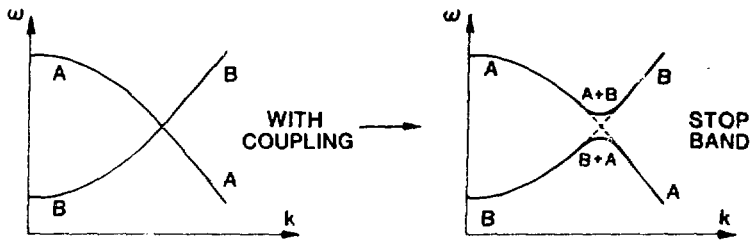

Fig. 11. Crossing of two coupled modes.

5.3. Zero-Mode Coupling — Confluence

Let us now consider the case where the dispersion curves join at zero mode. Unlike the previous case where only two modes were taken into account, now with $k \approx 0$, not only waves with $k > 0$, but also waves with $k < 0$ must be considered, because their velocity difference is very small.

One will then have, instead of Eq. (19),

$$\begin{cases} X_1' = -ik_{10}X_1 + i\alpha X_3 - i\alpha X_4 \ , \\ X_2' = +ik_{10}X_2 - i\alpha X_3 + i\alpha X_4 \ , \\ X_3' = -ik_{20}X_3 - i\beta X_1 + i\beta X_2 \ , \text{ and} \\ X_4' = +ik_{20}X_4 + i\beta X_1 - i\beta X_2 \ . \end{cases} \tag{24}$$

The condition for hybrid waves is now

$$\begin{vmatrix} k - k_{10} & 0 & +\alpha & -\alpha \\ 0 & k + k_{10} & -\alpha & +\alpha \\ -\beta & +\beta & k - k_{20} & 0 \\ +\beta & -\beta & 0 & k + k_{20} \end{vmatrix} = 0 \ , \tag{25}$$

which, after development, gives

$$(k^2 - k_{10}^2)(k^2 - k_{20}^2) + 4\alpha\beta k^2 = 0 \ . \tag{26}$$

For modes very close to the zero mode, k_{10}, $k_{20} \approx 0$. One may assume

$$k_{10}^2 + k_{20}^2 \ll \alpha\beta \ . \tag{27}$$

Eq. (26) then becomes

$$k^2 \approx -\frac{k_{10}^2 k_{20}^2}{4\alpha\beta} \ . \tag{28}$$

Around the zero mode, each dispersion curve can be represented by an expression of the form:

$$k_{10} = \sqrt{(\omega^2 - \omega_1^2)/K_1} \qquad k_{20} = \sqrt{(\omega_2^2 - \omega^2)/K_2} \ , \tag{29}$$

where K_1 and K_2 are proportional to the curvature of the dispersion curves around the zero mode, i.e., to their bandwidths.

Letting

$$\omega_1 = \omega_0 - \Delta\omega \ , \qquad \omega_2 = \omega_0 + \Delta\omega \ , \quad \text{and} \quad \omega = \omega_0 + \delta\omega \tag{30}$$

with $\Delta\omega,\ \delta\omega \ll \omega_0$, one obtains

$$k^2 \approx \frac{\omega_0^2}{\alpha\beta K_1 K_2}(\delta\omega^2 - \Delta\omega^2) \ , \tag{31}$$

and, for an exact "confluence" $(\Delta\omega = 0)$,

$$k \approx \pm\frac{\omega_0}{\sqrt{\alpha\beta K_1 K_2}}\,\delta\omega \ . \tag{32}$$

In such a case, there is no stop band; a confluence entails a nonzero group velocity (Fig. 12). This group velocity is proportional to the coupling coefficient $(\sqrt{\alpha\beta})$ and to the geometric average of the two passbands:

$$v_g = \sqrt{\alpha\beta K_1 K_2}/\omega_0 \ . \tag{33}$$

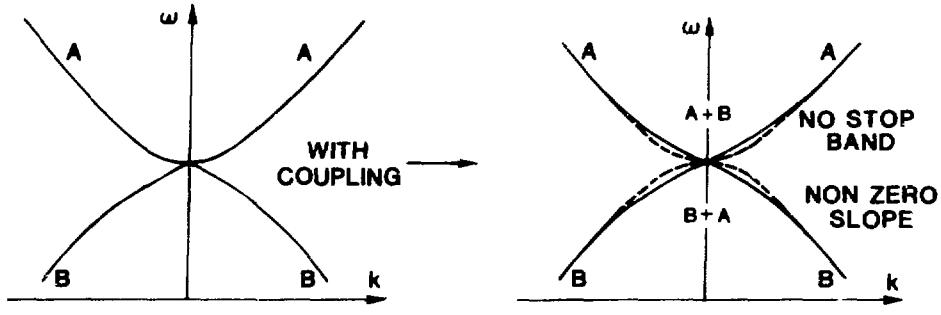

Fig. 12. Confluence.

The posts mentioned in Sec. 5.1 introduce in the cavity a band whose mode is slightly coupled to the Alvarez mode (the side alternance of the posts provides a favorable dispersion curve).

At confluence, $v_g \sim 0.1c$. In order to increase v_g, the coupling should be increased.

5.4 Stem Coupling [Giordano]

Stems supporting drift tubes resonate in a mode whose band does not normally interfere with the Alvarez mode. If, instead of one stem, two or more are used and their angle

and diameter are adjusted, it is possible to produce a confluence with the Alvarez mode (Fig. 13). The coupling is obviously larger than with posts that do not touch drift tubes.

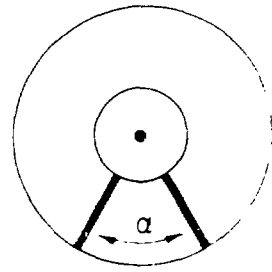

Fig. 13. Stem stabilization.

One obtains $v_g \sim c/3$. This device, however, is very inflexible. Posts, on the other hand, fitted with eccentric tabs at their ends allow, by rotating the posts, an adjustment of the field distribution along the structure [Swenson et al.] while still providing stability (but with $v_g \sim 0.1c$ only).

5.5 Remark on Zero-Mode Structures

(a) *Ordinary Structures.* At zero mode, the classical wave equation

$$\frac{\partial^2 E_z}{\partial z^2} + k^2 E_z = 0 \tag{34}$$

becomes

$$\partial^2 E_z / \partial z^2 = 0 \ ,$$

which exhibits the general solution

$$E_z = A + Bz \ . \tag{35}$$

In this solution, A represents a mode that, in a circular waveguide, corresponds to the classical TM_{010}. The term Bz represents a mode that turns out to be the limit of TM_{011} mode for an infinitely long cavity, $z = 0$ being the position of a magnetic wall (open cavity without radiation). [Dôme et al.](See Fig. 14).

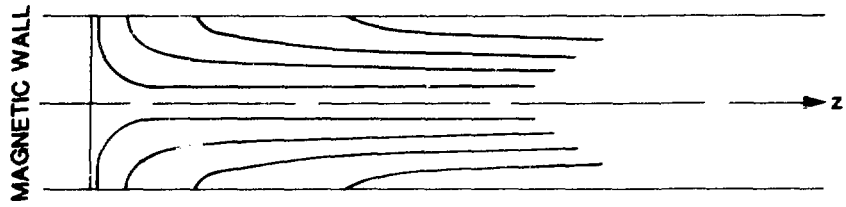

Fig. 14. Degenerate mode.

In such a mode, a purely imaginary flux of the Poynting vector maintains the field inequality along the structure. Such a flux can be produced at each end of a long cavity by a frequency perturbation that acts as a sink or a source of reactive power. Such perturbations then produce a field tilt as explained in Sec. 3.2. The larger the mode separation, the smaller the tilt (sensitivity factor S).

If A and B are not in phase, there is real power transmission. This is the case of transients that, because of the phase shift produced by rf joule losses, travel in an infinite structure at a velocity of the order of $c/\sqrt{Q}$.

(b) *Compensated Structures.* For "compensated structures," the situation is different. The sensitivity is no longer directly related to the group velocity. Let us consider a nonexact confluence, where $\Delta\omega \neq 0$. Instead of writing Eq. (28) as we did in Eq. (31), let us consider the neighborhood of ω_1 and, with Eq. (29), write

$$k^2 \approx (\omega^2 - \omega_1^2)\frac{\omega_1^2 - \omega_2^2}{4(v_g\omega_0)^2} \quad , \tag{36}$$

where v_g is the confluence value (Eq. 33).

This expression is of the same type as Eq. (29). It shows that mode separation around ω_1 of the accelerating mode is such that the sensitivity factor, instead of $S = 2K_1/(\omega L)^2$ as in Eq. (29), is now [Knapp et al.][Dôme, p. 673]

$$S \simeq \frac{8}{1-(\omega_2/\omega_1)^2}\left(\frac{v_g}{\omega_1 L}\right)^2 \quad . \tag{37}$$

The sensitivity to perturbation not only decreases (S increases) as a result of confluence, but also goes through zero and changes sign with the zero-mode frequency difference between accelerating and coupling modes. Equation (36) indeed indicates that the curvature around the ω_1 frequency of the accelerating mode changes with the sign of $\omega_2 - \omega_1$.

The situation is, however, not symmetrical. A closer look at Eq. (26) shows that Eq. (36) should be written

$$k^2 \approx (\omega^2 - \omega_1^2)(\omega_1^2 - \omega_2^2)/K_1(4\alpha\beta K_2 + \omega_1^2 - \omega_2^2)$$

in such a way that for $\omega_2^2 - \omega_1^2 \approx 4\alpha\beta K_2$, all stabilization vanishes before changing sign again.

At the confluence, experience shows that the two mode solutions of Eq. (34) are the zero accelerating mode and the zero coupling mode, both of constant amplitude but with a different parity (one symmetrical and the other antisymmetrical). [Dôme et al.] This property can be illustrated by comparison with a non-compensated case. Figure 15 shows the field distribution of the degenerate Alvarez mode and the pure post mode at confluence. For a similar flux of reactive energy at input (similar field configuration), there is in one case linear growth of the field and constant field in the other.

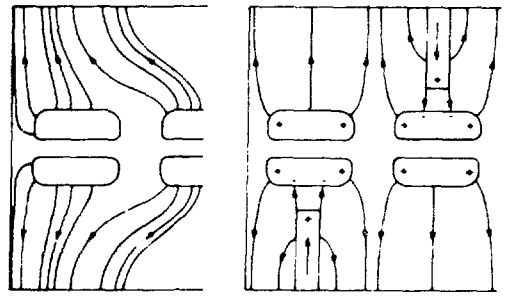

Fig. 15. Comparison of the degenerate Alvarez mode with the post mode at confluence.

The transient velocity at the confluence is, of course, still related to v_g, but, because of the complex shape of the dispersion curve, it may take a different value. Slightly away from the confluence, it decreases .

Further away from the confluence, when the coupling becomes weak, the velocity is $c/\sqrt{Q}$ again. As for stabilization, however, the situation is not symmetrical; for $\omega_2 > \omega_1$, the transient regime may become extremely bad, particularly when $\omega_2^2 - \omega_1^2 = 4\alpha\beta K_2$.

(c) *Sensitivity Factor and Group Velocity.* Equation (37), valid for compensated structures, does not show, as did Eq. (16) for a single structure, a direct relation between S and v_g. In practice, however, the group velocity value v_g is not at all irrelevant for field stabilization. The higher v_g is, the less important it is to guarantee a perfect confluence

and the less sensitive one is to possible accidental changes as produced by mechanical deformations. However, it is prudent to avoid $\omega_2 > \omega_1$, especially if the coupling mode has a small bandwidth.

6. OTHER TYPES OF LINACS

6.1 Variable Energy Linacs (Variable Velocity)

Such accelerators are particularly suited for heavy ions for which, according to mass, velocity may change in a relatively wide range.

(a) *Variable Frequency Linacs* [Odera]. RILAC in Japan is of this class. The Sloan-Lawrence structure ($\pi - 3\pi$ initially, then $\pi - \pi$) with a frequency range close to a factor of 3 can cover a wide range of energy per nucleon. Mechanical fabrication is delicate and rf losses relatively high.

(b) *Operation at Reduced Level Near the End of the Accelerating Cavity.* [Swenson et al.] *and* [Tanabe et al.] An insufficient field level entails a loss of trapping (inverted golf club). One may obtain several energy bands, but this operation would require more detailed studies in order to be practicable.

(c) *Additional Independent Cavities.* This is the device used in the UNILAC (GSI Darmstadt)[Böhne]. By a proper phase and amplitude adjustment of short additional reentrant cavities, one may reduce or increase the final energy while keeping a satisfactory longitudinal emittance.

6.2 Independent Cavity Linacs

(a) *Classical Reentrant Cavities.* Compared to a classical Alvarez structure, the rf consumption in such a device is notably higher at low velocity; for $\beta \geq 0.3$, however, the difference goes down and even changes sign for large βs.

(b) *Induction Cavities* [Smith]; [Fessenden].

These induction cavities are a type of pulse transformer where the accelerating field is applied only at the time the beam is crossing them. Independent pulses can be considered as part of an rf period of arbitrary length (Fig. 16).

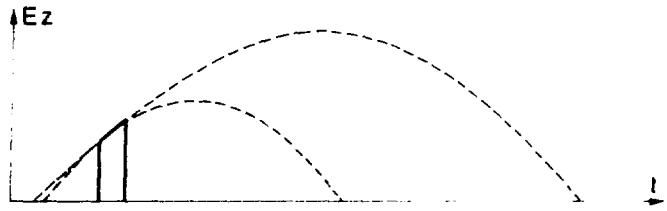

Fig. 16. Independent pulse operation.

These conditions may be expressed as

$$\begin{cases} E_z = \hat{E} \cos \phi & \text{and} \\ \dfrac{dE_z}{dt} = -\omega \hat{E} \sin \phi & , \end{cases} \tag{38}$$

which specify that acceleration and phase stability conditions may be satisfied by an infinite set of ω, $\hat{E}$ and ϕ values. A careful shaping of the pulse profile may even allow correction of some nonlinear effects (Chap. 2, Sec. 1.5).

(c) *Linac Boosters for Electrostatic Accelerators* [Schempp et al.] and [Bollinger et al.]. Such cavities, either at room temperature (Heidelberg) or superconducting (Argonne, Stonybrook, Saclay, etc.), usually have two or three gaps (spiral or split-ring resonators, see Fig. 17); the gaps can even be of a helical type ($\lambda/2$ or λ long) [Ramstein et al]. These indcpendent cavities, the phase of which is computer controlled, are potentially extremely flexible.

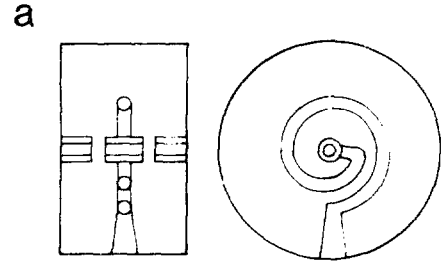

Fig. 17a. Spiral resonator.

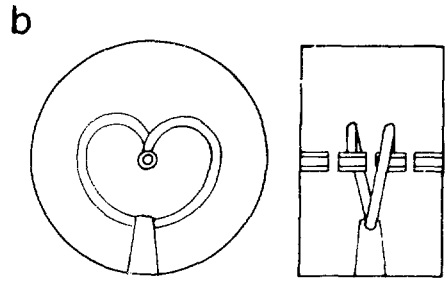

Fig. 17b. Split-ring resonator.

7. NOTES ON THE FIELD DISTRIBUTION COMPUTATION

[Halbach et al.]

Fields in a cavity satisfy Maxwell's equations, and the potential function ϕ must satisfy

$$\nabla^2\phi - \frac{\varepsilon\mu}{c^2}\frac{\partial^2\phi}{\partial t^2} = 0 \quad , \tag{39}$$

where ε and μ are the relative permittivity and permeability, respectively.

For circular symmetry, for instance, a mode having an E_z component on the axis will satisfy

$$\frac{1}{r}\frac{\partial}{\partial r}\left(r\frac{\partial E_z}{\partial r}\right) + \frac{\partial^2 E_z}{\partial z^2} - \frac{\varepsilon\mu}{c^2}\frac{\partial^2 E_z}{\partial t^2} = 0 \quad . \tag{40}$$

Computer codes exist for the solution of such partial derivative equations in free space ($\varepsilon = \mu = 1$), limited by boundary conditions such that, for instance, the electric field be normal to the walls.

In practice, this space is sometimes divided into subspaces limited by plane or cylindrical (or spherical) boundaries between which the fields can be expressed in the form of a series of modes with the usual functions [Bell et al.]. Other subspaces, including boundaries, are treated by finite difference equations applied to an appropriate mesh.

For the case of circular symmetry, instead of E_z and E_r, one often introduces the function

$$F = rH_\phi \quad , \tag{41}$$

for which Eq. (40) becomes

$$\frac{\partial^2 F}{\partial r^2} - \frac{1}{r}\frac{\partial F}{\partial r} + \frac{\partial^2 F}{\partial z^2} - \frac{1}{c^2}\frac{\partial^2 F}{\partial t^2} = 0 \quad . \tag{42}$$

One has to find the resonant frequency and field distribution simultaneously.

Usually, one starts computing the field distribution with an estimated value of the frequency. From this, various criteria lead to a new estimate, based in fact on an estimate of the difference between electric and magnetic stored energy. After a few iterations, the frequency and field are obtained.

It is then possible to compute joule losses (and heat deposition), peak electric and magnetic fields on the walls, frequency corrections as produced by perturbations not included in the computation (drift-tube stems, for instance), and various quantities relevant to beam dynamics computations (T, S, and their derivatives, see Chap. 5).

8. NOTES ON TRANSIENTS AND BEAM LOADING (Beam-induced Field Excitation)

Although of increasing importance, today, discussion of transients and beam loading will be limited here because detailed treatment presents relatively complex aspects.

8.1 Short Cavity [McMichael et al.]

When a bunch of charges crosses an rf cavity, it excites EM fields. We shall consider here a periodic train of bunches, the frequency of which is close to the resonant frequency of the cavity (or a harmonic frequency). Let $\tilde{I}$ be the corresponding intensity at that frequency (harmonic component of the Fourier spectral analysis). The field excited by this current can be computed from the fraction of the stored energy it absorbs from the cavity (assumed lossless):

$$\frac{dW_s}{dt} = -\tilde{I}VT\cos\phi \quad , \tag{43}$$

where V is the voltage in the cavity gap, T is the transit-time factor (see Chap. 5 for details), and ϕ is the relative phase between V and $\tilde{I}$.

The stored energy W_s can be expressed in terms of the voltage V with the help of an "impedance" Z, such that

$$W_s = V^2/2\omega_0 Z \quad . \tag{44}$$

If, for example, the cavity is a short section of an accelerating structure of shunt impedance Z_s with length L, quality factor Q, and angular frequency ω_0. then

$$Z = Z_s L/2Q \quad . \tag{45}$$

From Eqs. (43) and (44), one obtains

$$\frac{\vec{V}}{\omega_0 Z}\frac{d\vec{V}}{dt} = -\vec{\tilde{I}}\vec{V}T \tag{46}$$

whence

$$\frac{d\vec{V}}{dt} = -\vec{\tilde{I}}\cdot\omega_0 ZT = -\vec{\tilde{I}}\cdot\frac{\omega_0 Z_s LT}{2Q} \quad . \tag{47}$$

In these equations, vector notation has been used to show that the voltage derivative dV/dt is *opposite in phase* to the current $\tilde{I}$.

In a cavity with losses, another term must be added:

$$\frac{d\vec{V}}{dt} = -\vec{\tilde{I}}\omega_0 ZT - 2\frac{\vec{V}}{\tau} \quad , \tag{48}$$

where τ is the time constant of the empty cavity. A power feed from an external circuit would introduce an extra term. Without it, one sees that, after a transient period, the beam would maintain a constant field level equal to

$$\vec{V}_b = -\vec{\tilde{I}}\omega_0 ZT\ \tau/2 \quad . \tag{49}$$

This voltage must be compensated for by a correction of the signal injected by the power feeder into the cavity. Correction must be made in amplitude and in phase because $\tilde{I}$ is usually not in phase with the voltage V (V and V_b are not opposite in phase: they even are in quadrature in a buncher). In the case of high beam loading, V_b may be much larger than V; phase and amplitude controls become difficult [Boussard] (in bunchers, one sometimes damps the cavity in order to reduce V_b). Superconducting cavities are obviously an extreme case; the situation is, however, slightly simpler for electron linacs where the accelerating phase is very close to the crest of the wave.

In the previous Fourier analysis of the beam bunches only the fundamental frequency has been considered. In case the cavity can be excited at harmonic frequencies, methods must be found to damp the corresponding modes.

8.2 Accelerating Structure

(a) *Zero-Mode Alvarez Structure.* In a long structure, if one neglects the possible variation of ϕ_s with energy, all accelerating gaps are excited in phase. If one assumes the radial field distribution is unaffected by the beam, neglecting the transient propagation there, and if one neglects the variation of other parameters with energy, the equation that governs the axial field distribution may be written according to Eq. (40), taking the losses into account, as:

$$\frac{\partial^2 E_z}{\partial t^2} + \frac{2}{\tau}\frac{\partial E_z}{\partial t} - \frac{c^2}{\varepsilon\mu}\frac{\partial^2 E_z}{\partial z^2} + \omega_c^2 E_z = 0 \quad , \tag{50}$$

where E_z is the average accelerating field amplitude and $\omega_c = \omega_0$ corresponds to the zero-mode (cutoff) frequency. Beam excitation would add a term on the right-hand side of Eq. (50)

$$-\frac{di}{dt} \cdot \omega_0 Z_s T/2Q$$

as in Eq (47). Here i is the instantaneous value of the beam current, assumed independent of z, and of which one can compute the spectral component in the neighborhood of the frequency ω_0.

It is easily seen that in steady-state conditions, one has

$$\vec{E}_z = -\vec{I}\omega_0 Z_s T\tau/4Q \quad , \tag{51}$$

and all the remarks pertaining to the case of a short cavity apply here.

However, while the beam absorbs energy in a uniform way along the structure, feedback from an external circuit is usually done at a single point. In order to study how the cavity is filled and to understand its transient aspects, one has to solve Eq. (50), which is a telegrapher's type. This analysis will not be developed here [Hereward et al.]. One may also consider that several modes are excited [Nishikawa].

Let us say that in steady-state conditions, for an uncompensated zero mode, energy propagation in the cavity (for compensating beam loading as well as rf losses) entails a small amplitude drop and a progressive phase shift, which may be of a few degrees. Under transient conditions, propagation is made along the axis of an infinite

cavity only through losses (no propagation for τ_∞), and the velocity is of the order of $c/\sqrt{Q}$. Phase shifts can be several tens of degrees in a long cavity. In a short cavity, however, due to reflections phenomena are more complex and one cannot speak any longer even of a propagation velocity, because the initial filling time is approximately proportional to the square of the length and almost independent of the losses. In the superconducting case, cavities that are not too long are preferable.

Under such conditions, any feedback control of amplitude and phase of a cavity will always be imperfect. It is, however, acceptable. It is better to control a point not too far in the cavity from the feed coupling in order not to complicate the feedback loop.

(b) *Nonzero Mode. Nonzero Group Velocity.* In Eq. (50), ω_c is no longer equal to ω_0, the operation frequency. If there is still a slight phase shift along the cavity because of losses, it is now very small. Energy propagation from the feed point is at the group velocity, usually much faster and without any appreciable phase shift.

(c) *Compensated Structure.* In this case, energy propagation takes place at a velocity of the order of the confluence group velocity and a little slower if the confluence is not perfect (see Sec. 5.5.b). There is no phase shift except from structure imperfections or losses.

CHAPTER 5

DETAILED PARTICLE DYNAMICS COMPUTATIONS

The general theory described in Chaps. 2 and 3 for longitudinal and transverse motions assumes the existence of a constant amplitude synchronous wave. We saw that such an existence is often compromised by changes in parameters, the effect of which has yet to be analyzed.

The choice of a constant ϕ_s is not necessarily the best if one considers the rapid increase of the stability area (while the beam, according to Liouville's theorem, occupies a constant area). One may also introduce "longitudinal beam gymnastics," either to improve matching or for any other purpose. Such an operation can, indeed, be adopted easily in separated cavity linacs, where each of them can be adjusted in amplitude and phase.

It is then necessary to compute such cases with good accuracy. General theory remains, of course, a valuable tool for obtaining a quick overview of the phenomena and for guiding one to the achievement of special effects, but an accurate computation is still necessary.

The treatment described here is the computation of each gap or each independent cavity for longitudinal as well as transverse motion in a "thin lens" formalism, as it is current practice for beam transport devices.

1. INITIAL METHOD [Panofsky et al.]

1.1 Panofsky Equation

Let us consider an accelerating gap (Fig. 1) across which exists a longitudinal electric field E_z with an rf voltage $V \cos(\omega t + \phi)$ crossed by a particle with charge q. The energy gain from point A to point B will be

$$\Delta W = q \int_{-L/2}^{L/2} E_z(z) \cos(\omega t + \phi) dz \quad , \tag{1}$$

and it is always smaller than qV, whatever the phase ϕ is. This reduction in energy gain is what is called the *transit time effect.*

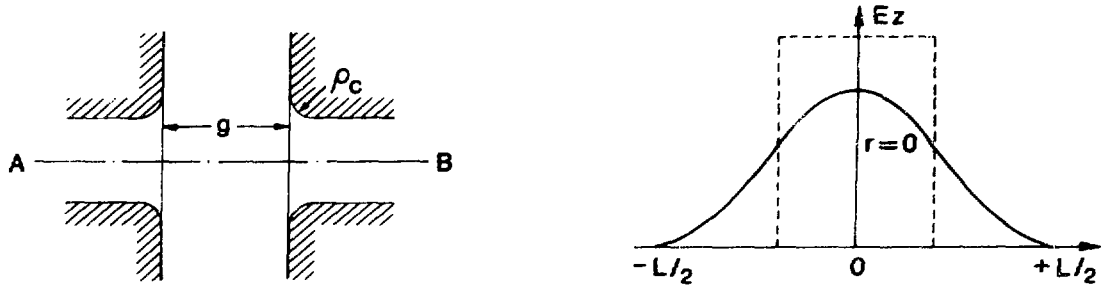

Fig. 1. Accelerating gap.

Let us assume, for instance, a constant velocity v for the particle (we shall later on extend the computation). If $t = 0$ is the time when the particle crosses the center $z = 0$,

$$z = vt \quad , \tag{2}$$

and for a symmetrical gap

$$\Delta W = q \int_{-L/2}^{L/2} E_z(z) \cos\left(\frac{\omega z}{v} + \phi\right) dz = q \int_{-L/2}^{L/2} E_z(z) \cos\frac{\omega z}{v} \cos\phi \, dz \quad .$$

If one writes

$$V = \int_{-L/2}^{L/2} E_z(z) dz \tag{3}$$

and

$$VT_0 = \int_{-L/2}^{L/2} E_z(z) \cos\frac{\omega z}{v} dz < V \quad , \tag{4}$$

one gets

$$\Delta W = qVT_0 \cos\phi \quad , \tag{5}$$

sometimes referred to as Panofsky's equation. The term T_0 is the transit time coefficient, a function of the velocity v; it is very close to 1 for very fast particles, but always <1.

In the commonly considered case of a constant field in a gap of length g (Fig. 2), one has

$$T_0 = \frac{\sin\theta/2}{\theta/2} \quad \text{with } \theta = \omega g/v \quad . \tag{6}$$

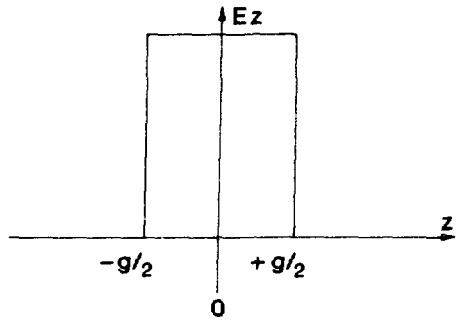

Fig. 2. Uniform field in a gap.

Fig. 3 shows the well-known variations of T_0 with ω/v.

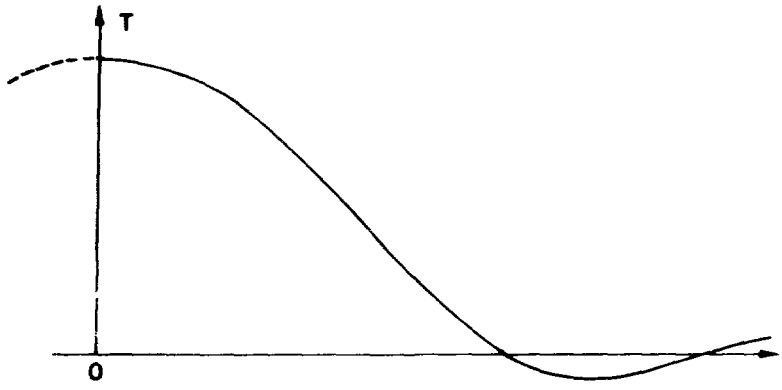

Fig. 3. Transit time factor variations with ω/v.

In practice, the beam holes on the faces of the electrodes modify this value. On its edge is usually a chamfer to avoid breakdowns (radius ρ_c, see Fig. 1). In addition, the field penetrates into the hole giving a different value for T_0 according to the distance from the axis. Such effects can be expressed by replacing g by the empirical expression

$$g_c = g + 0.85\rho_c \quad , \tag{7}$$

and putting (with $\theta_c = \omega g_c/v$)

$$T_0 = \frac{\sin \theta_c/2}{\theta_c/2} \frac{I_0(k_r r)}{I_0(k_r a)} \quad , \tag{8}$$

where

$$k_r^2 = (\omega/v)^2 - (\omega/c)^2 \quad . \tag{9}$$

In this expression, r is the distance from the axis to the particle, and a is the hole radius (see Sec. 2.2 in this chapter).

In a linac design, v would be the synchronous velocity. As shown in Chap. 2, however, particles in a bunch oscillate around a synchronous particle with continuous velocity and phase spectra; v is then not unique but depends on the particles.

1.2 Emittance Nonconservation

In the previous (*thin lens*) treatment, the phase is not modified when crossing the median plane of the gap where the energy gain is applied. Let us consider four particles (Fig. 4) around a central particle; two are of the same energy but displaced in phase by $\pm\Delta\phi$ (A and B) and two are of equal phase but displaced in energy by $\pm\Delta W$ (C and D)(displaced in velocity by $\pm v_s \Delta W/2W_s$). Look at the position of these four particles with respect to the central one after crossing the *thin lens*. With constant phase, A and B will be displaced in energy by equal but opposite amounts ($\Delta\phi$ assumed small). A′ and B′. However, C, more energetic than the central particle, will have a larger transit time coefficient T and will move up to C′. On the contrary, D will move down to D′.

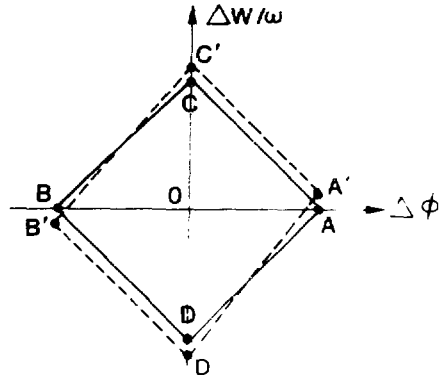

Fig. 4. Non-Liouvillian transformation: the dotted parallelogram has an area larger than the solid one.

Comparing the areas of parallelograms, ABCD and A'B'C'D', it is clear that there is a growth in area. Emittance is not conserved. Liouville's theorem is not satisfied as it must be. One way to avoid this difficulty, as suggested in 1963 at a Linac Conference, would be to ignore the energy dependence of T. This approach is not very satisfactory. Another solution [Carne et al.] is to introduce a $\Delta\phi$ change at the *thin lens* crossing.

2. ACCURATE COMPUTATION OF LONGITUDINAL AND TRANSVERSE MOTIONS. FIRST ORDER [Carne et al.]

2.1 Description of an Accelerating Gap

In practice, the field distribution in a gap can be measured experimentally (Chap. 4) or rather, nowadays, can be calculated by using computer codes. The electric field on the axis can then be expressed in the form of a Fourier series, or integral

$$E_z(z, r = 0) = \frac{V}{2\pi} \int_{-\infty}^{+\infty} T(k_z) \cos k_z z \, dk_z \quad , \tag{10}$$

with the inverse relation

$$VT(k_z) = \int_{-\infty}^{+\infty} E_z(z, 0) \cos k_z z \, dz \quad . \tag{11}$$

One recognizes a relation of the type used in Eq. (4) with the notation already used in Chap. 4,

$$k_z = \omega / v_\phi \quad . \tag{12}$$

The gap is assumed symmetrical and, for purposes of this study, the only gap.

In circular symmetry, electromagnetic fields can be expressed in the form of modes.* The term $T(k_z)$ can then be considered as the amplitude function with wave number k_z in the spectrum of a stationary wave for which

$$E_z(z, r, t) = \frac{V}{2\pi} \int_{-\infty}^{+\infty} T(k_z) I_0(k_r r) \cos k_z z \cos(\omega t + \phi) dk_z \quad , \tag{13}$$

* For synchronous waves, only TM or E modes interact with particles, and they are the only ones that will be considered here.

$$E_r(z,r,t) = \frac{V}{2\pi}\int_{-\infty}^{+\infty} T(k_z)\frac{k_z}{k_r} I_1(k_r r)\,\sin k_z z\,\cos(\omega t+\phi)dk_z \quad , \tag{14}$$

and

$$cB_\theta(z,r,t) = \frac{V}{2\pi}\int_{-\infty}^{+\infty} T(k_z)\frac{\omega}{ck_r} I_1(k_r r)\,\cos k_z z\,\sin(\omega t+\phi)dk_z \quad , \tag{15}$$

with k_r as defined by Eq. (9) where v is replaced by v_ϕ.

2.2 Energy Gain

With the previous expressions, the energy gain of a particle of velocity v assumed constant and parallel to the axis is easily computed:

$$\Delta W = q\int_{-\infty}^{+\infty} E_z\left(z,r,\frac{z}{v}\right)dz \quad .$$

With a derivation similar to the one used in Sec. 1, and making use of inverse Fourier relations (Eqs. 10 and 11), one obtains

$$\Delta W = q\ VT(k)I_0(k_r r)\cos\phi \quad . \tag{16}$$

This equation is exactly like Eq. (8), which is then justified as far as the radial variation of the transit time factor is concerned. (It must be noted that the Bessel function term is not included in the new definition of $T(k_z)$, which relates to the axis.) As explained, $T(k_z)$ is a spectral amplitude, and it is important to notice that the only thing that matters is the amplitude corresponding to

$$k = \omega/v \quad , \tag{17}$$

which is related to the particle mid-gap velocity.

2.3 Phase Equation

The energy gain computation, assuming a constant velocity and a rectilinear trajectory, can be considered as a first-order approximation of a *perturbation method* in which, with a higher order, the velocity will change with energy. Let us consider the way energy and phase change when a particle crosses an acceleration gap (Fig. 5).

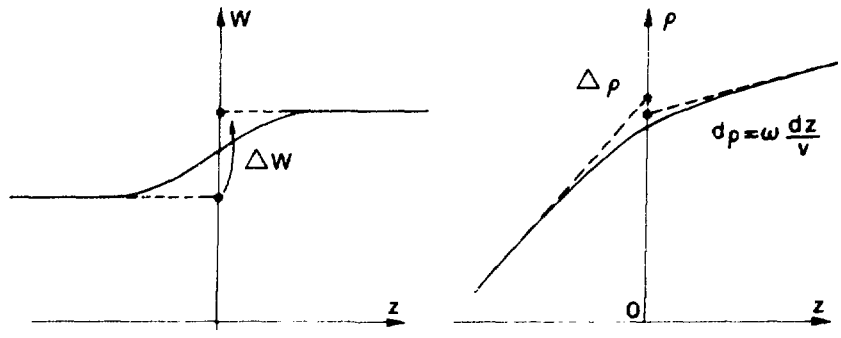

Fig. 5. Detailed evolution of phase and energy across a gap.

For the energy, the *thin lens* formalism leads to replacing the curve shown by the two dotted straight lines, the distance ΔW between them being given by Eq. (16) (the mid-gap value is assumed to be known). For the phase, there is a continuous slip, but it is also possible to extend the straight lines corresponding to the outside portions up to mid-gap (see dotted lines). The two extensions have no reason to cross at this mid-gap point. One should then introduce a $\Delta\phi$ jump, which we shall now compute. Between the true law and the dotted line, the differential phase slip is

$$\delta\phi = \omega \int_{-\infty}^{z} \delta\left(\frac{1}{v}\right) dz \quad , \tag{18}$$

with

$$\delta\left(\frac{1}{v}\right) \approx -\frac{1}{2vW}\delta W = -\frac{1}{2vW}\int_{-\infty}^{z} qE_z(s,t)ds \quad . \tag{19}$$

The $\Delta\phi$ jump is then given by

$$\Delta\phi = -\frac{\omega}{2vW}\int_{-\infty}^{0} dz \int_{-\infty}^{z} q\ E_z(s,t)ds + \frac{\omega}{2vW}\int_{0}^{\infty} dz \int_{z}^{\infty} q\ E_z(s,t)ds \quad . \tag{20}$$

By inverting the order of integration in the domain shown on Fig. 6 and with the help of Eq. (17), one obtains

$$\delta\phi = \frac{k}{2W}\int_{-\infty}^{+\infty} q\ E(s,t)ds \int_{0}^{s} dz \tag{21}$$

and

$$\Delta\phi = \frac{k}{2W}\int_{-\infty}^{+\infty} s\ ds \int_{-\infty}^{+\infty} \frac{qV}{2\pi} T(k_z) I_0(k_r r) \cos k_z s \cos(ks + \phi) dk_z \quad . \tag{22}$$

Because

$$s \cos(ks + \phi) = \frac{\partial}{\partial k} \sin(ks + \phi) \quad , \tag{23}$$

with the help of Fourier transform relations, one obtains

$$\Delta\phi = \frac{qV}{2W} k \frac{\partial}{\partial k} \left[T(k) I_0(k_r r) \right] \sin \phi \quad . \tag{24}$$

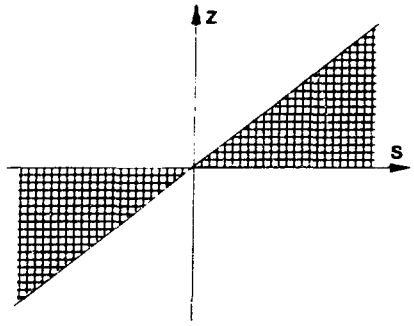

Fig. 6. Integration domain.

Coming back to the discussion in Sec. 1.1, one may see that points A and B of Fig. 4 are now moving inwards in $\Delta\phi$ as are C and D moving outwards in ΔW. This motion allows phase space conservation, at least to first order (Fig. 7).

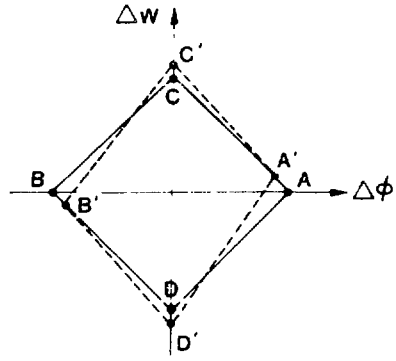

Fig. 7. Liouvillian transformation: the area is conserved.

Putting

$$H = -qVT(k) I_0(k_r r) \sin \phi \quad , \tag{25}$$

it is easy to check that Eqs. (16) and (24) are such that

$$\begin{cases} \Delta W &= -\partial H/\partial\phi \\ \Delta\phi &= \partial H/\partial W \end{cases} ; \tag{26}$$

$\Delta\phi$ and ΔW proceed from a Hamiltonian formalism (see Chap. 2, Sec. 3.1.1) and Liouville's theorem is satisfied to the first order.

2.4 Radial Motion

With the help of Eqs. (14) and (15), one can similarly treat the radial motion and compute $\Delta r'$ and Δr jumps in slope and position at the mid-gap plane in a *thin lens* formulation similar to the one sketched in Fig. 5. One must be aware that the conjugate variable of r is mv_r and not r' and that transverse fields E_r and B_θ act on mv_r and not on

$$r' = \frac{mv_r}{mv_z} \ . \tag{27}$$

One then has

$$\Delta r' = \frac{\Delta(mv_r)}{mv_z} - \frac{mv_r}{(mv_z)^2}\Delta(mv_z) \ ,$$

and

$$\Delta r' = \frac{\Delta(mv_r)}{mv_z} - r'\frac{\Delta W}{2W} \ . \tag{28}$$

It is also possible to take into account the effect of the trajectory slope at the mid-gap plane by writing

$$I_0[k_r(r + r'z)] \approx I_0(k_r r) + k_r r' I_1(k_r r)z \tag{29}$$

and repeating for the r' term a derivation similar to the above. One eventually obtains

$$\begin{aligned}
\Delta W &= qVT(k)I_0(k_r r)\cos\phi + qV\frac{\partial}{\partial k}[T(k)k_r I_1(k_r r)]r'\sin\phi \ , \\
\Delta\phi &= \frac{qV}{2W}\,k\,\frac{\partial}{\partial k}[T(k)I_0(k_r r)]\sin\phi - \frac{qV}{2W}k\frac{\partial^2}{\partial k^2}[T(k)k_r I_1(k_r r)]r'\cos\phi \ , \\
\Delta r' &= -\frac{qV}{2W}\,T(k)\,\frac{k_r}{k}\,I_1(k_r r)\sin\phi + \frac{qV}{2W}\left\{\frac{\partial}{\partial k}\left[T(k)\,\frac{k_r^2}{k}\,I_1'(k_r r)\right] - T(k)I_0(k_r r)\right\}r'\cos\phi \ , \\
\Delta r &= -\frac{qV}{2W}\frac{\partial}{\partial k}\left[T(k)\frac{k_r}{k}I_1(k_r r)\right]\cos\phi - \frac{qV}{2W}\left\{\frac{\partial^2}{\partial k^2}\left[T(k)\frac{k_r^2}{k}I_1'(k_r r)\right]\right. \\
&\quad \left. - \frac{\partial}{\partial k}\left[T(k)I_0(k_r r)\right]\right\}r'\sin\phi \ .
\end{aligned} \tag{30}$$

One may again check that previous relations have Hamiltonian character by putting

$$H = -qVT(k)I_0(k_r r)\sin\phi + qV\frac{\partial}{\partial k}\left[T(k)k_r I_1(k_r r)\right]r'\cos\phi \quad , \tag{31}$$

and that they satisfy Liouville's theorem at least to first order.

Remark. The previous relations, in particular those in r and r', present a matrix character. They can easily be included in a beam-transport program either to express the effect of rebuncher cavities or the effect of independent accelerating cavities.

2.5 Mid-Gap Plane Coordinates

In the previous relations, $k(W)$, ϕ, r', and r relate to mid-gap crossing. Such values are unknown and may even be outside the range limited by input and output values of the thin lens (see Fig. 5, the case of the phase). It is possible to compute them in the following way. The previous derivation referred to a symmetric gap. A similar formalism can be derived for an antisymmetric case; this would be the case of a two-gap system (see Sec. 4 in this chapter).

One can then imagine an antisymmetrical system as shown in Fig. 8 for the first part of which the field would be exactly equal to the gap field; the field would be equal and opposite for the second half, like an image field. Such a system is not physical but it can be considered analytically.

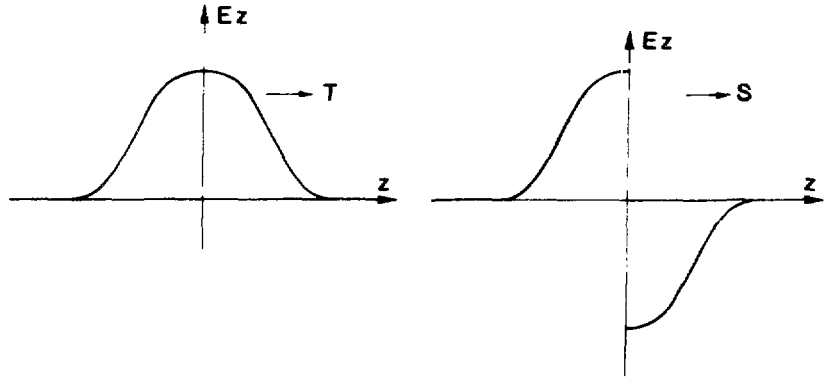

Fig. 8. Symmetrical and antisymmetrical fields for mid-gap computations.

The fields in such a system are no longer expressed with the help of the spectral amplitude $T(k_z)$, but with the help of $S(k_z)$ such that

$$S(k_z) = -\frac{2}{V}\int_0^\infty E(z)\,\sin k_z z\; dz \quad , \tag{32}$$

through expressions similar to Eqs. (13), (14), and (15), where $\cos k_z z$ is replaced by $\sin k_z z$, $\sin k_z z$ by $-\cos k_z z$ and, of course, $T(k_z)$ by $S(k_z)$. With such relations a system analogous to Eq. (30) can be computed.

But the half sum of T and S fields is equal to the gap field from input to mid-plane and zero further on. The thin-lens computation through such a system will then give, at output, the unknown mid-gap values.* Such values, of course, can be obtained only by iteration; in practice, a single iteration is often enough. It might even be possible to compute them with thin-lens input values. Also, it is possible to neglect the r' terms for many beams.

3. SECOND-ORDER COMPUTATION [Lapostolle et al.]

In order to increase accuracy, it is possible to go in the perturbation method to higher order by introducing in the ΔW computation a $\delta\phi$ correction leading to the replacement of $\cos(\omega z/v + \phi)$ by $\cos(\omega z/v + \phi + \delta\phi)$ and computing $\delta\phi$ as in Eq. (19) but with an integration from 0 to z.

It is also possible to compute a second-order correction in $\Delta\phi$ as well as in $\Delta r'$ and Δr, including the effects of δW, $\delta\phi$, and δr. Such second-order terms appear in the form of integrals of second-order expressions in $T(k_z)$ and its derivatives. Such relations are of no practical use.

---

* In real terms, the antisymmetric field considered here has for $z = 0$ a discontinuity that cannot fulfill Maxwell's equations. The $S(k_z)$ waves do not behave radially like the $T(k_z)$ waves. It is nevertheless acceptable behavior in practice, for usual beams ($kz < 1, r' < 10$ mrad) because one only wants to find mid-gap values, the effect of which is second order in Eq. (30), simply to add, in the equation for $\Delta r'$, to the term $-qV/2WS(k)(k_r/k)I_1(k_r r)\cos\phi$, the correction $-q(E_z(0)/2W)(k_r^2/k^2)r\cos\phi$.

3.1 Fourier Integrals and Series

Instead of integrals, the fields in the accelerating gap, even if given in the form of a series of period L_0, can be expressed through simple circular relations in the form of a Fourier series of period $L > L_0$. If

$$kL = 2n\pi \quad . \tag{33}$$

with n integer ($n = 1$, for instance, for a short gap), all the computations of Sec. 2 can be repeated in a similar way. Only one term of the series expression (the term of order n) acts on the particle. One finds again the set of Eq. (30).

Second-order computation, on the other hand, leads to series instead of integrals. For instance, one has

$$\begin{aligned}\Delta W_{\text{corr}} = \frac{q^2V^2n \sin 2\phi}{8\pi W}\Bigg[&2k\frac{\partial T(k)}{\partial k}\sum_{j=0,\neq n}^{\infty}\frac{T(jk/n)}{j^2-n^2} - 2T(k)\sum_{j=0,\neq n}^{\infty}\frac{T(jk/n)(j^2+n^2)}{(j^2-n^2)^2} \\ &+ \sum_{j=0,\neq n}^{\infty}\frac{T(2n-j)k/n)T(jk/n)}{(j-n)^2} \\ &+ \sum_{j=0}^{\infty}\frac{T[(2n+j)k/n]T(jk/n)}{(j+n)^2} - \frac{T^2(k)}{4n^2} - \frac{\partial T(k)}{\partial k}T(k)\frac{k}{2n^2} \\ &+ \frac{\partial^2 T(k)}{\partial k^2}T(k)\frac{k^2}{2n^2}\Bigg] \quad .\end{aligned} \tag{34}$$

Such an expression may look complicated, but it can be handled on a computer (much more easily than an integral) inasmuch as $T(k)$ decreases quickly with k (see Fig. 9 relating to a classical gap). The term $T(k)$ is the normal transit time factor, $T(2k)$ would correspond to 4π or $2\beta\lambda$ mode in the Alvarez structure where at 50 or 100 MeV, $T(2k)$ is small. The quantity $T(3k)$ is always negligible.

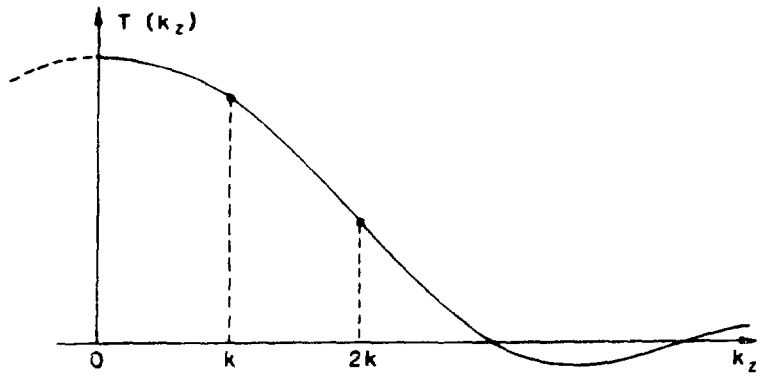

Fig. 9. Transit time coefficients of harmonic modes.

In the series, only a few terms [in $T(0), T(k), T(2k)...$, and the corresponding derivatives] have to be introduced inasmuch as the denominators still reduce the effect of higher order terms.

Normally, only ΔW_{corr} would have to be computed. At most, $\Delta\phi_{\text{corr}}$ is usually equal to $0.1°$, and radial corrections are of no practical interest—much less than alignment error effects, which require correcting and adjusting devices. In second-order radial corrections one, the $\Delta r'$, term would correspond to the focusing effect of an electrostatic lens—an effect which, as already mentioned, is usually negligible compared to the defocusing effect of a linac gap. Such second-order radial corrections, in order to be accurate, should also include the effect of H or TE modes because, in the second-order approximation, particles are no longer fixed in the synchronous wave.

3.2 Liouville's Theorem

If only the ΔW term is used, in order to conserve emittance without the $\Delta\phi$ term, one can give to the $T(k)$ terms the same value for all the particles of a bunch (but not the same ϕ), and the accuracy is normally good. According to the cases treated, one may add to the first-order terms a correction to satisfy Liouville's theorem to second order in qV/W, if necessary.

3.3 Remark on Fourier Coefficients

It is good to notice that all the information concerning the field distribution can be contained in only a few coefficients and not in a complete function as in the integral representation.

The ΔW_{corr} computation from Eq. (34) gives the same value even if one changes the value of n (Eq. 33), that is to say all the terms in Eq. (34). Of course, if n is increased, more terms may have to be computed [always up to $T(2k)$ or $T(3k)$, for instance]. This is a very important remark because it is an easy way to check the accuracy of a code.

4. OTHER TYPES OF CAVITIES. INDEPENDENT CAVITIES

[Lapostolle et al.]

In heavy-ion linacs with variable energy and velocity, use is frequently made of independent cavities (see Chap. 4), each cavity often including several gaps (Fig. 10) or even having a different nature like a helix (Fig. 11).

In multigap cavities, each gap can be treated independently (although the zero field zone in drift tubes is sometimes reduced almost to a point). One may also treat the full cavity at one time; this is the only possibility in the case of a helix.

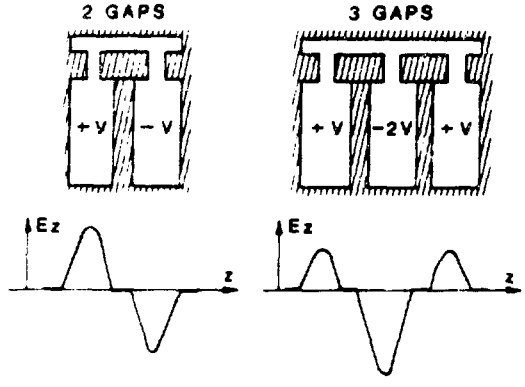

Fig. 10. Two- or three-gap cavities.

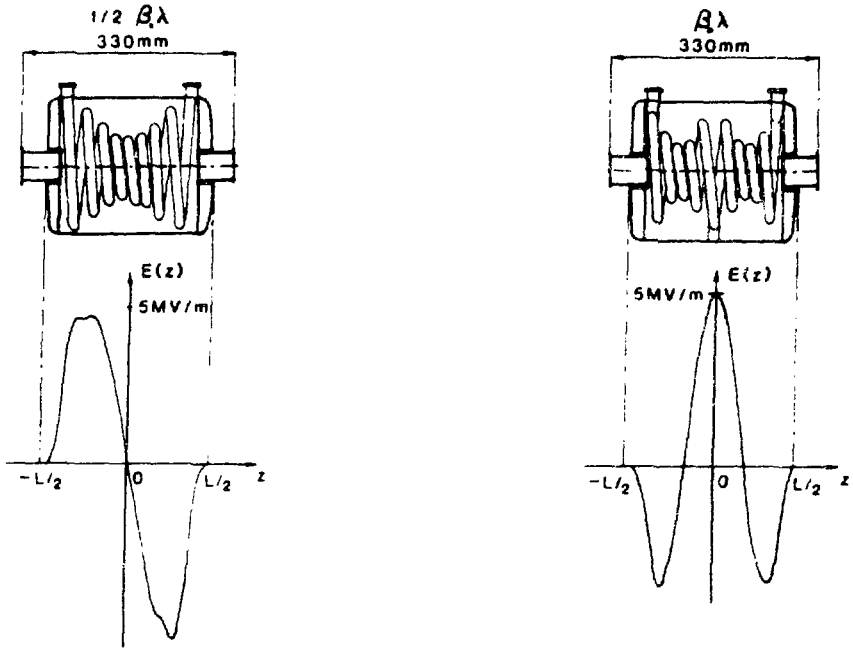

Fig. 11. Helix resonators ($\lambda/2$ orλ).

A two-gap cavity is then antisymmetrical. As seen in Sec. 2.5, the field is then expressed in terms of $S(k_z)$ coefficients. One will, in fact, write

$$S(k_z)[V] = \int_{-\infty}^{+\infty} E(z) \sin k_z z \, dz \quad , \tag{35}$$

where $[V]$ is an arbitrary normalizing factor such that S is dimensionless. For example, for two equal gaps with transit time coefficient $T(k_z)$, separated by a distance D (Fig. 12), one may write

$$S(k_z) = 2T(k_z) \sin \frac{k_z D}{2} \quad . \tag{36}$$

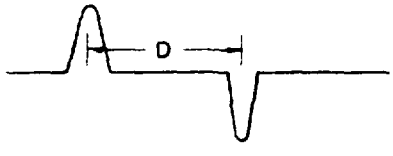

Fig. 12. Field distribution in a two-gap system.

Then

$$\Delta W = V S(k) I_0(k_r r) \sin \phi \quad , \tag{37}$$

where V is the voltage across each gap. One can write similar expressions for $\Delta\phi$, $\Delta r'$, and Δr.

For a two- or three-gap cavity or a $\beta\lambda/2$ or $\beta\lambda$ helix, one gets for $S(k)$ or $T(k)$ variations of the type shown in Fig. 13.

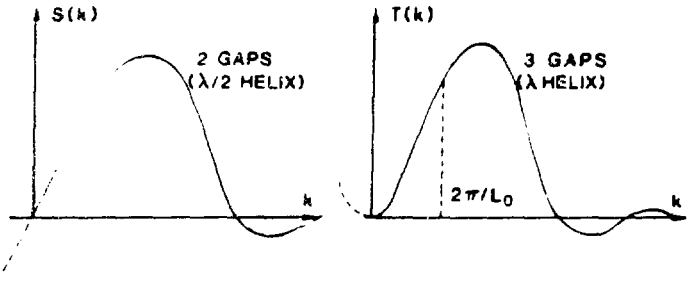

Fig. 13. Transit time factors for two or three gaps.

4.1 Accelerating Systems Without Symmetry

To compute particle dynamics in a system that is neither symmetrical nor antisymmetrical, one may add to the principal term (T or S) a contribution of the other parity (S or T). This correction must also, of course, apply to mid-gap coordinates computation. Computing time is increased but not doubled (an appreciable time is used for mid-gap values).

4.2 Fictitious Cavity of Double Length

It is possible to avoid the computation of mid-gap values by making the cavity input the middle of a fictitious cavity of double length, either symmetrical or antisymmetrical (Fig. 14), for which the sum would be 0 in the first half and equal to the real cavity in the second half. In this method, no symmetry is required for the real cavity.*

* Here, the footnote in Sec. 2.5 does not apply because the two fields, symmetrical and antisymmetrical, both can satisfy Maxwell's equation. Relations in T and S of the type given in Eq. (30) both apply rigorously.

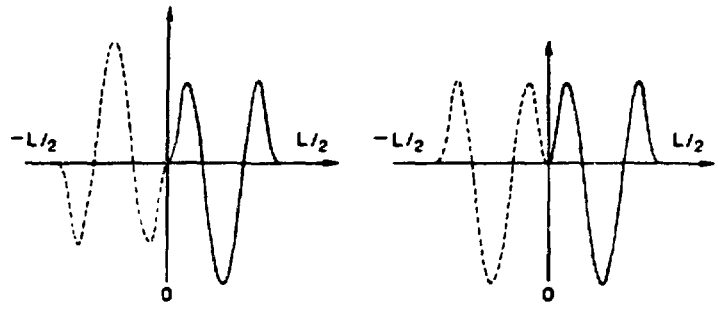

Fig. 14. Symmetrical and antisymmetrical fictitious cavities.

Because fictitious cavities may be very long (transit time of more than 10π in some test cases), it may be necessary to introduce second-order computation. One then has to add to the term (Eq. 34) an S term (but that term is equal to the T term because the field is the same) and two cross terms $T \times S$ and $S \times T$ (equal together). For such long cavities, n must, of course, be taken larger and may be equal to 5 or 6. Computing time for a bunch of trajectories (100 for example) still remains, however, much shorter than for a step-by-step integration of a similar accuracy.

Figure 15 shows trajectory coordinates inside a helix cavity of $\beta\lambda$ length optimized for $\beta \approx 0.08$; results of first- and second-order accuracies for a slow and a fast particle are indicated on Fig. 16. Such computations satisfy Liouville's theorem (see Sec. 3.2); from their increase (or decrease) when computing effective or rms emittances (see Chap. 6, Sec. 4), one sees the effect of nonlinearities (or couplings) that distort the emittance shape.

5. COMPARISON WITH CLASSICAL THEORY

In first-order expressions (Eq. 30), particle dynamics is the same as in a succession of steps with constant field, the field amplitude being, however, a function of the velocity (transit time factor T). Such a variation results from the nonconstant character of the real field. Let us consider the simple case of a sinusoidal variation (see Sec. 6.2, the case of an RFQ structure) that we shall divide into $\beta\lambda$ periods. Let us take, for instance, a field in

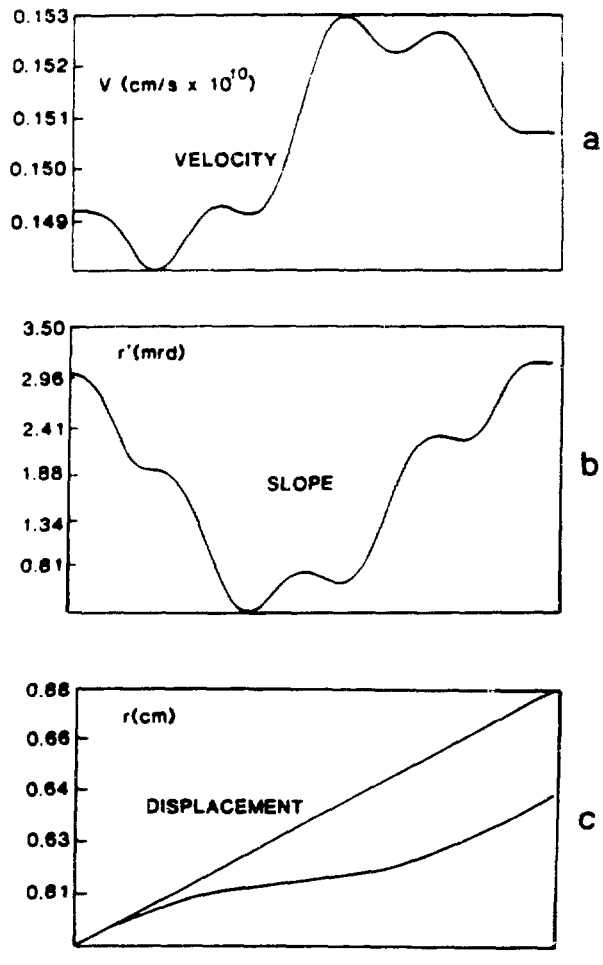

Fig. 15. Velocity v, slope r', and radial position r for a slow particle crossing a helix.

cos z between $-\pi$ and $+\pi$. One finds

$$T(k) = \int_{-\pi}^{+\pi} \cos kz \cos z \, dz \tag{38}$$

and

$$T(k) = \frac{\sin (k-1)\pi}{k-1} + \frac{\sin (k+1)\pi}{k+1} \quad . \tag{39}$$

For a synchronous particle, k = 1 and

$$T(1) = \pi \quad \text{and} \quad \partial T(1)/\partial k = \pi/2 \quad . \tag{40}$$

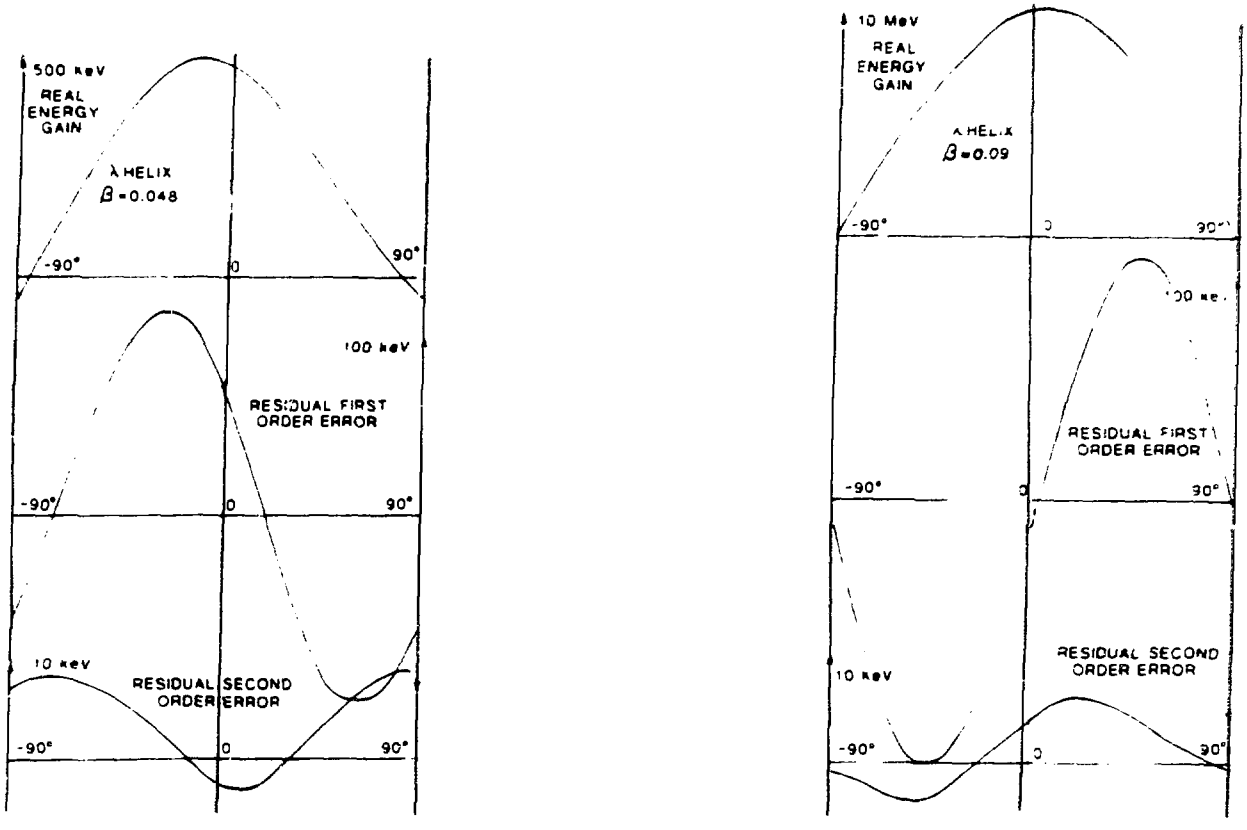

Fig. 16. Energy gain as a function of input phase for slow and medium velocity particles.

If, on the contrary, one had taken the periods from $-\pi$ to $+\pi$ with a field in sin z, one would have obtained

$$S(k) = \int_{-\pi}^{+\pi} \sin kz \sin z \, dz \tag{41}$$

and

$$S(k) = \frac{\sin (k-1)\pi}{k-1} - \frac{\sin (k+1)\pi}{k+1} \tag{42}$$

from where

$$S(1) = \pi \quad \text{and} \quad \partial S(1)/\partial k = -\pi/2 \ . \tag{43}$$

The complete variations of $T(k)$ and $S(k)$ are shown on Fig. 17, which shows also the results for segments $2\beta\lambda$ long.

There is clearly a difference in beam dynamics computations according to the segmentation used. Such a difference is real because periodic acceleration presents similar

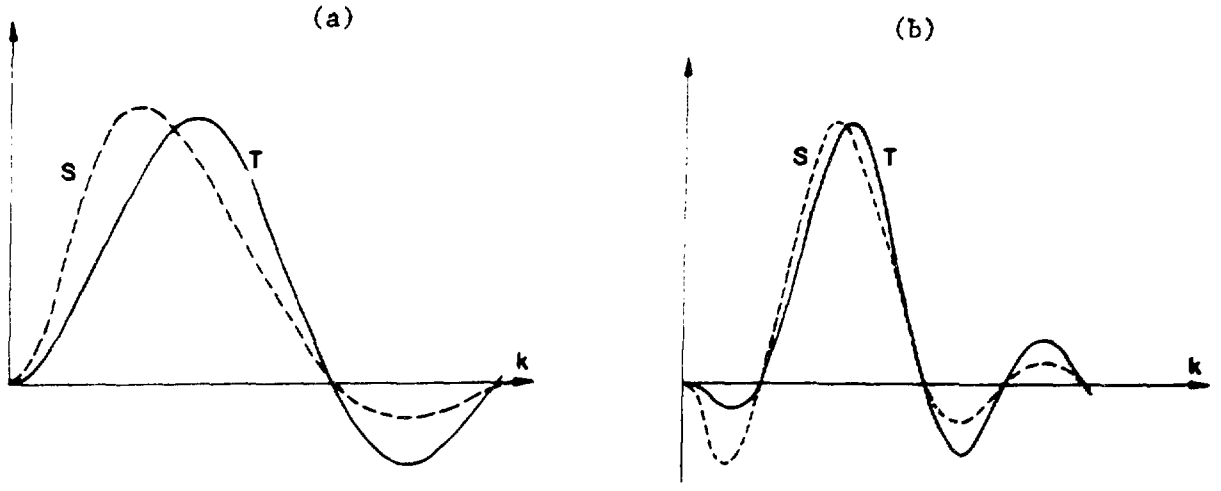

Fig. 17. Transit time T and S factors for a sinusoidal field and two types of segmentation. (a) segments $\beta\lambda$ long and (b) segments $2\beta\lambda$ long.

properties in phase space to periodic focusing; according to the point of observation, the matched figure does not present the same shape (2π and 4π, however, lead for $k = 1$ to the same values).

First-order relations (Eq. 30) take into account this property of the field, assuming, however, a thin-lens approximation. In second-order expressions, some terms in $T^2(k)$ correspond to a thick-lens correction while other terms provide a finer analysis of the effect of field distribution.

Instead of looking for the highest accuracy, one may be satisfied with a *smooth approximation.* This is what is obtained by neglecting the second term in Eqs. (39) or (42). This is the classical theory case. It would then be easy to take into account thick-lens corrections by taking the ellipses mentioned in Chap. 2, Sec. 2.1 for the trajectory in phase space.

6. DYNAMICS CODES INCLUDING FOCUSING

6.1 Drift-Tube Linacs

Various expressions given previously concern only gaps; in a drift-tube linac, focusing is generally provided by quadrupole lenses in drift tubes, i.e., between the gaps. In a way

similar to beam transport codes, one can compute in succession the effect of gaps and quads with a formalism of the matrix type (in particular for transverse motion). For gaps, most codes use expressions of the type found in Eq. (30) using mid-gap coordinates. This is the case when space charge is to be computed (see Chap. 6) because these codes require the knowledge of bunch shapes in the gaps. Second-order corrections are always ignored [Promé et al.]. For zero space-charge computations and in particular for heavy ion boosters with long cavities, a code exists following the method described in Sec. 6.2 with second-order corrections (ΔW_{corr} and Liouville's terms).

6.2 RFQ Linacs

A classical integration is generally used by segmenting the RFQ field (see Chap. 3, Eq. 13), for instance, in 20 parts per $\beta\lambda$ period. This $\beta\lambda$ period is the structure period for acceleration as well as for quadrupole field properties. Each segment not having any symmetry (see Sec. 4.1) might require the computation of two factors, T and S, with their derivatives. Terms in r' giving the effect of the slope of the trajectories are neglected. Some codes add to the phase term (Eq. 24) (but with T and S terms) a small correcting term to satisfy completely Liouville's theorem (and not only to first order). Transverse motion includes two terms in A and X (see Eq. 13 of Chap. 3) and is computed in a matrix form.

According to the results found in Sec. 4, it should be possible to treat the dynamics with much longer segments: one or two per $\beta\lambda$ period, or even segments of several $\beta\lambda$ length, inasmuch as space charge (see Chap. 6) that requires relatively long computing time is usually computed only once or twice per period. Also, one may take only the smooth approximation (see Sec. 5); however, one would lose the knowledge of periodic emittance variations.

CHAPTER 6

HIGH INTENSITIES AND SPACE-CHARGE EFFECTS

Several types of difficulties arise when one tries to increase the beam intensity in a linac. Some of these difficulties depend on the average intensity while others are peak intensity dependent. A large average intensity requires a large rf power and, therefore, efficient cooling of the rf structure. In the case of beam loss, there is also a risk of local heating and contamination (relative losses increase with intensity). In peak intensity, one must also distinguish between pulse intensity and bunch intensity (not equal when all the buckets are not filled).

During a pulse (or even the crossing of a long bunch), the beam takes out a fraction of the stored energy and the structure has to be refilled (as mentioned in Chap. 4, Sec. 8). For good beam quality, rf tolerances are usually about 1% in amplitude and 1° in phase (sometimes even less); such an accuracy is not easy to achieve under transient operation. Even in cw operation, when the beam absorbs several times more power than the rf losses, and the cavity impedance depends essentially on the beam amplitude and phase, the feedback loop, as said in Chap. 4, is not easy to adjust (especially if beam intensity can be changed).

The intensity of a bunch, i.e., its charge, is limited by interparticle repulsion. This effect is usually referred to as "space charge," and this chapter will be devoted to this subject.

Charge neutralization to counteract space charge — by electrons for positively charged ions, for example, — is possible and may occur spontaneously. This neutralization will occur by gas ionization, for instance, if the vacuum is not high enough. Another neutralization process results from secondary emission from particle collision with diagnostics devices, grids, or other losses. Much experimental and theoretical work needs to be done to take advantage of neutralization and guarantee its stability, reproducibility, and compatibility with acceleration.

1. CHARGE DISTRIBUTION IN A LINEAR REGIME

The assembly of charges of the same sign in a continuous beam or a succession of bunches produces an electric field that adds to the focusing and phase stable fields, acting against them and hence reducing beam stability. Such a *space-charge field* distribution depends on the charge distribution. To start with, it is interesting to consider the case where such a field would be linear in order to maintain the linear character of the focusing.

Space-charge fields satisfy

$$\nabla \cdot \mathbf{E}_{s.c.} = \rho/\varepsilon_0 \tag{1}$$

and only a uniform distribution will give linear fields (a necessary but not sufficient condition; image effects usually introduce nonlinear fields). In free space, one can show that a continuous uniform beam of circular or elliptic cross section produces a linear field inside it. This linear character is also true for a uniformly charged ellipsoid.

In a linear motion, a beam that is matched in all directions is defined by quadratic invariants. For an elliptical or ellipsoidal distribution in configuration space, the phase-space distribution is hyperellipsoidal in four or six dimensions.

Let us try to find the hyperellipsoidal distribution to which there is a corresponding uniform distribution in the configuration space. Let us consider a hypersphere (for simplicity) and take

$$\left.\begin{aligned} t_2 &= r_2^2 = x_1^2 + x_2^2 \\ t_3 &= r_3^2 = x_1^2 + x_2^2 + x_3^2 \\ t_4 &= \ldots \end{aligned}\right\} \tag{2}$$

corresponding to 2, 3, ... dimensions, and let us call $\rho_2(t)$, $\rho_3(t)$, $\rho_4(t)$, ... the corresponding density distributions. From a classical derivation, if ρ_2 is the projection of ρ_4 [Lapostolle, 1966], one has

$$-\pi\rho_4(t) = \frac{d}{dt}\rho_2(t) \quad . \tag{3}$$

Similarly, one would have

$$\pi^2\rho_6(t) = \frac{d^2}{dt^2}\rho_2(t) \quad . \tag{4}$$

Through a slightly longer derivation, one finds

$$\rho_3(t) = 2\pi \int_t^\infty \rho_6(t_6)\sqrt{t - t_6}\, dt_6 \quad . \tag{5}$$

and

$$\pi^2 \rho_6(t) = \frac{d^2}{dt^2} \int_t^\infty \frac{\rho_3(t_3)}{\sqrt{t_3 - t}}\, dt_3 \quad . \tag{6}$$

These relations show that for a uniform continuous beam, the 4-D phase-space distribution is a surface distribution on a hyperellipsoid (called *Kapchinskij-Vladimirskij or K-V distribution*) [Kapchinskij et al.]. Such a distribution is not realistic.

For an ellipsoidal bunch, the 6-D distribution would also go to infinity on a 6-D hyperellipsoid with the addition of a sheath of the other sign. This is totally nonphysical.

For weak space charge, where $\mathbf{E}_{\text{s.c.}}$ can be neglected with respect to external fields, the previous relations easily give configuration space densities corresponding to uniform or Gaussian phase-space distributions.

2. LINEAR ENVELOPE EQUATIONS. K-V EQUATIONS

Let $\pm k^2(s)$ be the periodic focusing gradient applied and $\mathbf{E}_{\text{s.c.}}$ the space-charge field. The transverse equations of motion of the beam particles can be written:

$$x'' \pm k_x^2(s)x - \frac{q}{m\gamma^3 v^2} E_{x,\text{s.c.}}(x, y, s) = 0 \quad , \tag{7}$$

with a similar equation in y, the derivatives being taken with respect to s. If the space-charge field is computed in a frame moving with the beam at velocity v, it is purely electrostatic (the changes in the beam cross section are assumed sufficiently slow). In the laboratory system then, there is a magnetic field, the action of which is equal to β^2 times the electric field and subtracts from it, multiplying its value by $1 - \beta^2 = 1/\gamma^2$. This explains the γ^3 term added to the relativistic correction in the last part of Eq. (7).

In such a general equation, $E_{x,\text{s.c.}}(x, y, s)$ is usually complex. For a uniform density, however, it is linear in x and independent of y. For a circular beam, the relations are particularly simple. One has

$$E_{r,\text{s.c.}}(r) = \frac{\rho_0 r}{2\varepsilon_0} \quad , \tag{8}$$

and one can write

$$E_{x,\text{s.c.}}(x,s) = \frac{\rho_0(s)x}{2\varepsilon_0} = \frac{I}{2\pi\varepsilon_0 v a^2(s)}\, x \quad , \tag{9}$$

where a is the beam radius. For an elliptic beam of semiaxes a and b, one would have

$$E_{x,\text{s.c.}} = \frac{I}{\pi\varepsilon_0 v(a+b)}\frac{x}{a} \quad . \tag{10}$$

From such relations, using a derivation similar to the one used by Courant [Courant et al.] to compute the so-called β function, one easily gets the K-V envelope equations* [Kapchinskij et al.]:

$$\begin{cases} a'' \pm k_x^2(s)a - \dfrac{EM_x^2}{a^3} - \dfrac{2K_2}{a+b} = 0 \\ b'' \pm k_y^2(s)b - \dfrac{EM_y^2}{b^3} - \dfrac{2K_2}{a+b} = 0 \end{cases} , \tag{11}$$

where EM_x and EM_y are the beam emittances in x and y (the area of elliptic surfaces uniformly filled in the planes xx' and yy' divided by π).

One has

$$K_2 = \frac{Iq}{2\pi\varepsilon_0 m\gamma^3 v^3} \quad , \tag{12}$$

where I is the beam current and q is the particle charge.

In the case of circular symmetry, there is only one equation instead of two, as in Eq. (11):

$$a'' \pm k^2(s)a - \frac{EM^2}{a^3} - \frac{K_2}{a} = 0 \quad . \tag{13}$$

This system can be extended to three dimensions (but for a distribution that has been seen as unphysical), and for a sphere, one has

$$a'' \pm k^2(s)a - \frac{EM^2}{a^3} - \frac{K_3}{a^2} = 0 \quad . \tag{14}$$

For ellipsoidal bunches, the last term can be expressed (in the general case of three different half-axes a, b, and c) with the help of elliptic integrals of the second kind. When

* In order to find these equations, one may look in Eq. (7) [with its last term expressed by Eq. (9)] for a solution of the form $x(s) = a(s)\cos[\psi(s) + \phi]$. It is easy to obtain the relation $\psi'(s) = \text{const}/a^2(s)$ and to notice that the constant is simply the emittance.

a, b, and c are not different by a factor larger than 2 or 3, one may use approximate expressions (to $\pm 10\%$) such as:

$$\frac{9K_3}{(a+b+c)^2} \quad or \quad \frac{3K_3}{ab+bc+ca}$$

with

$$K_3 = \frac{qQ}{4\pi\varepsilon_0 m\gamma^3 v^2} \quad , \tag{15}$$

where Q is the total charge of the bunch. One can also use the more classical but complicated relations with an f factor introduced by Lapostolle [1965] and given by Gluckstern [1970 page 828].

3. NONUNIFORM DENSITY DISTRIBUTIONS. UNIFORM DENSITY IN PHASE SPACE (Waterbag) [Kapchinskij, 1966] [Lapostolle, 1969]

It is possible to compute stationary distributions other than K-V. It is interesting, for instance, to consider a uniform distribution in phase space (waterbag) or a Gaussian distribution.

The two-dimensional waterbag distribution (4-D in phase space) is particularly simple, especially for circular symmetry. It can be obtained with the help of the Vlasov and Poisson equations. Letting ϕ be the total potential (external + space charge) in the reference frame moving with the beam, one finds that it must satisfy

$$\nabla^2\phi = C \cdot \phi \tag{16}$$

(in the 3-D case, a similar expression holds with slight corrections). The constant C is proportional to the density in the 4-D phase space, i.e., beam brightness.

For high densities, the charge distribution in the beam takes the form shown in Fig. 1, governed by the relation:

$$\rho = \rho_0\left[1 - \frac{I_0(r\sqrt{C})}{I_0(R\sqrt{C})}\right] \quad , \tag{17}$$

where R is the external radius of the beam. The density is uniform for most of the beam, just cancelling the external field by its own space charge with a fast drop at the edges, in

a thickness equal to the Debye length λ_D. Particles then move freely in the beam (as they do in a neutral plasma) bouncing on the edges of the beam.

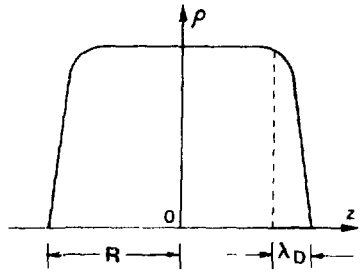

Fig. 1. Radial density distribution in a space-charge-dominated beam.

I. Hofmann [Hofmann, 1987] has shown that for high space charge, if the average tune depression is σ/σ_0, one has for a rotationally symmetrical beam

$$\lambda_D/R \approx \pi\sigma/\sigma_0 \tag{18}$$

with

$$\sigma_0/\sigma - \sigma/\sigma_0 = \delta = \text{const} \cdot \; I/EM \quad . \tag{19}$$

For a spherical bunch, one would have

$$\lambda_D/R \approx \frac{2\pi}{3}\,\sigma/\sigma_0 \quad .$$

Such a situation corresponds to a highly nonlinear motion. The emittance shape, in a projection over xx' or yy' planes, becomes rectangular with the density decreasing towards the edges.

A Gaussian-type distribution would give similar results, except for a smoother edge with a thin tail going to infinity.

Remark. As will be seen later, a tune depression σ/σ_0 (Eq. 18) or space-charge coefficient δ (Eq. 19) may present limits above which any beam transport becomes difficult. Because a single-valued relation exists between $R\sqrt{C}$ and these two coefficients, one way to make the transport of a very intense and very low emittance beam easier is to split it into several minipencil beams of the same brightness C, but with a smaller radius R.

4. EFFECTIVE (OR RMS) ENVELOPE EQUATIONS [Lapostolle, 1971]

Let us again consider the particle motion of Eq. (7), multiply each term by x, and take the average over all particles. The result is

$$\overline{xx''} \pm k_x^2(s)\overline{x^2} - \frac{q}{m\gamma^3 v^2}\overline{xE_{x,s.c.}}(x,y,s) = 0 \quad . \tag{20}$$

For circular symmetry, the averages are easy to compute with the help of the relations

$$\left.\begin{aligned} \frac{d}{ds}\overline{x^2} &= 2\overline{xx'} \\ \frac{d^2}{ds^2}\overline{x^2} &= 2\overline{xx''} + 2\overline{x'^2} \end{aligned}\right\} \quad ; \tag{21}$$

letting

$$q(r) = \int_0^r \rho(r) 2\pi\, r\, dr \tag{22}$$

such that

$$E_r(r) = \frac{q(r)}{2\pi\varepsilon_0 r}$$

and

$$\int_0^R rE_r(r)\rho(r)2\pi\, r\, dr = \frac{1}{2\pi\varepsilon_0}\int_0^R q(r)\frac{dq(r)}{dr}\, dr \quad ,$$

one gets

$$\tilde{a}'' \pm k^2(s)\tilde{a} - \frac{\widetilde{EM}^2}{\tilde{a}^3} - \frac{K_2}{\tilde{a}} = 0 \quad , \tag{23}$$

where

$$\tilde{a} = 2\sqrt{\overline{x^2}} \tag{24}$$

and

$$\widetilde{EM} = 4\sqrt{\overline{x^2}\;\overline{x'^2} - \overline{xx'}^2} \quad . \tag{25}$$

This last expression is the second-order invariant for a linear motion. The term K_2 is given by Eq. (12), and I is the total current;

Equation (23) is exactly the same as the K-V Eq. (13) provided rms-type dimensions as expressed by Eqs. (24) and (25) are used. Factors 2 and 4 have been introduced for the sake of consistency with the usual beam size and emittance values for a uniform beam. In

order to avoid any confusion, we shall call the *effective half axis* the quantity (Eq. 24) and the *effective emittance* the value (Eq. 25), with similar expressions for the y axis. For an exactly elliptical distribution, F. Sacherer [Sacherer] has shown that Eq. (11) applies in the same manner also.

For 3-D bunches, I. Hofmann [Hofmann, 1987] has obtained equations similar to the ones referred to in Eqs. (14) and (15) with, however, very small correcting terms.

The K-V envelope equations, provided they are written with the *effective beam dimensions and emittances* given from rms values by Eqs. (24) and (25), have a real physical meaning, which is valid for real beams, and they constitute a very valuable tool for studying beam evolution and matching problems as long as the effective emittances $\widetilde{EM}$ do not change, as will be seen later. Simulation codes show that envelope oscillations are accurately represented by such equations, provided the length of the computation is not too long.

5. ENERGY EQUATIONS [Lapostolle, 1971]

If instead of multiplying each term of Eq. (7) by x, as above, one multiplies by x', one gets

$$\overline{x'x''} \pm k_x^2(s)\overline{xx'} - \frac{q}{m\gamma^3 v^2}\,\overline{x'E}_{x,s.c.}(x,y,s) = 0 \quad , \tag{26}$$

where one immediately sees that the first two terms represent the derivatives of the average kinetic energy and potential energy of the particles in the external focusing field. The last term is then the derivative of the space-charge energy $W_{s.c.}$ (per unit length of beam or per bunch). This space-charge energy can be considered either as the electrostatic energy of the space-charge field or as half the potential energy of the particles in this space-charge potential (the factor 1/2, which appears usually in energy computations, is the same as the factor that appears in the energy of a condenser).

The kinetic energy can be written, with the help of Eq. (25),

$$\overline{x'^2} = \frac{\widetilde{EM}^2/16 + \overline{xx'}^2}{\overline{x}^2} \quad , \tag{27}$$

and one may obtain a new form of K-V equations. New terms appear, however. To isolate them, it is convenient to subtract Eq. (23), where each term has been multiplied by $\tilde{a}'$, from the equation now obtained and then do the same for each coordinate. Adding the two or three residues (2- or 3-D cases), the result can be written in the form [Wangler et al.]

$$\sum_{x,y,z} \frac{1}{4\tilde{a}^2} \frac{d}{ds} \widetilde{EM}_x^2 \approx -K \frac{d}{ds} \left(\frac{W_{s.c.} - W_{s.c.,u}}{W_0} \right) , \tag{28}$$

where $W_{s.c.}$ is the beam space-charge energy, $W_{s.c.,u}$ is the space-charge energy corresponding to a uniform density distribution with the same effective dimensions (this term corresponds to the last term of Eq. (23) with the K-V form, i.e., uniform density), and W_0 is a normalizing factor. (In the case of a nonelliptic distribution or for three dimensions, whether they are ellipsoidal or not, small but complicated correcting terms should be added). The space-charge energy $W_{s.c.}$ depends on the charge distribution. The distribution, which gives the minimum energy with the constraint of fixed rms dimensions, is uniform (see Sec. 11). This energy is higher for both hollow and peaked distributions.

Equation (28) shows that if a *mismatched* distribution entails density oscillations, these will produce emittance oscillations. More generally, a charge redistribution will take place, leading to a new emittance value. According to Eq. (28), one may also expect emittance transfers, or rather *kinetic energy* ($\sim \widetilde{EM}^2/\tilde{a}^2$) transfers, with the possibility of thermalization or equipartition. Eventually, in the case of resonances between density oscillations and envelope oscillations resulting from a mismatch or periodic focusing (or through neglected image effect terms), there may be a relatively slow emittance growth if the relative phase allows it.

6. DENSITY OSCILLATIONS AND INSTABILITIES

R. Gluckstern [Gluckstern, 1970] has studied the set of oscillation modes for a K-V circular beam. Apart from the well-known coherent and envelope oscillations (breathing and quadrupolar modes), there exists a full set of modes defined by an azimuthal and a radial order similar to EM waves in a circular waveguide. Frequency oscillations depend

on beam intensity and many of the modes become unstable when space charge is above some threshold. The first unstable mode appears for a tune depression (see Sec. 3):

$$\begin{cases} \sigma \approx 0.4\sigma_0 \\ \text{or } \delta \approx 2 \end{cases} \tag{29}$$

Gluckstern's work was extended to elliptic beams by I. Hofmann. [Hofmann, 1980]

For nonuniform distributions, no similar theory has been derived. It has been shown, however, that no instability occurs when the density in phase space is monotonically decreasing when moving away from the center. Approximate computations and simulations have confirmed this result, exhibiting oscillations that do not differ very much from the K-V case except for stability. It is observed, however, that if there are stable situations in a continuous beam and continuous focusing, unstable bands may appear in periodic focusing through resonance effects. [Laslett et al.]

7. CURRENT LIMITS. ACCELERATOR DESIGN

It is possible to write envelope equations for a linac in a normalized form to take into account the energy change, using as emittances the input transverse emittances and a longitudinal emittance resulting from the bunching process. According to the available aperture (including some effect from misalignments) and the longitudinal acceptance (taking into account the slight displacement of stable phase under space-charge conditions), one may derive maximum current values transportable without loss. For example, one may compute the influence of focusing strength on this current limit. Figure 2 shows a typical result. For weak focusing, the beam is wide and only a small increase in intensity is enough to make the beam hit the aperture. For stronger focusing, the transverse dimension of the bunches becomes small, also leading to an increased space-charge field in the longitudinal direction where particles may be lost. Focusing must not be too strong in order to avoid resonances with periodic focusing. The phase shift per period σ_0 without space charge must never be larger than 90° (60° is even a safer limit) to avoid the depressed tune σ coming into any resonance.

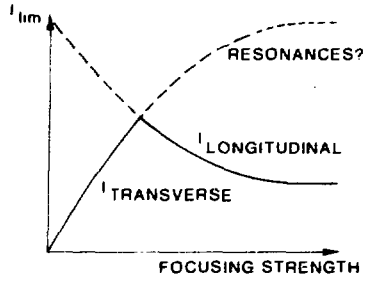

Fig. 2. Maximum current resulting from transverse and longitudinal limitations.

From these limitations, there is an optimum focusing value (as indeed observed and used experimentally). The value of this optimum is not, however, obtained exactly without taking into account a change in emittance values, as will now be explained. This technique has been successfully used for the design of the CERN Linac 2 [Warner] and [Weiss].

8. EMITTANCE GROWTH. COMPUTER SIMULATION. HALO FORMATION LOSSES [Wangler et al.]

In the previous paragraph, the emittances were assumed constant. Equation (28) has shown, however, that there could be emittance growth or exchange. For several effects, estimates or limits can be computed today. However, details of the process still remain unclear.

Simulation with Monte Carlo type computations, which are relatively accurate, remains a preferred tool, and it is possible to estimate emittance increases and to include them in envelope equations in order to optimize a linac design. Such simulations show that density oscillations produce wrinkles on 4-D or 6-D phase-space boundaries. Even for a distribution of limited extent, halos appear around the beam (such an effect is obviously less clear for Gaussian-type distributions for which there is always a halo).

An empirical law found by R. Chasman and M. Promé [Chasman and Promé] stated that the sum of initial effective emittances increases (quadratically) through a linac by an amount proportional to the intensity. Such a property has now found a theoretical interpretation [Wangler et al.]. Particles going into such halos or tails of distribution

are at risk of being lost (in such a case, $\widetilde{EM}$ goes down, limiting the predicted increase experimentally).

9. TRANSVERSE MODES. BEAM BLOWUP [Gluckstern, 1984]

The beam blowup (BBU) phenomenon resulting from transverse mode excitation, which is very dangerous for electron linacs (see Chap. 7, Sec. 4), is not a concern for Alvarez or drift-tube linacs with present intensities. Transverse mode penetration in the gaps is very small. R. Gluckstern has derived a theory to evaluate such a risk in any type of structure.

10. CONCLUSIONS

One may say, in general, that when one tries to accelerate a very bright beam (high current — low emittances), even if one avoids resonances that occur in particular for $\sigma_{x,y,z} \approx 60°$, charge redistribution often leads to an initial fast emittance growth; this is followed by a slow growth when velocity distributions tend to equalize. The velocity distributions become of thermal type with some halo formation, leading to particle losses. There is not yet a theory predicting the exact type of distribution in such halos. Simulation cannot give an accurate representation, especially if these halos are sparse and widely spread. In a very high intensity machine, where losses must be limited to 10^{-3} or even 10^{-4} at high energy, this unknown remains a challenge for designers. Fortunately, experimental results (as well as simulation) show that losses decrease very fast when energy increases. However, the values are difficult to use because nonlinearities that are responsible for the halos also depend on image effects, which are very sensitive themselves to misalignments that are not well known. Of course, it is known experimentally that an intentional misalignment changes the beam quality.

It has been confirmed experimentally [Kim et al.] that a continuous beam in a beam transport channel can accept very high intensities with tune depressions down to $\sigma/\sigma_0 = 0.1$ (the extreme limit reached in standard linacs does not exceed 0.4). Such a possibility had been foreseen from simulation work done in the 1970s [Lapostolle, 1978].

It might be that very high intensities could be accelerated in induction linacs where the longitudinal–transverse coupling is weak when there are very long bunches. Simulation results are not accurate enough for this case. Since the beginning of the 1980s, scientists at Berkeley have been conducting experiments that should shed light on this important question [Kim et al.].

11. EXPRESSION OF SPACE-CHARGE ENERGY. NONLINEAR ENERGY.

For the sake of simplicity, we shall discuss only the case of a continuous beam with circular symmetry. Let us then consider a beam of density $\rho(r)$ for $r \leq r_0$ inside a metallic pipe of radius $R(R > r_0)$. The space-charge energy

$$W_{s.c} = \varepsilon_0 \int_0^R \frac{E_{s.c.}^2(r)}{2} 2\pi r dr \tag{30}$$

equals, according to

$$E_{s.c.}(r) = \frac{q(r)}{2\pi\varepsilon_0 r} \tag{31}$$

$$W_{s.c.} = \int_0^R \frac{q^2(r)}{4\pi\varepsilon_0 r} dr \quad , \tag{32}$$

where $q(r)$ is given by Eq. (22).

Letting

$$u = r^2 \quad , \tag{33}$$

one obtains

$$W_{s.c.} = \int_0^U \frac{q^2(u)}{8\pi\varepsilon_0 u} du \quad , \tag{34}$$

which one can use to compute the space-charge energy and its variations with the distribution $\rho(\mathrm{u})$ or $q(u)$, such that

$$q(u) = \pi \int_0^u \rho(u) du \quad . \tag{35}$$

If one then compares distributions with the same total charge Q, the same effective radius, and $\tilde{u}$, they will be such that

$$Q\tilde{u} = \pi \int_0^U u\rho(u) du = UQ - \int_0^U q(u) du \tag{36}$$

does not depend on the distribution $q(u)$. The distribution that minimizes $W_{s.c.}$ will also be such that Eq. (34) is independent of small changes in $q(u)$ so that, whatever the constant λ is (Lagrange multiplier principle),

$$W_{s.c.} + \lambda(Q\tilde{u} - UQ) \tag{37}$$

is also independent of small changes in $q(u)$. There exists, then, a value of λ for which Eq. (37) is equal to zero. From Eqs. (34) and (36), one has

$$q(u) = 8\pi\varepsilon_0\lambda u \quad , \tag{38}$$

and from Eq. (35),

$$\rho(u) = \text{const} \quad . \tag{39}$$

A uniform distribution minimizes space-charge energy so that the right-hand side of Eq. (28), which contains the *nonlinear space-charge energy* [Wangler et al.], also contains the difference with a minimum. As was stated earlier, because a bright beam takes a given uniform distribution, the energy in the right-hand part of Eq. (28) tends to zero, leading to an emittance growth if the initial distribution was not uniform (charge redistribution mentioned in Sec. 10).

12. NOTES ON SIMULATION CODES

In Monte Carlo simulation codes, charge distribution is usually represented by a few thousand *macrobeamlets* or *macroparticles*. Two main computational methods are used.

12.1 Particle-to-Particle Interaction

In this method, the forces between *macrobeamlets* or *macroparticles* are computed in a two- or three-dimensional space, including, if necessary, image charges. One difficulty results from *collision effects*, the importance of which comes from the concentration of relatively big charges in each *macroparticle*. In a real system, such charges are in particles that are distributed over a certain volume, and such volumes can interpenetrate

without collision. A way to avoid collisions is to give a nonzero radius a to the macrobeamlets or particles, either giving the repulsive field a law in r/a for $r \leq a$ and in a/r (2D) $[a^2/r^2(3D)]$ for $r \geq a$ or a law in $1/(r+a)(2D)[1/(r^2+a^2)(3D)]$. In this last case, space charge is slightly reduced, but not appreciably. For space-charge energy computation, one may also assume the charge distributed in volumes of radius a (Eq. 32). The choice of a is, of course, arbitrary and results from empirical tests.

12.2 Particle in Cell Codes (PIC)

In this method, the charge distribution is defined by the number of particles in each cell of a mesh. From this distribution, one computes the field (potential), first on each node and then everywhere using interpolation. Field computation can be made directly by putting all the charges of each cell in its center or, more rapidly, by a fast Fourier transform (FFT) routine. It is again possible to take image effects into account or make a free-space computation with a mesh matched to the beam dimensions. (With the FFT method, one then computes the potential on the outer mesh boundary from an external expansion that, in order to converge (radius of convergence), requires a square mesh. A rectangular mesh may be used for a flat beam in a second, more accurate computation). Irregular mesh dimensions may sometimes cause a transfer of energy or a *heating* of the beam (emittance growth).

There are no more collision effects, but the displacement of all the charges in the middle of the cells entails a loss of accuracy. It is possible to improve the computation by distributing the charge of each particle according to its position in three to five neighboring cells. In any case, however, the mesh size still fixes a limit to the resolution of the field or potential definition.

12.3 Integration Steps

An integration routine must be chosen that will satisfy Liouville's theorem. This is not often the case with formulas that are too elaborate. One therefore frequently uses very simple methods (e.g., leap frog) with relatively short integration steps.

CHAPTER 7

ELECTRON LINACS COMPARED TO PROTON MACHINES

Electrons are very light particles, and they reach relativistic velocities very quickly. They travel inside a linac at an almost constant velocity, the velocity of light. No phase stability exists; on the contrary, energy gain depends on the accelerating field. Accelerating cavities are usually of a traveling-wave type. They may propagate higher order modes that are beam excited, which can induce the beam breakup (BBU) phenomenon.

Relatively recent developments have led to an energy increase of 50% without changing the input power, but by reducing the pulse length. Positron acceleration, currently made for e^+e^- colliders, may eventually offer some surprising effects.

1. PARTICLE DYNAMICS AT A VELOCITY EQUAL OR CLOSE TO THE VELOCITY OF LIGHT

The classical stability diagram of constant nonrelativistic velocity protons (Fig. 1) progressively changes when the synchronous velocity approches c (Fig. 2), because more and more energy is needed to pass this synchronous velocity during phase oscillations. When the synchronous velocity equals the velocity of light c, the diagram opens up and no phase oscillation can take place: the phase is fixed.

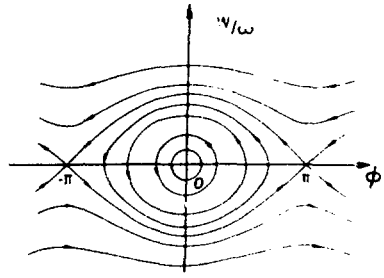

Fig. 1. Phase-space trajectories for constant velocity $v \ll c$.

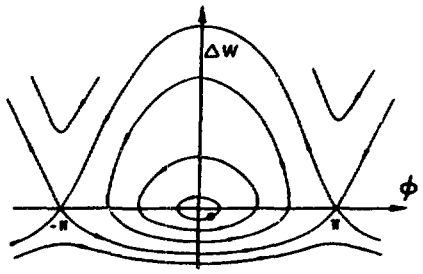

Fig. 2. Phase-space trajectories for constant velocity $v \approx c$.

Integration of the relativistic equation,* instead of using the method in Chap. 2, can be derived in the following way:

$$\frac{d}{dt}(mv_z) = eE_z \sin\left(\omega t - \frac{\omega z}{c}\right) \tag{1}$$

leads, multiplying both members by $u' = du/dt$ where

$$u = z - ct \tag{2}$$

and

$$\Delta\phi = -\frac{2\pi u}{\lambda} \tag{3}$$

to

$$\frac{1}{\sqrt{-2c/u' - 1}} = \frac{\alpha}{2\pi}\left\{\cos\Delta\phi - \cos\phi_0\right\} \tag{4}$$

with

$$\alpha = \frac{eE_z\lambda}{m_0c^2} \tag{5}$$

where λ is the rf wavelength

$$2\pi\lambda = c/\omega \ , \tag{6}$$

and the kinetic energy W is related to $u' = du/dt$ by the relativistic relation

* It is a common practice to use a sine expression for electrons and a cosine expression for protons; $\phi = 0$ corresponds here to zero field.

$$\frac{W + m_0c^2}{m_0c^2} = \frac{-c/u'}{\sqrt{-2c/u' - 1}} \quad . \tag{7}$$

The relation between W and ϕ, which results from Eqs. (4) and (7), is shown in Fig. 3.

According to the value of α [Eq. (5)], the shape of the curves changes slightly in such a way that for $\alpha > \pi$, very low energy particles may reach relativistic velocities (also see Fig. 11). For protons, α would always remain very small, and this cannot be. Therefore, it is necessary to use low-velocity structures in order to accelerate them.

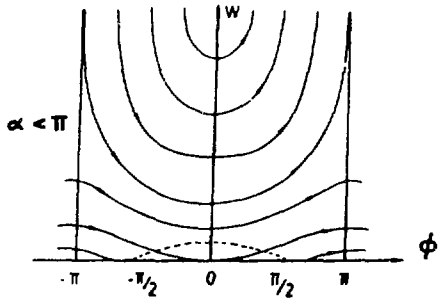

Fig. 3. Phase-space trajectories for $v = c$.

2. BEAM LOADING

A consequence of the type of dynamics described above is that output energy does not depend on the geometry. It depends on the phase of the particle and on the rf field level. Because the energy given to the particles comes from the rf field, the field level decreases for high intensities, and that entails a drop in the final energy. The energy obtained from an electron linac depends on the accelerated intensity (number of particles per pulse).

3. RF CAVITIES

The rf structures used in electron linacs are usually of the disk-loaded waveguide type (Fig. 4). Irises reduce the phase velocity, which is larger than c in a smooth waveguide, to c. The structure mode (see Chap. 4) is usually $\pi/2$ or rather $2\pi/3$, which gives a slightly

better shunt impedance Z_s. [For the $2\pi/3$ mode, there are fewer irises per wavelength (three instead of four). An integral number is essential to allow exact cell-by-cell adjustment during fabrication.]

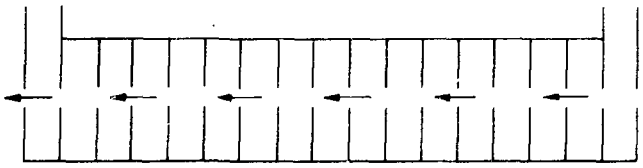

Fig. 4. Disk-loaded waveguide structure.

The group velocity (not much smaller for the $2\pi/3$ mode than for the $\pi/2$ mode) is always very low (between $c/50$ and $c/150$) because the bandwidth is very narrow. (The structure can be considered as a stack of pillbox resonators slightly coupled through the irises.) The group velocity v_g depends on the iris diameter, while Z_s is not very sensitive to it.

The structures are used in traveling-wave operation (the backward wave is only accelerating for π, 2π, ..., $n\pi$ structure modes). The attenuation A depends on the iris diameter, as does v_g. The iris diameter can be optimized in order to produce the maximal energy gain for a given input power. With the E_z field of the form

$$E_z(z) = E_z(0)e^{-Az} \quad , \tag{8}$$

the energy gain over the length L is

$$eV = e\int_0^L E_z(0)e^{-Az}dz = eE_z(0)L\,\frac{1-e^{-AL}}{AL} \tag{9}$$

with

$$\frac{V^2}{P} = 2A\,Z_s\frac{V^2}{E_z(0)^2} = 2Z_sL\,\frac{(1-e^{-AL})^2}{AL} \quad . \tag{10}$$

Assuming Z_s = const, the optimum value of A is such that

$$AL \simeq 1.25 \quad . \tag{11}$$

Then

$$V \simeq 0.9(P\,L\,Z_s)^{1/2} \quad . \tag{12}$$

The output power at the end of the structure is only about 10% of input power, so that the loss is not large. Thus, traveling-wave operation is justified inasmuch as it simplifies, in a short pulse operation, the coupling between the feeder and the structure itself at very high power levels (several 10s of MW at 3 GHz).

As just seen, the drop of rf level along the structure, due to losses, reduces the energy gain. It is possible to change the iris diameter along the structure to keep the accelerating gradient constant. Equation (12), however, remains approximately true as does the total attenuation and output power.

Electron linacs that require extremely high rf powers usually operate with very short pulses (a few microseconds at most), not much longer than the filling time of the cavities with very low group velocity. Thus, the useful time for beam acceleration is very short. The energy drop due to beam loading, as mentioned before, may be reduced by a proper adjustment of pulse shapes and, above all, by an accurate timing of the beam pulse inside the rf pulse.

4. BEAM BREAKUP

4.1 Regenerative Beam Breakup

Apart from the accelerating TM_0 mode, a disk-loaded waveguide also supports higher order modes. In particular, a transverse hybrid HEM_1 mode exists at a frequency of about 4 GHz for classical structures operated around 3 GHz (a hybrid TE-TM mode can deflect a particle even at the velocity of light)[Montague, p. 574]. For $v_\phi = c$, this mode is of the backward type (Fig. 5), with phase and group velocities being of the opposite sign.

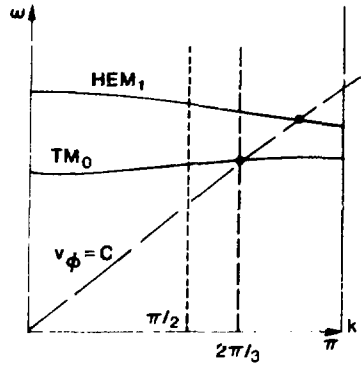

Fig. 5. Dispersion diagram for a disk-loaded waveguide.

When there is synchronism between a wave and particles, an energy transfer may take place from the wave to the particles (as in acceleration), but it can also take place the other way if proper phase conditions exist. This is indeed the mechanism set forth in traveling-wave tubes (microwave amplifiers). In such traveling-wave tubes (TWT), use is normally made of a longitudinal TM_0 mode, but the mechanism also exists for transverse modes (and these may be responsible for spurious oscillations). In an accelerating structure, such a transverse interaction leading to oscillations can take place inasmuch as the backward character of the mode gives a direct feedback without need of reflection (as in backward wave oscillators (BWO), sometimes called "carcinotron" oscillators). Above some current threshold, the structure behaves as a *self-oscillator*. This phenomenon in accelerators is called "regenerative beam breakup."

This phenomenon was discovered in the early 1960s, but the way to cure it already existed in some machines. A progressive change in iris diameter (see Sec. 3), made to keep the accelerating gradient constant (with a slight corresponding adjustment of cell diameter to keep v_ϕ constant), displaces the HEM_1 passband slightly and destroys the synchronism, which is now limited to shorter lengths that are too short to lead to oscillations. The instability threshold is then greatly increased.

4.2 Cumulative Beam Breakup

Before leading to an oscillation, the interaction between the beam and the HEM mode produces *amplification*. In very long machines, such as in the Stanford Linear Accelerator Center (SLAC) at Stanford, each cavity, with tapered geometry, acts like an amplifier of relatively wide bandwidth. None of the cavities oscillate, but their gain adds together. Any transverse noise coming from the electron gun or from any other origin can reach an amplitude such that the beam hits the edge of the irises when the current (which governs the gain) exceeds some value. This is *cumulative beam breakup*. The theory of cumulative BBU is complicated because short pulse operation limits BBU to its transient aspects. Stronger beam focusing can reduce the gain and push up the cumulative BBU threshold.

The risk of BBU, of both types, is greatly increased when the losses are negligible as is the case in new superconducting linacs. A method developed to move up BBU threshold is then to damp the HEM modes through proper coupling into an external loss circuit.

5. METHOD TO INCREASE BEAM ENERGY

SLED (Stanford Linac Energy Development) and *LIPS* (LEP Injector Power Saver).

The Stanford linac was originally designed with the idea that at a later date, its energy could be increased by increasing the number of klystrons by a factor of 2 or 4, leading to an energy doubling in the final state (or even more energy with more powerful klystrons). When such an extension was considered after an initial operation period, energy and klystron prices dictated that alternatives had to be found.

Recirculation of the beam with a second pass in the structure seemed difficult and hazardous at that time. The idea proposed was to *store the electromagnetic energy* of a klystron pulse and send it back into the structure *in a shorter time*. This led to the SLED principle based on transient properties of EM cavities.

Let us consider first the impedance seen from the feeder at the beginning of a square rf pulse sent into a resonant cavity. In the case of *overcoupling*, the impedance starts from 0, crosses the characteristic impedance Z_c, and reaches the value corresponding to

cw operation (see a Smith diagram in Fig. 6 where a case of slight detuning is also shown). Such a property entails a reflection at the input port, first with one phase (between 0 and Z_c) and then with the opposite phase.

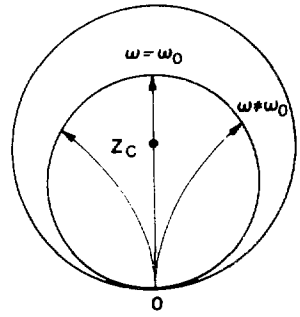

Fig. 6. Transient input impedance of an rf cavity (overcoupled) on the Smith diagram.

Let us now consider a system (Fig. 7) where, apart from the klystron and the accelerating structure, there is a high-Q cavity, all three elements being connected through a three-port circulator. At the beginning of the pulse, the klystron fills the cavity and the reflected wave goes to the structure. Nothing comes back to the klystron because the structure in TW mode is matched, and there is no reflection on its input.

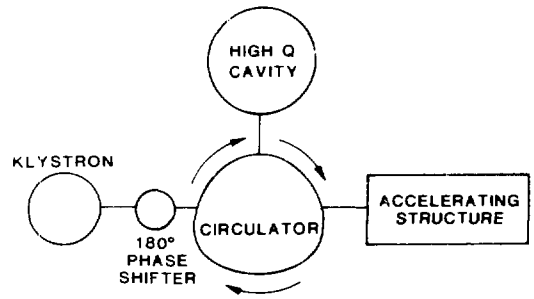

Fig. 7. Storage scheme in SLED.

Near the end of the pulse, a fast phase shifter reverses the signal by a 180° phase shift. Such a reversal is equivalent to the start of a new pulse of opposite sign and double amplitude that will initially be reflected on the cavity, adding to the remaining signal of the first pulse (Fig. 8). Forced by a signal of the opposite sign, the cavity is very quickly emptied before being filled again with the new phase. In practice, the klystron pulse is

stopped when the cavity is empty at the latest. During a very short period, the reflected wave going to the structure is almost doubled (tripled at most).

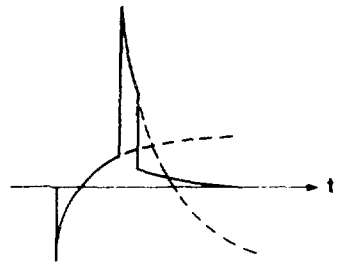

Fig. 8. Pulse diagram in SLED.

Of course, phase reversal is not instantaneous. In addition, the field level in the structure varies very quickly with time, so that taking into account the long transit time, particles only partially benefit from that increase. In practice, the energy gain can be increased by about 50%. With a proper timing between rf and beam pulses and the phase reversal, one can obtain a relatively flat energy spectrum during the beam pulse. A shaping of the pulses may even improve it.

In the scheme as shown, the elements added to the initial klystron structure circuit (phase shifter, cavity, and circulator) must hold very high field levels. In practice, the phase shifter can be put before the klystron at low level. The high-Q cavity under a short pulse is not a problem. However, there is no circulator for this high level; therefore, it is replaced by a 3-dB coupler connected to a double cavity (Fig. 9).

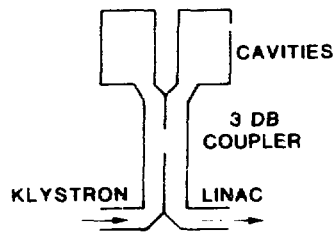

Fig. 9. Actual SLED circuit.

In the 3-dB coupler, the two hybrid waves (see Chap. 4, Sec. 5.2) must turn, respectively, in phase of $\pm 45°$ in such a way that their sum reaches the required -3-dB level.

Figure 10, as a matter of fact, shows these hybrid waves at input and output of the coupling zone. These waves, H_1 and H_2, add in circuit 1 and subtract in circuit 2. At input they are in phase and of equal amplitude ($E_2 = 0$). At output they must have rotated $\pm 45°$. Then in circuits 1 and 2, E_1 and E_2 have equal amplitude, each of them equal to $E_{1\ \text{input}}/\sqrt{2}$. They are 90° apart in phase.

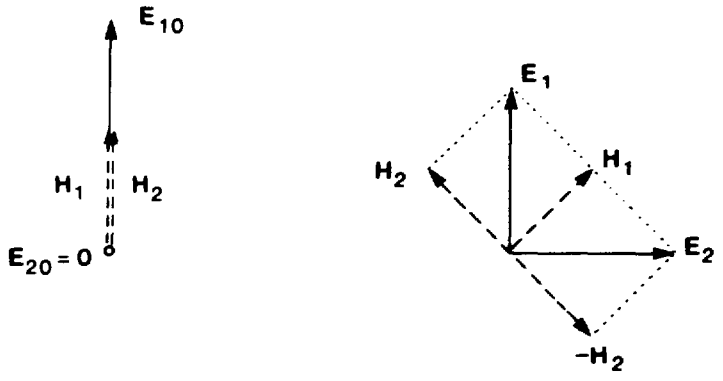

Fig. 10. Hybrid wave composition in a 3-dB coupler.

The two cavities are then filled with rf fields in quadrature. This 90° phase shift also exists in their reflected waves, which after crossing the 3-dB coupler in the other way, will become 180° in such a way that the reflected waves will enter circuit 2 to the linac whereas no signal will go back to the klystron.

6. POSITRON ACCELERATION

Positron acceleration is relatively common today. An intense electron beam of a few hundred MeV or more is directed onto a target where some of the gamma rays that are produced create e^+e^- pairs. A solenoidal lens focuses the secondaries (a few MeV in energy) into a second linac, properly phased, where they are accelerated. The conversion efficiency ranges from 1% to a few percent, except when the conversion energy is very high, such as at SLAC, where the efficiency can be larger than 1 (efficiency is roughly proportional to energy).

The first tests of positron acceleration led, however, to a surprising observation. Together with positrons an almost equal (if not higher) electron beam was accelerated; a

phase reversal of the accelerating field did not affect the result appreciably. This somewhat astonishing effect can be understood from Fig. 11, which is similar to the Fig. 3 diagram, but drawn for a value of α close to π, which is the common condition for electron linacs.

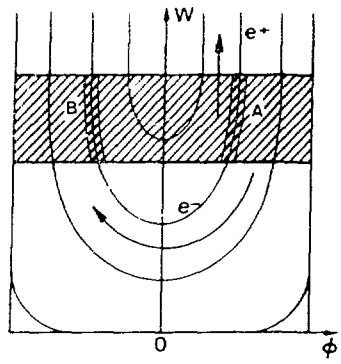

Fig. 11. Electron and positron acceleration.

Positrons are injected around A (small phase spread but relatively wide energy spectrum) simultaneously with the corresponding electrons of the pairs. For accelerating these electrons, one would, of course, choose the phase corresponding to B. In practice, however, electrons injected around A are first decelerated until they can slip in phase and be accelerated. Their final energy is a little lower, of course, but not much. A change in phase of 180° just inverts the relative situation of e^+e^-.

It is obvious that, in pairs, there is the same number of e^+ and e^-. However, depending on the thickness of the conversion target, some fraction of the primary electrons could emerge from it with a smaller emittance than the secondaries. One may then have an e^- beam that is more intense than the e^+ beam. In practice, the two species of particles are separated by deflecting elements that are used for alignment and optimization of the beam, thereby increasing the e^+/e^- ratio. Nevertheless, the possible presence of e^- in e^+ linacs is a concern for machine builders and users, inasmuch as cavity beam loading is produced by e^- as well as by e^+.

REFERENCES

Chapter 1

Alvarez, L. W., "The Design of a Proton Linear Accelerator," *Phys. Rev.* **70**, 799 (1946).

Alvarez, L. W., H. Bradner, J. V. Franck, H. Gordon, J. D. Gow, L. C. Marshall, F. Oppenheimer, W. K. H. Panofsky, C. Richman, and J. R. Woodyard, "Berkeley Proton Linear Accelerator," *Rev. Sci. Instrum.* **26**, 111–133, 210–219 (1955).

Blewett, J. P., "Radial Focusing in the Linear Accelerator" *Phys. Rev.* **88**, 1197 (1952).

Blewett, J. P., "The History of Linear Accelerators," in *Linear Accelerators,* P. M. Lapostolle and A. L. Septier, Eds. (North-Holland Publishing Company, Amsterdam, The Netherlands, 1970), Chap. A.1, p. 1.

Chamouard, P. A., J. M. Lagniel, J. L. Lemaire, "Saturne Linac Performances in $2\beta\lambda$ Mode for Polarized Protons Acceleration." Proc. Linear Accelerator Conf., Los Alamos National Laboratory report LA-9234-C, 352 (1981).

Ising, G., "Arkiv for Matematik," *Astronomi och Fyzik* **18**, p. 1 (1924).

Kapchinskij, I. M., "Linear Resonant Accelerators" (in Russian), Atomizdat, Moscow, "Particle Dynamics in Linacs," Los Alamos Scientific Laboratory translation LA-TR-80-10 (1966).

Kapchinskij, I. M., and V. Vladimirskij, Proc. Int. Conf. on High Energy Accelerators, Geneva, Switzerland, CERN, p. 274 (1959).

Kim, C., et al., "High Current Beam Transport Experiment at LBL," Proc. Int. Symposium on Heavy Ion Accelerators, Institute for Nucl. Study, Tokyo (1984), p. 460.

Lapostolle, P., "Density Distribution in Intense Beams," Proc. Conf. on High Energy Accelerators, Yerevan, Vol I, p. 205 (1969).

Sloan, D. H., and E. O. Lawrence, "Production of Heavy High Speed Ions Without High Voltage," *Phys. Rev.* **38**, 2021–2032 (1931).

Sloan, D. H., and W. M. Coates, "Recent Advances in the Production of Heavy High Speed Ions," *Phys. Rev.* **46**, 539 (1934).

Wideröe, R., *Archiv für Electrotechnik* **21**, 387 (1928).

Chapter 2

Alvarez, L. W., "The Design of a Proton Linear Accelerator," *Phys. Rev.* **70**, 799 (1946).

Alvarez, L. W., H. Bradner, J. V. Franck, H. Gordon, J. D. Gow, L. C. Marshall, "Berkeley Proton Linac," *Rev. Sci. Instrum.* **26**, 111–133, 210–219 (1955).

Becker, G. E., *Introduction to Theoretical Mechanics,* (McGraw-Hill, New York, 1956).

Bruck, H., *Accélérateurs Circulaires de Particules*, Institut National des Sciences et Techniques Nucléaires (Presses Universitaires de France, Paris, 1966); Los Alamos Scientific Laboratory translation, "Circular Particle Accelerators," LA-TR-72-10 Rev. (1972).

Corben, H., and P. Stehle, *Classical Mechanics*, 2nd ed. (J. Wiley and Sons, New York, 1960).

Hereward, H. G., "The General Theory of Linear Accelerators," in *Linear Accelerators,* P. M. Lapostolle and A. L. Septier, Eds. (North-Holland Publishing Company, Amsterdam, The Netherlands, 1970), Chap. A.2, p. 19.

Kapchinskij, I. M., *Theory of Resonance Linear Accelerators* (Harwood Acad. Publ., New York, 1985).

Lawson, J. D., *Physics of Charged Particle Beams*, 2nd ed. (Clarendon Press, Oxford 1987), Chap. 2.

Lichtenberg, A., *Phase Space Dynamics of Particles* (J. Wiley and Sons, New York, 1969).

MacMillan, E. M., "The Synchrotron," *Phys. Rev.* **68**, 143 (1945)

Sloan, D. H., and E. O. Lawrence, "Production of Heavy High Speed Ions," *Phys. Rev.* **38**, 2021–2032 (1931).

Smith, Lloyd, "Linear Accelerators" in *Handbuch der Physik,* Band XLIV (Springer, Berlin), 361–389 (1959).

Taylor, R., "Acceptance of Axially and Radially Oscillating Particles in the Harwell Linac Injector," AERE report 3013, U.K.A.E.A. Harwell, Berkshire, UK (1959).

Veksler, V. I., "A New Method of Acceleration of Relativistic Particles," *J. of Phy.* (Moscow), USSR **9**, 153 (1945).

Chapter 3

Abramowitz, M., and I. Stegun, Eds., *Handbook of Mathematical Functions, Applied Math*, Series 55 (National Bureau of Standards, Washington, DC, 1964).

Adlam, J. H., "A Method of Simultaneously Focusing and Accelerating," AERE GP/M 146, U.K.A.E.A., Harwell, Berkshire, UK (1953).

Angot, A., *Compléments de Mathématiques á l'usage des Ingenieurs,* 6th ed. (Masson, Paris, 1972).

Anisimov, G., and V. Teplyakov, *Prib. Tekh. Eksp.* **1**, 21 (1963) [Instrum. Exp. Tech. **1** (USSR), 15 (1963)].

Baev, V. K., et al., "Resonant Ion Linac with Fast Wave Focusing," *Dok Akad Nauk USSR* **275** (April 1984), pp. 870–872.

Blewett, J. B., *Phys. Rev.* **88**, 1197 (1952).

Boussard, D., "Radio Frequency Focusing in Heavy Ion Linear Accelerators," in *Linear Accelerators,* P. M. Lapostolle and A. L. Septier, Eds. (North-Holland Publishing Company, Amsterdam, The Netherlands, 1970), Chap. D.3, p. 1073.

Bruck, H., *Accélérateurs Circulaires de Particules*, Institut National des Sciences et Techniques Nucléaires (Presses Universitaires de France, Paris, 1966); Los Alamos Scientific Laboratory translation, "Circular Particle Accelerators," LA-TR-72-10 Rev. (1972).

Courant, E. D., et al., "The Strong Focusing Synchrotron," *Phys. Rev.* **88**, 1190 (1952).

Courant, E. D., and H. S. Snyder, "Theory of the Alternating Gradient Synchrotron," *Ann. Phys.* **3**, (New York) 1–48 (1958).

Dietinghoff, et al., "Properties of Linacs with APF," Proc. Linac Conf., Chalk River, AECL 5677, 238–250 (1976).

Fainberg, I. B., "Alternating Phase Focusing," Proc. Conf. on High Energy Accelerators, CERN, Geneva, Switzerland, 91 (1956).

Good, M. L., "Phase Reversal Focusing in Linear Accelerators" (Berkeley Radiation Laboratory report), *Phys. Rev.* **92**, 538 (1953).

Hereward, H. G., and K. Johnsen, "AG Focusing in Linacs," Proc. Conf. on High Energy Accelelerator, CERN, Geneva Switzerland, p. 167 (1956).

Humphries, S., *Principles of Charged Particle Acceleration* (J. Wiley and Sons, New York, 1986), Chap. 14.

Kapchinskij, I. M., *Theory of Resonance Linear Accelerators* (Harwood Academic Publ., New York, 1985), para. 2.8.

Kapchinskij, I. M., et al., *Prib. Tekh. Eksp.* **17**, 19–22 (1970).

Kapchinskij, I. M., "The Linac with Space Uniform Quadrupole Focusing," *IEEE Trans. Nucl. Sci.* **26**, 3462 (1970).

Junior, P., H. Deitinghoff, K. D. Halfmann, H. Klein, and A. Schempp, "A RFQ Concept Using Circular Rods," Proc. Linear Accelerator Conf., Los Alamos National Laboratory report LA-9234C, 81 (1981).

Knapp, E. A., and D. A. Swenson, "The Pigmi Program at LASL," Proc. Proton Linear Accelerator Conf., Chalk River Nuclear Laboratories report AECL-5677, 230 (1976).

Lapostolle, P., et al., "Cross Gradient Focusing in Linacs," Proc. Int. Conf. on High Energy Accelerator, Dubna (Atomizdat, Moscow), p. 513 (1963). (U.S. AEC translation, p. 672–682.)

Lasslett, J., in *Focusing of Charged Particles,* (A. Septier, Ed.) (Academic Press, New York, 1967) Vol. 2, p. 355.

Lawson, J. D., *Physics of Particle Beams* (Clarendon Press, Oxford, 1987), Chap. 2.

Maltsev, A., and V. Teplyakov, *Prib. Tekh. Eksp.* **4**, 29 (1965) [*Instrum. Exp. Tech.* **4**, 763 (1965)]

McMillan, E. M., "The Relation Between Phase Stability and First Order Focusing," *Phys. Rev.* **80**, 493 (1950).

Müller, R., "Work on RFQ Structures at GSI," Proc. Linear Accelerator Conf., Montauk, Brookhaven National Laboratory report BNL-51134, 148 (1979).

Müller, R. W., H. Deitinghoff, K. Halfmann, P. Junior, H. Klein, K. Langbein, J. Müller, and A. Schempp, "Proton Model of a Heavy-Ion RFQ Linac," *IEEE Trans. Nucl. Sci.* **28**, 2862 (1981).

Potter, J. M., S. W. Williams, F. J. Humphry, and G. W. Rodenz, "Radio Frequency Quadruople Accelerating Structure Research at Los Alamos," *IEEE Trans. Nucl. Sci.* **26**, 3745 (1979).

Promé, M., "Focusing," in *Linear Accelerators,* Chap. C.1.2c, p.785.

Smith, L., and R. L. Gluckstern, "Focusing in Linacs," *Rev. Sci. Instrum.* **26**, 220 (1955).

Smith, L., "Linear Accelerators," in *Handbuch der Physik* **44** (Springer Verlag, Berlin 1959) pp. 341–389.

Stokes, R. H., K. R. Crandall, J. E. Stovall, and D. A. Swenson, "RF Quadrupole Beam Dynamics," *IEEE Trans. Nucl. Sci.* **26**, 3469 (1979).

Swenson, D. A., "Beam Dynamics in the Low Energy End of PIGMI," Proc. Proton Linear Accelerator, Conf., Chalk River Nuclear Laboratories report, AECL-5677, 234 (1976).

Swenson, D. A., "Low Beta Linac Structures," Proc. Linear Accelerator Conf., Brookhaven National Laboratory report BNL-51134, 129 (1979).

Teng, L. C., "AG Focusing for Linacs," *Rev. Sci. Instrum.* **25**, 264 (1954).

Vladimirskij, V., *Prib. Tekh. Eksp.* **3**, 35 (1956).

Chapter 4

Alvarez, L., et al., "Berkeley Proton Linear Accelerator," *Rev. Sci. Instrum.* **26**, 111–132, 210–219 (1955).

Bell, M., et al., "Numerical Computation of Field Distribution," Proc. Linear Accelerator Conf., Batavia, NAL, p. 329, 1970.

Böhne, D., "The UNILAC," Proc. Linear Accelerator Conf., Chalk River AECL 5677, 2 (1976).

Bollinger, L., et al., "Concept of a Superconducting Linac," Proc. Linear Accelerator Conf., Darmstadt report GSI 84-11, 217 (1984).

Boussard, D., "Control of Cavities with High Beam Loading, *IEEE Trans. Nucl. Sci.* **32** (5), 1852 (1985).

Carne, A., "Low and Medium Energies, Alvarez Structures," in *Linear Accelerators*, Chap. C.1.1b, p. 587.

Dôme, G., "Review and Survey of Accelerating Structures," in *Linear Accelerators*, Chap. C.1.1e, p. 637.

Dôme, G., and P. Lapostolle, "A New Interpretation of Structure Compensation," Proc. Linear Accelerator Conf., Brookhaven National Laboratory report BNL-50120 (C54), 445 (1968).

Fessenden, T., "Induction Linacs for HIF," Proc. Linear Accelerator Conf., Darmstadt GSI 84-11, 485 (1984).

Fukushima, T., T. Hattori, T. Hori, K. Sato, E. Tojyo, and K. Yoshida, "Measurement of Model Inter-digital H Type Linac," Proc. Linear Accelerator Conf., Los Alamos National Laboratory report LA-9234-C, 296 (1982).

Giordano, S., et al., "Multistem Drift Tube Structure," Proc. Linear Accelerator Conf., Los Alamos Scientific Laboratory report LA-3609, 88, (1966).

Halbach, K., et al., "Properties of the Code Superfish," Proc. Linear Accelerator Conf., Chalk River AECL 5677, 122 (1976) and "Superfish," *Particle Accelerators* **7**, 213–222 (1976).

Hereward, H. G., and P. Lapostolle, "Energy Flow and Transients in Alvarez Structures" Proc. 5th Int. Conf. on High Energy Accelerators, Frascati, p. 742 (1965).

Humphries, S., *Principles of Charged Particle Acceleration* (John Wiley & Sons, Inc., New York, 1986), Chap. 14.

Kaspar, K., "The Prestripper Accelerator of UNILAC," Proc. Linear Accelerator Conf., Chalk River AECL 5677, 73 (1976).

Knapp, E. A., "High Energy Structures," in *Linear Accelerators*, Chap. C.1.1c, p. 601.

Knapp, E. A., B. C. Knapp, and J. M. Potter, "Standing Wave High-Energy Linear Accelerator Structures," *Rev. Sci. Instrum.* **39**, 979–991 (1968).

McMichael, G., et al., "Beam Loading Experiments," Proc. Linear Accelerator Conf., Brookhaven National Laboratory report BNL-51134, 180 (1979).

Moretti, A., et al., "The Design of a 12.5 MHz Wideröe Linac," Proc. Linear Accelerator Conf., Brookhaven National Laboratory report BNL-51134, 152 (1979).

Nassibian, G., J. Bennett, Jr., D. Broadbent, S. Devons, R. W. R. Hoisington, and V. E. Miller, "A One MeV/Nucleon Sloan Lawrence Linear Accelerator," *Rev. Sci. Instrum.* **32**, 1316 (1961).

Nishikawa, T., "Normal Mode Analysis of Standing Wave Linacs," Proc. 5th Int. Conf. on High Energy Accelerators, Frascati, p. 651 (1965) and "Beam Loading Effects in Standing Wave Linacs," Proc. Linear Accelerator Conf., Los Alamos Scientific Laboratory report LA-3609, 294 (1966).

Nishikawa, T., "Transients and Beam Loading Effect," in *Linear Accelertors*, Chap. C.1.3b, p. 809.

Nolte, E., et al., "The Munich Heavy Ion Post Accelerator," *IEEE Trans. Nucl. Sci.* **26**, 3724 (1979).

Odera, M., "A Variable Frequency Linac," Proc. Linear Accelerator Conf., Chalk River AECL 5677, 62 (1976).

Odera, M., et al., "Status of RILAC," Proc. Linear Accelerator Conf., Brookhaven National Laboratory report BNL-51134, 28 (1979).

Ramstein, G., et al., "Cavité supraconductrice a hélice," *Revue Phys. Appl.* **23**, 1483-1488 (1988).

Schempp, A., et al., "A Heavy Ion Post Accelerator," Proc. Linear Accelerator Conf., Brookhaven National Laboratory report BNL-51134, 159 (1979).

Slater, J. C., *Microwave Electronics* (Van Nostrand, New York, 1950), p. 81 and Chap. 4 and 5.

Slater, J. C., et al, "Field Strength Measurements" *J. of App. Phys.* **23**, 68–83 (1952)

Sloan, D. H., and E. O. Lawrence, "The Production of Heavy High Speed Ions Without the Use of High Voltages," *Phys. Rev.* **38**, 2021–2032 (1931).

Smith, L., "Beam Dynamics in Heavy Ion Induction Linacs," Proc. Linear Accelerator Conf., Los Alamos National Laboratory report LA-9234-C, 111 (1981).

Swenson, D. A., E. A. Knapp, J. M. Potter, and E. J. Schneider, "Stabilization of the Drift-Tube Linac by Operation in the $\pi/2$ Cavity Mode," Proc. 6th Conf. on High Energy Accelerators, Cambridge CEAL 2000, 167 (1967).

Swenson, D. A., T. J. Boyd, Jr., J. M. Potter, and J. E. Stovall, "Variable-Energy Drift-Tube Linac," Proc. Linear Accelerator Conf., Los Alamos National Laboratory report LA-9234-C, 187 (1981).

Tanabe, E., and G. Meddaugh, "Variable Energy Standing Wave Linear Accelerator Structure," Proc. Linear Accelerator Conf., Los Alamos National Laboratory report LA-9234-C, 191 (1981).

Vassallo, C. *Théorie des Guides dÓndes Électromagnétiques* (Eyrolles, Paris, 1985), Chap. II.

Watkins, D., *Topics in EM Theory*, (John Wiley & Sons, Inc., New York, 1958).

Watson, J., et al., "A 12.5-MHz Heavy Ion Linac," *IEEE Trans. Nucl. Sci.* **26**, 3045 (1979) and "The Status of the Argonne Low Beta Linac," *IEEE Trans. Nucl. Sci.* **28**, 3449 (1981).

Zeidlitz, P., et al., "Accelerating Systems Employing H Type Waves," *Plasma Physics* **4**, 121–127 (1962).

Chapter 5

Alvarez, L. W., H. Bradner, J. V. Franck, H. Gordon, J. D. Gow, L. C. Marshall, F. Oppenheimer, W. K. H. Panofsky, Ch. Richman, and J. R. Woodyard, "Berkeley Proton Linac," *Rev. Sci. Instrum.* **26**, 119 (1955).

Carne A., et al., "Design Equations in a Linac," Proc. Linear Accelerator Conf, Los Alamos Scientific Laboratory report LA-3609, 201 (1966) and Proc. 5th Int. Conf. on High Energy Accelerators, Frascati, p. 656 (1965).

Carne, A., B. Schnizer, P. Lapostolle, and M. Promé, "Numerical Methods. Acceleration by a Gap," in *Linear Accelerators*, P. M. Lapostolle and A. L. Septier, Eds. (North-Holland Publishing Company, Amsterdam, The Netherlands, 1970), Chap. C.1.2b, p. 747.

Lapostolle, P., "Equations de la Dynamique des Particules," CERN report AR/Int SG 5/11 (1965).

Lapostolle, P., and S. Valero, "Beam Dynamics in Long Transit Time Cavities," Proc. Linear Accelerator Conf., Stanford Linear Accelerator Center report SLAC 303, 315 (1986).

Promé, M., and M. Martini, "Beam Dynamics in a Proton Linac with Space Charge," Proc. Int. Conf. on High Energy Accelerators, Yerevan, Vol I, p. 223–235 (1969)

Promé, M., and M. Martini, "Computer Studies of Beam Dynamics," *Particle Accelerators* **9**, 289–299 (1971).

Schnizer, B. "General Properties of Fields and Beam Dynamics," CERN report 69-3 (1969).

Chapter 6

Chasman, R., "Numerical Calculation of Transverse Emittance Growth," *IEEE Trans. Nucl. Sci.* **16**, 202 (1969).

Courant, E., and H. Snyder, "Theory of the Alternating Gradient Synchrotron," *Ann. Phys.* (New York) 3, 1.48 (1958).

Gluckstern, R. L., "Beam Cavity Interaction," Proc. Linear Accelerator Conf., Darmstadt report GSI-84-11, **265** (1984).

Gluckstern, R. L., "Oscillation Modes in 2D Beams," Proc. Linear Accelerator Conf. Batavia, NAL, p. 811 (1970).

Gluckstern, R. L., "Space Charge Effects," in *Linear Accelerators*, P. M. Lapostolle and A. L. Septier, Eds. (North-Holland Publishing Company, Amsterdam, The Netherlands, 1970), Ch C1.3.c., p. 827.

Hofmann, I., "Negative Energy Oscillations and Instability of Intense Beams," *Particle Accelerators* **10**, 253–258 (1980).

Hofmann, I., in *Applied Charged Particle Optics*, A. L. Septier, Ed. (Academic Press, New York, 1983), p. 49–140.

Hofmann, I., "Generalized 3D Equations for the Emittance and Field Energy of High-Current Beams in Periodic Focusing Structures," *Particle Accelerators* **21**, 69–98 (1987).

Jameson, R. A., "Equipartioning in Linear Accelerators," Proc. Linear Accelerator Conf., Los Alamos LA-9234-C, 125 (1981).

Kapchinskij, I. M., " Linear Resonant Accelerators" (in Russian), Atomizdat Moscow, "Particle Dynamics in Linacs," Los Alamos Scientific Laboratory translation LA-TR 80-10 (1966).

Kapchinskij, I., and V. Vladiimirskij, "Limitations of Proton Beam Current in a Strong Focusing Linear Accelerator Associated with the Beam Space Charge," Proc. Int. Conf. on High Energy Accelerators, CERN, p. 274 (1959).

Kapchinskij, I. M., *Theory of Resonance Linear Accelerators*, (Harwood Acad. Publ., New York, 1985) Chap. 3 and 4.

Kim, C., et al., "High Current Beam Transport Experiment at LBL," Proc. Int Symposium on Heavy Ion Accelerators, Tokyo Institute for Nuclear Study, p. 460 (1984).

Lapostolle, P., "Effects de la Charge d'Espace dans un Accélérateur Linéaire," CERN report AR/INT SG/65–15 (1965).

Lapostolle, P., "Relations Entre Les Distributions de Type Hyperellipsoidal," CERN report ISR 300 LIN/66-32 (1966).

Lapostolle, P., "Density Distribution in Intense Beams," Proc. Conf. on High Energy Accelerators, Yerevan, Vol. I, p. 205 (1969).

Lapostolle, P., "Relations Energetiques dans les Faisceaux Continus," CERN report ISRD 1/71-6, Los Alamos National Laboratory translation LA-TR-80-8 (1971).

Lapostolle, P., "Etude Numérique de Charge d'Espace, CERN report ISR/78-13 (1978).

Lasslett, L., et al., "Stability of the KV Distribution," *Particle Accelerators* **13**, 165–178 (1983).

Lawson, J. D., *Physics of Charge Particle Beams*, 2nd ed. (Clarendon Press, Oxford, 1987), Chap. VI.

Promé, M., et al. "Beam Dynamics in a Proton Linac with Space Charge," Proc Conf. on High Energy Accelerators, Yerevan, Vol. I, 223–235 (1969).

Promé, M., et al., 1971, "Computer Studies of Beam Dynamics," *Particle Accelerators* **2**. 289–299 (1971) and Thesis, Orsay, 761 (1971).

Sacherer, F., "RMS Envelope Equations with Space Charge," *IEEE Trans. Nucl. Sci.* **18**, 1105 (1971).

Wangler, T. P., "Relation Between Field Energy and RMS Emittance," *IEEE Trans. Nucl. Sci.* **32**, 2196 (1985).

Wangler, T.P., K. R. Crandall, R. S. Mills, and M. Reiser, "Field Energy and RMS Emittance in Intense Particle Beams," Workshop on High Brightness, High Current, High Duty Factor Ion Injectors, San Diego, AIP Conf. Proc. **139**, 133 (1986).

Warner, D., "Accelerating Structure of CERN Linac," Proc. Linear Accelerator Conf., Chalk River report AECL 5677, 49 (1976).

Weiss, M., "The New CERN Linac," Proc. Linear Accelerator Conf., Montauk, Brookhaven National Laboratory report BNL 51134, 67 (1979).

Chapter 7

Amman, F., "Positron Accelerators," in *Linear Accelerators*, P. M. Lapostolle and A. L. Septier, Eds. (North-Holland Publishing Company, Amsterdam, The Netherlands, 1970) Chap. B.3.5, p. 523.

Farkas, Z., et al., "SLED A Method of Doubling SLAC's Energy," Proc. Conf. on High Energy Accel, Stanford, 576 (1976).

Farkas, Z., et al., "Recent Progress on SLED," *IEEE Trans. Nucl. Sci.* **22**, 1299 (1975).

Farkas, Z., et al., "Microwave Developments at SLAC," *IEEE Trans. Nucl. Sci.* **24**, 1827 (1975).

Helm, R. H., and G. A. Loew, "Beam Breakup," in *Linear Accelerators*, Chap. B.1.4, p. 173.

Helm, R. H., and R. Miller, "Particle Dynamics," in *Linear Accelerators*, Chap. B.1.2, p. 115.

Leiss, J. E., "Beam Loading and Transient Behavior in Traveling Wave Electron Linear Accelerators," in *Linear Accelerators*, Chap. B.1.3, p. 147.

Loew, G. A., and R. B. Neal, "Accelerating Structures," in *Linear Accelerators*, Chap. B.1.1, p. 39.

Montague, B. W., "Radiofrequency Separators," in *Linear Accelerators*, Chap. B.3.7, p. 569.

☆ U.S. GOVERNMENT PRINTING OFFICE: 1980-673-034/00153